ACCESSIBILITY
Open

OSLO METROPOLITAN UNIVERSITY
STORBYUNIVERSITETET

Master's Degree in
Structural Engineering and Building Technology
Department of Civil Engineering and Energy Technology

MASTER THESIS

THESIS TITLE	DATE
Impact of urban morphology on pressure coefficient on building facades and wind velocity in street canyons - The case of Oslo	09.06.2021
	NUMBER OF PAGES 92/3
AUTHOR(S) Arun Adhikari Øystein Løken Bergum	SUPERVISOR(S) Dimitrios Kraniotis Arnab Chaudhuri

IN COLLABORATION WITH	CONTACT PERSON
-	-

SUMMARY
By 2050 the number of people living in urban areas will be increased by 2.5 billion. To deal with such an inflow of people, cities will have to build taller, bigger, and denser. This will lead to a severe change in the urban morphology, which will impact the local wind conditions. This project aims to study the impacts of urban morphology on pressure coefficients on building facades and wind velocity in street canyons within the city of Oslo.

Two 3D-models of areas within the city has been created using Revit Placemaker to import the buildings, and Autodesk AutoCAD to edit them. One of the areas represents the city center (Downtown) containing high and medium-rise buildings, the other represents Bygdøy, a residential area with low-rise buildings. CFD-simulations for these have been made using STAR-CCM+.

The results have shown that that urban morphology affects the wind conditions. Both differences between the models, and within each model has been spotted. Effects have been found both regarding the pressure coefficient on building facades and the wind velocity in street canyons.

3 KEYWORDS
Computational Fluid Dynamics – CFD
Pressure Coefficient
Wind Velocity

Acknowledgements

This master thesis was conducted at Oslo Metropolitan University (OsloMet) as the concluding work of the master's degree Programme in Structural Engineering and Building Technology.

The thesis has been conducted during a difficult time for everyone with an ongoing global pandemic. This has influenced us in many ways, challenging both us and our supervisors to find new ways to communicate and cooperate. We are thankful that OsloMet has strived to keep the campus open for the students as much as possible. This has been important for us to be able to carry out necessary simulations.

We would like to thank our excellent supervisors, Associate Professors Dimitrios Kraniotis and Arnab Chaudhuri. Both have contributed with professional guidance and inspiration, as well as motivation through the challenging phases of the project. We would also like to thank our fellow students for good discussions and great support throughout the project.

Finally, we would like to thank our families, friends, and each other for invaluable support and motivation.

Oslo Metropolitan University

Oslo, 09.06.2021

_____ _____

Arun Adhikari ***Øystein Løken Bergum***

Abstract

By 2050 the number of people living in urban areas will be increased by 2.5 billion. To deal with such an inflow of people, cities will have to build taller, bigger, and denser. This will lead to a severe change in the urban morphology and have impacts on the local wind conditions. Understanding how this relate will become more important in the years to come. This project aims to study the impacts of urban morphology on pressure coefficients on building facades and wind velocity in street canyons within the city of Oslo.

Two 3D-models of areas within the city has been created using Revit Placemaker to import the buildings, and Autodesk AutoCAD to edit them. One of the areas represents the city center (Downtown) containing high and medium-rise buildings. The other represents Bygdøy, a residential area with low-rise buildings. The models are limited to containing buildings where all roofs are considered flat.

These models are then imported to the CFD-tool STAR-CCM+ where a domain is created, a mesh is made, and relevant physics are applied. A simulation is then performed with the target of getting results regarding pressure coefficient of building facades and wind velocity in street canyons.

The results have shown that urban morphology affects the wind conditions in several ways. The pressure coefficient values are positive on facades facing the inlet and mainly negative on other facades. The highest magnitudes occur in exposed areas and in areas with tall buildings. It is seen that the area with low-rise buildings receives significantly smaller pressure coefficient values.

The wind velocity tends to increase around tall buildings and open areas in the Downtown model. This is more significant at the pedestrian level height ($2.5m$) than at $17m$. There are large differences between the areas, as the Bygdøy model has very few areas with increased wind velocity.

Contents

List of Figures

List of Tables

Nomenclature

CFD	Computational Fluid Dynamics
CPU	Central Processing Unit
U_{eq}	Equivalent mean wind speed $[m/s]$
$\Sigma\ \sigma_u$	Standard deviation of the wind speed $[m/s]$
p_k	Peak factor
P	Probability
U_{max}	Threshold for equivalent mean wind speed $[m/s]$
U_i	Instantaneous velocity vector $[m/s]$
X_i	Position vector $[m]$
T	Time $[s]$
P	Density $[kg/m^3]$
P	Pressure $[Pa]$
V	Kinematic viscosity $[m^2/s]$
U_i'	Fluctuation velocity vector $[m/s]$
β^*, σ^*	Closure coefficients in the turbulent kinetic energy equation.
$\alpha, \beta, \sigma, \sigma_d$	Closure coefficients in the specific dissipation rate
P_x	Static pressure at any point on the building facades $[Pa]$
P_d	The dynamic pressure $[Pa]$
P_o	The reference static pressure $[Pa]$
P	Density of air $[kg/m^3]$
U_{ref}	Reference wind speed at the reference height $[m/s^2]$
K	Von Karman's constant

1 Introduction

According to the United Nations Department of Economic and Social Affairs, 55% of the world's population were accommodated in urban areas in 2018. The urbanization is ongoing, and it is projected that by 2050 it will be increased to 68%. The United Nations also projects that by 2050 the number of people living in urban areas will be increased by 2.5 billion [1]. To deal with the great inflow of people, cities will have to build taller, bigger, and denser. As the urban morphology changes, it is important to understand that it has a large influence on the local urban environment.

An important part of the local urban environment is the wind conditions. A study from 2020 showed that in an urban area in the city of Beijing, the average wind velocity varied between 56% and 160% of the suburban wind velocity [2]. This shows that urbanization not only makes the wind weaker, but it can also make it significantly stronger. In the years to come, city areas will be introduced to more high-rise buildings, narrower street-canyons, and a more compact building mass. When designing the city areas, it is important to have knowledge about how the local environment will react to the changes.

It is known that the urban morphology does influence the airflow around the buildings and the wind loads on the buildings [3]. It is important to study these conditions as they influence several factors, including wind-induced air infiltration, energy consumption, urban heat islands, and air pollution [4]. The wind conditions are also important regarding the structural design of the buildings. This thesis will focus on the pressure coefficient on the building facades and the wind velocity in street canyons, two factors which are important in different ways.

In 2017, buildings were accountable for 39% of all carbon emissions in the world [5]. Therefore, it is important to take measures to reduce the emissions. One way this could be done is to improve the energy performance of new buildings. The air infiltration and ventilation are key parts to buildings total energy use, and the pressure coefficients are a part of this. Studying the wind conditions and finding the correct pressure coefficients is important, as studies show that using sources as databases and analytical methods can give large deviations in energy calculations [6].

The wind velocity in street canyons is often used to determine the pedestrian wind comfort. It is known that high wind velocities often occur around high-rise buildings, which in many cases can be uncomfortable or dangerous for pedestrians [7]. By analyzing the wind conditions during

the designing phase, it is possible to improve the pedestrian comfort, and avoid dangerous situations.

Studying the impact of urban morphology on wind conditions are mainly done by either wind-tunnel experiment, computational fluid dynamics (CFD), or field measurements. There have been questions whether CFD-simulations are accurate enough to give an adequate result compared to wind-tunnel experiments. However, with improving methods and documentation over the later years, a properly executed CFD-simulation should be considered equivalent to the result of wind-tunnel experiments, according to Kataoka et. al. [8]. This has been verified by several other studies, i.e., by Yoshie et.al. which showed that their CFD-simulation gave results within 10% of wind-tunnel results [9].

Studying the impact of urban morphology on wind conditions for real urban areas using CFD-simulations is a complex task, which requires good data, sufficient knowledge, high CPU-power, and plenty of time. Even though similar studies have been made for other urban areas, the situation can be completely different from area to area. Therefore, doing such studies is important do discover the local conditions.

1.1 Scope

The scope of this project is to investigate how the wind conditions, in terms of pressure coefficient on building facades and wind velocity at street level, relates to the urban morphology in urban areas in Oslo. This will be done by performing CFD-simulations in the software Simcenter STAR-CCM+. The project also includes the creation of 3D-models from existing geodata, and the process of linking it to the CFD-software.

Two different urban areas in Oslo will be analyzed, both areas of approximately $2x2\ km$. One area is located in the city center, containing mainly high and medium-rise buildings, while the other is located in Bygdøy, which mainly contains low-rise residential buildings. The aim is to see how the wind conditions varies related to different urban morphology factors, both between the two areas, but also internally in the same area.

1.2 Research question

This project includes two main parts. One contains the creation of the 3D-models that will be used in the simulation, while the other contains the simulation itself and the associated results. There will be two different research questions in the project:

- *Find the best way to link geodata to the CFD-software STAR-CCM+ and create two models for two different urban areas within the city of Oslo.*
- *Analyze how the urban morphology affects the pressure coefficient on building facades and wind velocity in street canyons within different parts of Oslo and analyze the differences between areas of high-rise buildings and areas of low-rise buildings.*

1.3 Limitations

Investigating the impact of urban morphology on wind conditions within the city of Oslo is a large task, and not everything can be done within the time scope of a master thesis. Therefore, some limitations are made:

- Area limited to two areas of approximately $2x2km$
- 3D-model contains only buildings. Terrain and other features are not included
- All roofs are considered as flat
- Height of buildings are in some cases assumed

2 Theory

Impact of urban morphology on the pressure coefficient and pedestrian wind environment in an urban street canyon like Oslo, rife with low-rise and high-rise buildings, involves substantial theoretical parameters. This chapters deals with the most of these theoretical parameters, including CFD.

2.1 Wind conditions

Wind is known as relative movement of the air with respect to the earth surface. It is dependent on several driving forces of which pressure difference in the atmosphere is the major one. Pressure difference in the earth's surface is dependent on differential solar heating at different parts of an earth surface, force due to the rotation of the earth about its own axis and the morphology of a place [10].

Wind speed is generally described in terms of the mean velocities at the pedestrian level. Despite gust effect being possibly argued for major influence in the pedestrian wind environment, several city planners need the certain fulfilment of mean velocities with a specified probability of exceedance.

At the urban street canyons, when a gust of wind strikes urban dwellings, high wind speed can be generated due to deflection of wind. Mainly vortex flow between buildings at ground level, descending air around the building corners at leeward side and the air flow passing through the opening in the ground levels are some important features to investigate regarding the wind environment in the street canyons.

Air flow pattern with some important terminologies is explained and illustrated in Figure 2-1. As most of the buildings are designed to withstand the larger external air forces, the understanding of the air flow pattern around the buildings is an essential part in the CFD.

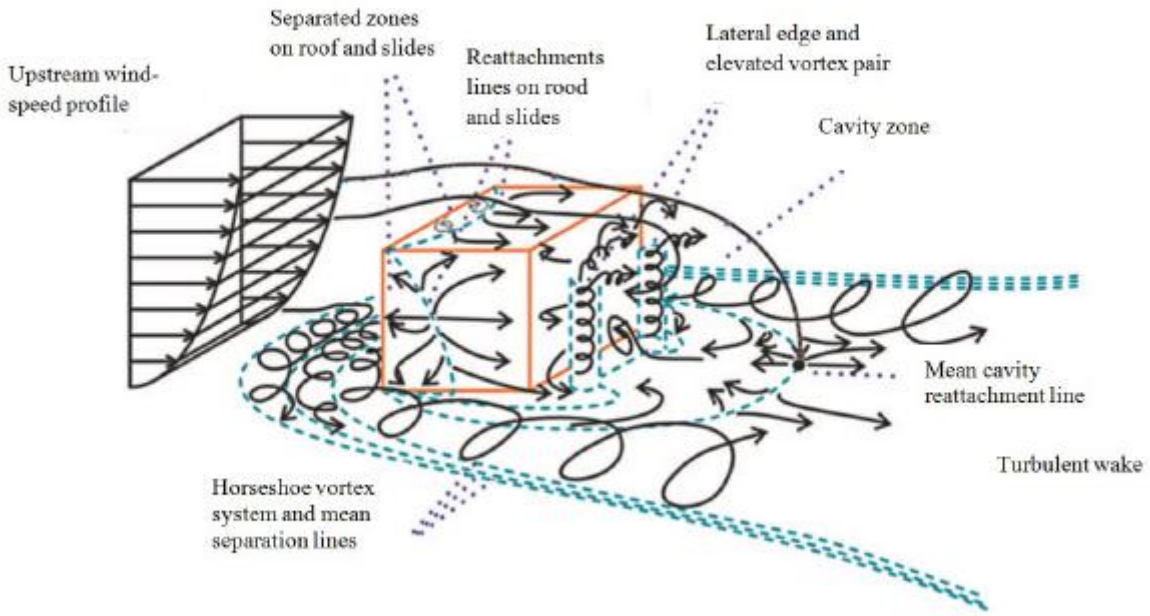

Figure 2-1. Air flow pattern around a building [11]

The air flow pattern illustrates turbulent shear flow at the boundary layer and the flow diverges as it approaches the building. Windward side though clearly not visible has a stagnation point with maximum pressure situated in two third the upper part of the building. The separated recirculation zone on sides, roof, turbulent wake, and wake cavity zone are important aspect of this diagram. Stagnation point separates the low-pressure zone flow as upward, sideward, and downward flow. Recirculation zone or the separation bubble at the upper edge helps to separate the upward and sideward flow and has low velocity and highly turbulent fluid at this zone.

The dotted line in the figure is the reattachment line where separated flow can reattach based on turbulence and the building dimension. The vortex at the ground, also called frontal, standing or horseshoe vortex is formed by downward flow from stagnation point and it creates corner streams around the building base at high wind speed. Leeward side of the building is usually underpressurized side and forms the cavity zone along with dotted lines (mean cavity reattachment line) representing the end of cavity zone. The diagram represents the mean wind flow pattern for a single building and complexity may increase for multiple building due to the interaction between the fluid flow.

2.2 Pedestrian wind Environment

Understanding of wind condition at pedestrian level for denser urban street canyons becomes vital these days. Generally, wind condition at street canyons is expressed in terms of human comfortability and it is expressed by the following mathematical expression.

$$U_{eq} = U + p_k.\sigma_u \geq U_{max} \quad (1)$$

$$P(U_e) \geq U_{max} \quad (2)$$

Where:

U_{eq} Equivalent mean wind speed $[m/s]$

$\Sigma\ \sigma_u$ Standard deviation of the wind speed $[m/s]$

p_k Peak factor

P Probability

U_{max} Threshold for equivalent mean wind speed $[m/s]$

Equation 1 interprets that for a certain activity a combination of certain U and σ_u beyond the given threshold U_{max} is unacceptable. σ in the expression can be related to the wind speed or to the streamwise u-component only or to the total horizontal turbulence, so it is not same at all conditions. Peak factor depends on gust duration, total averaging time and probability density function of the wind speed, and the peak factor is generally between 0 and 3.5. However, there is no universally valid expression for evaluating probability density function of wind speed [12].

Figure 2-2 and Figure 2-3 shows the wind comfort and danger criteria based on the Dutch Wind Nuisance standard NEN8100, a first wind comfort standard in the world [13]. Based on this standard, different exceedance probabilities point to different comfort classes for three types of activities as traversing, strolling and sitting. And this exceedance probability for different comfort classes corresponds to the threshold wind speed of $5m/s$ and null peak factor (k). Figure 2-4 illustrates other wind comfort criteria and their comparison with the NEN8100.

$P(U_{THR} > 5$ m/s (in % hours per year)	Grade	Activity		
		Traversing	Strolling	Sitting
<2.5	A	Good	Good	Good
2.5–5.0	B	Good	Good	Moderate
5.0–10	C	Good	Moderate	Poor
10–20	D	Moderate	Poor	Poor
>20	E	Poor	Poor	Poor

Figure 2-2. Criteria for wind comfort according to NEN8100 [14]

$P(U_{THR} > 15$ m/s (in % hours per year)	Grade	Activity		
		Traversing	Strolling	Sitting
0.05–0.30	Limited risk	Acceptable	Not acceptable	Not acceptable
≥0.30	Dangerous	Not acceptable	Not acceptable	Not acceptable

Figure 2-3. Criteria for wind danger according to NEN 8100 [14]

Reference	Threshold (moderate/tolerable wind climate)	P_{max}	Description of activity
***A (Sitting long)**: Sitting for a long period of time, laying in steady position, pedestrian sitting, terrace, street café or restaurant, open field theatre, pool*			
Isyumov & Davenport [20]	U > 3.6 m/s (3 Bft)	1.5% (1/week)	"Tolerable climate for sitting - long exposure (outdoor restaurants, bandshells, theatres)"
Lawson [21]	U > 1.8 m/s (2 Bft)	2%	"Tolerable for covered areas"
Melbourne [22]	$U + 3.5\sigma_u > 10$ m/s	0.022% (2 h/year)	"Generally acceptable for stationary, long–exposure activities (outdoor restaurants, theatres)"
NEN 8100 [19]	U > 5 m/s	2.5%	Quality Class A: "good climate for sitting long (parks)". Note: the Dutch Standard does not focus on café or restaurant terraces
***B (Sitting short)**:Pedestrian standing, standing/sitting over a short period of time, short steady positions, public park, playing field, shopping street, mall*			
Isyumov & Davenport [20]	U > 5.3 m/s (4 Bft)	1.5% (1/week)	"Tolerable climate for standing, short exposure (parks, plaza areas)"
Lawson [21]	U > 3.6 m/s (3 Bft)	2%	"Tolerable for pedestrian stand around"
Melbourne [22]	$U + 3.5\sigma_u > 13$ m/s	0.022% (2 h/year)	"Generally acceptable for stationary short-exposure activities (window shopping, standing or sitting in plazas)"
NEN 8100 [19]	U > 5 m/s	5%	Quality Class B: "moderate climate for sitting long (parks)"
***C (Strolling)**: Pedestrian walking, leisurely walking, normal walking, ramble, stroll, walkway, building entrance, shopping street, mall*			
Isyumov & Davenport [20]	U > 7.6 m/s (5 Bft)	1.5% (1/week)	"Tolerable climate for strolling, skating (parks, entrances, skating rinks)"
Lawson [21]	U > 5.3 m/s (4 Bft)	2%	"Tolerable for pedestrian walk-thru"
Melbourne [22]	$U + 3.5\sigma_u > 16$ m/s	0.022% (2 h/year)	"Generally acceptable for main public access-ways"
NEN 8100 [19]	U > 5 m/s	10%	Quality Class C: "moderate climate for strolling"
***D (Walking fast)**:Objective business walking, brisk or fast walking, car park, avenue, sidewalk, belvedere*			
Isyumov & Davenport [20]	U > 9.8 m/s (6 Bft)	1.5% (1/week)	"Tolerable for walking fast (sidewalks)"
Lawson [21]	U > 7.6 m/s (5 Bft)	2%	"Tolerable for roads, car parks"
NEN 8100 [19]	U > 5 m/s	20%	Quality Class D: "moderate climate for walking fast"
***Unacceptable, poor wind climate** → region in between D and Danger*			
Danger		**P_{min}**	***Description of activity***
Isyumov & Davenport [20]	U > 15.1 m/s (U > 8 Bft)	0.01% (1/year)	"Dangerous"
Melbourne [22]	$U + 3.5\sigma_u > 23$ m/s	0.022% (2 h/year)	"Completely unacceptable – the gust speed at which people get blown over"
NEN 8100 [19]	U > 15 m/s	0.05%	"limited risk" and "dangerous"

Figure 2-4. Different wind comfort and wind danger criteria consisting of wind speed threshold and maximum allowed exceedance probabilities for different pedestrian activity categories [14]

Wind danger criterion illustrated in Figure 2-3 is based on the exceedance of $15 m/s$ uniform wind speed.

2.3 Wind pressure and Pressure coefficient

As mentioned earlier, global pressure difference at the atmospheric level is due to the differences in the temperature of the earth surface due to solar radiations. Wind pressures act as a vital driving force in the natural ventilation. Air flows from the region of higher pressure to the region of lower pressure in order to compensate the pressure differences created by the uneven surface heating due to solar radiations. The direction of the air movement is dependent on pressure gradient, Coriolis force and friction on the earth's surface. Pressure decreases with the altitude but not at a uniform rate. It decreases most rapidly at lower elevation while it tapers of gradually at higher altitudes. But, at the earth surface, all recording meteorological stations are reduced to sea-level pressure in order to make horizontal comparisons.

Pressure gradient generally represents the pressure drop per unit length [10]. There are two pressure gradients as horizontal and vertical pressure gradients. Horizontal pressure gradients are small values even across large areas under normal conditions; whereas vertical pressure gradients are larger as pressure always decrease with the altitude and can be considered as the extreme cases of horizontal pressure gradients in terms of numbers.

$$Pressure\ gradient\ force\ /\ unit\ mass\ =\ -\frac{1}{\rho_\alpha} * \frac{\partial p}{\partial x} \qquad (3)$$

According to the expression above, in fluid mechanics, there is a resulting force per unit mass at a point in a fluid where there is a pressure gradient ($\partial p/\partial x$), x, in a cartesian co-ordinate system. ρ_α is the density of air in the above expression [10].

Another important driving force, Coriolis force, occurs due to the rotation of the earth. It is zero at the equator; while it acts right of the direction of the motion in the northern hemisphere and left of the velocity vector in southern hemisphere of the earth [10].

The Coriolis force: $F_c\ =\ 2\Omega sin(\Phi)v$

Where, Ω is the Earth's rotation rate, Φ is the latitude and v is the velocity.

Wind pressure around the building envelope is usually represented by the pressure coefficient C_p. It is generally calculated based on the pressure difference between static pressure (P_x) on the surfaces of the building and static pressure (P_o) at the reference point. Mathematically, pressure coefficient is represented by the following equation:

$$Pressure\ coefficient\ C_p = \frac{(P_x - P_o)}{P_d} \tag{4}$$

$$P_d = \rho * \frac{U_{ref}^2}{2} \tag{5}$$

P_x $[Pa]$ represents static pressure at any point on the building facades, P_d $[Pa]$ is the dynamic pressure, P_o $[Pa]$ is the reference static pressure, ρ $[kg/m^3]$ is the density of air and U_{ref} $[m/s^2]$ is the reference wind speed at the reference height. Static pressure at the reference height usually represents the pressure at the height when the wind achieves the free stream state. In CFD, the domain height should be properly understood in order to locate the probe point for the static pressure.

2.4 Mathematical Basics for the atmospheric flow description

Generally, Navier Stokes equations are considered as a basic mathematical tool to describe a fluid flow. Fluid with lower Mach number, less than 0.3, is considered to be incompressible. Basically, for a fluid when the viscous stresses arising from its flow is linearly corelated to the local strain rate then such fluid is termed as Newtonian fluid. Navier-Stokes equations for an incompressible Newtonian fluid is given by:

$$\frac{\partial u_j}{\partial x_j} = 0 \tag{6}$$

$$\frac{\partial u_i}{\partial t} + \frac{\partial u_i u_j}{\partial x_j} = -\frac{1}{\rho}\frac{\partial \rho}{\partial x_j} + v\frac{\partial}{\partial x_j}\left(\frac{\partial u_i}{\partial x_j} + \frac{\partial u_j}{\partial x_i}\right) \tag{7}$$

Where:

U_i	Instantaneous velocity vector $[m/s]$
X_i	position vector $[m]$
T	time $[s]$
P	density $[kg/m^3]$
P	pressure $[Pa]$
V	kinematic viscosity $[m^2/s]$

Considering computational costs, direct numerical solution of Navier-Stokes equations is superseded by other solution techniques, which falls into two different categories, Reynolds Averaged Navier-Stokes equations (RANS) and Large Eddy Simulation (LES). For mean flow solution with the time dependent eddies of a turbulent flow model, RANS are used, and for the transient large-scale flow with the eddies, LES is used. Detached Eddy Simulation (DES) is the combination of both of the above solution techniques, where LES is used to resolve the free stream flow, and the near wall is modelled by RANS. RANS equation can be obtained by time averaging from the previous Navier-Stokes equation.

$$\frac{\partial u_i}{\partial x_i} = 0 \tag{8}$$

$$\frac{\partial u_i}{\partial t} + \frac{\partial u_i \partial u_j}{\partial x_j} = -\frac{1}{\rho}\frac{\partial \overline{p}}{\partial x_j} + v\frac{\partial}{\partial x_j}\left(\frac{\partial u_i}{\partial x_j} + \frac{\partial u_j}{\partial x_i}\right) - \frac{\partial u'_i u'_j}{\partial x_j} \tag{9}$$

Where:

U_i mean velocity $[m/s]$

U_i' Fluctuation velocity vector $[m/s]$

The equation above introduces six different unknowns that can be better explained with the turbulence model.

2.5 Computational fluid dynamics (CFD)

CFD is a popular tool which has been in practice for several decades now. There are several intensive CFD studies carried out in the past regarding evaluation of indoor environment of the buildings, heat and mass transfer between buildings and the envelope, pedestrian wind environment, thermal comfort, wind driven rain, pollutant dispersion, exterior building surface heat transfer, natural ventilation, wind loads on the building structure and so on [15].

In CFD, modelling of the atmospheric boundary layer appropriately becomes vital when it comes to the degree of reliability in the outcome of the simulation. The atmospheric boundary layer is the bottom part of the earth's atmosphere that is in contact to the earth's surface. Within this layer, frictional effects and temperature creates turbulence and vertical mixing and above this layer rotational effects dominates the turbulence.

2.5.1 Inlet boundary condition

Inlet condition is the vital boundary condition. Generally, horizontal wind profile at the atmospheric boundary layer is computed by two main laws, the logarithmic law and the power law. Above rough walls, velocity profile is not same as that of the ground level and above uniform plane terrain wind profile is logarithmic. Considering Richard and Hoxey's law as the preferred method of modelling the roughness of an atmospheric boundary layer, vertical velocity is assumed to be zero with constant pressure and shear stress and the K-Epsilon model is in equilibrium. The K-Epsilon turbulence model at equilibrium gives solutions for the stream wise velocity component u, turbulent kinetic energy k, and the turbulent dissipation rate $\in$, which is valid throughout the entire domain [16].

Inlet velocity profile for the boundary condition is given by the logarithmic law as following:

$$u = \frac{u_*}{k} \ln\left(\frac{y_0 + y}{y_0}\right) \tag{10}$$

$$k = \frac{u_*^2}{\sqrt{c_\mu}} \tag{11}$$

$$\in = \frac{u_*^3}{k(y + y_0)} \tag{12}$$

k is the Von Karman's constant with the recommended value of 0.4. y_o is the surface roughness length, y is the wall distance to the nearest wall and c_μ is a parameter of K-Epsilon model with

the recommended value of 0.09. The aerodynamic roughness length (y_o) can be assigned based on the landscape description from Figure 2-6. u_* is the friction velocity which can be explained from the following equation.

$$u_* = \frac{k u_h}{\ln\left(\frac{h + y_o}{y_o}\right)} \tag{13}$$

U_h is the specified velocity at the reference height, h. STAR-CCM+ wall roughness equation to model atmospheric boundary layer is expressed by the following expression.

$$r = \frac{E y_o}{C_\mu} \tag{14}$$

E and C_μ in the expression are the wall function coefficients. For $u^+ > 0$, there must be $y >> y_0$ in order to make physical result more reliable, especially where wall distance to wall-cell centroids is larger than the roughness length [16].

Regarding the reference velocity, the average annual local atmospheric wind conditions and the wind rose at the desired meteorological station becomes vital. Figure 2-5 illustrates the wind rose frequency distribution of wind at Blindern, meteorological station of Oslo for the period of five years on hourly basis along the entire year. The dominant wind direction is to be from west of south towards east of north with the average being $5.7\ m/s$.

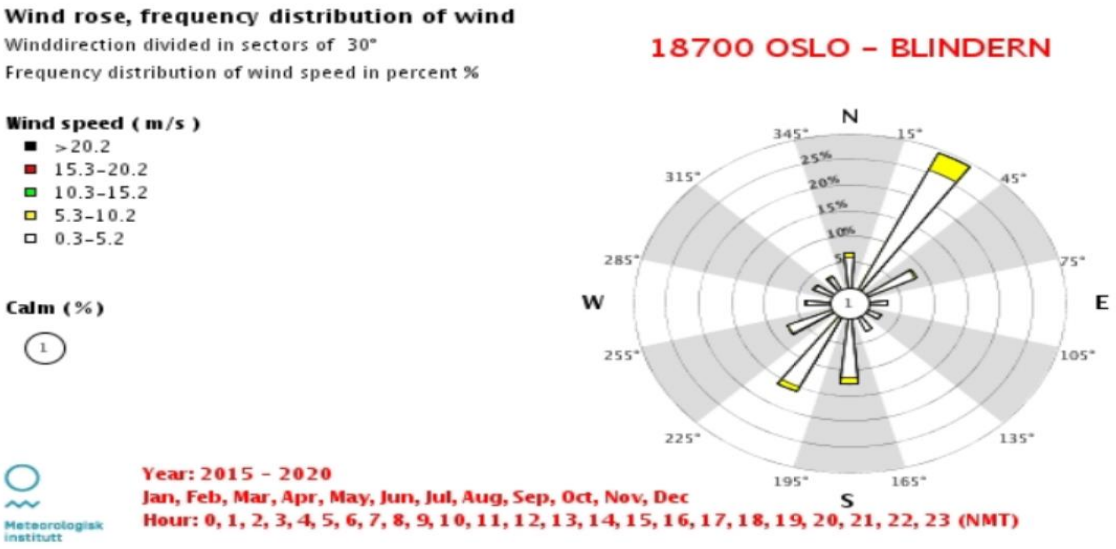

Figure 2-5. Wind rose for Oslo - Blindern

Aerodynamic roughness length (y_0) (m)	Landscape description
0.0002 (sea)	Open sea or lake (irrespective of the wave size), tidal flat, snow covered flat plain, featureless desert, tarmac and concrete, with a free fetch of several kilometers.
0.005 (smooth)	Featureless land surface without any noticeable obstacles and with negligible vegetation; e.g. beaches, pack ice without large ridges, morass, and snow-covered or fallow open country.
0.03 (open)	Level country with low vegetation (e.g. grass) and isolated obstacles with separations of at least 50 obstacle heights; e.g. grazing land without windbreaks, heather, moor and tundra, runway area of airports.
0.1 (roughly open)	Cultivated area with regular cover of low crops, or moderately open country with occasional obstacles (e.g. low hedges, single rows of trees, isolated farms) at relative horizontal distances of at least 20 obstacle heights.
0.25 (rough)	Recently-developed "young" landscape with high crops or crops of varying height, and scattered obstacles (e.g. dense shelterbelts, vineyards) at relative distances of about 15 obstacle heights.
0.5 (very rough)	"Old" cultivated landscape with many rather large obstacle groups (large farms, clumps of forest) separated by open spaces of about 10 obstacle heights. Also, low large vegetation with small inter- spaces, such as bushland, orchards, young densely-planted forest,
1.0 (closed)	Landscape totally and quite regularly covered with similar-size large obstacles, with open spaces comparable to the obstacle heights; e.g. mature regular forests, homogeneous cities or villages.
2.0 (chaotic)	Centers of large towns with mixture of low-rise and high-rise buildings. Also, irregular large forests with many clearings.

Figure 2-6. Updated Davenport roughness classification [17]

Wall treatment

Walls act as a source of vorticity in most fluid flow cases. Therefore, an accurate flow prediction across the boundary layer becomes essential. Wall boundary layer is a thin viscosity affected layer near a wall where the flow velocity of fluid changes from zero to the free stream value away from the wall. Boundary layer can be defined as a layer beyond which the effect of viscous stresses can be neglected, and its nominal thickness considered to be up to a point where the velocity of the fluid is 99% of the free stream velocity. The turbulent flow can be divided into two layers with outer layer dominated by turbulent effects and inner layer divided into three sub-layers.

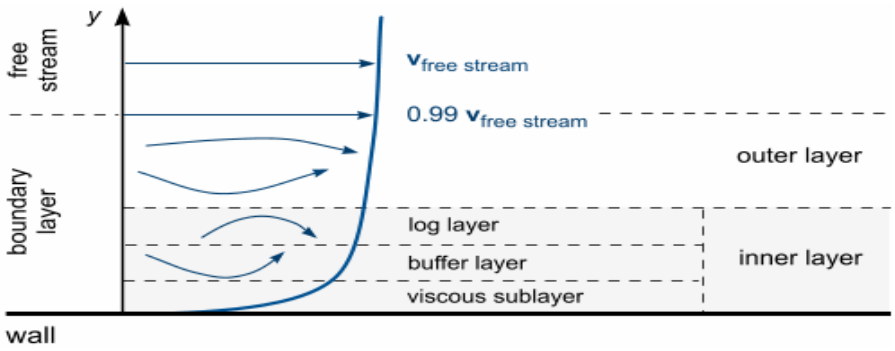

Figure 2-7. Velocity profile of turbulent boundary layer[18]

Among three sub-layers, viscous layer is in contact with the wall with almost laminar flow in it, turbulent log layer is equally dominated by viscous and turbulent effects and the buffer layer is the transitional layer. For the near wall modelling with the local and non-local effects that the wall has on turbulence, STAR-CCM+ uses low-Reynold number approach (including two-layer approach using damping function to account blocking effects) and high-Reynold number approach (includes turbulence damping effects). Wall treatment basically provides boundary conditions to the solver in the CFD tool for turbulence and it applies the transported turbulence quantities on the centroids of the near wall cells for the appropriate post processing. All y^+ wall treatment provides valid boundary conditions for flow, energy and turbulence using blended wall functions for all near wall mesh densities.

Figure 2-8 illustrates distribution of the non-dimensional quantity u^+ in the sub-layers of the turbulent boundary layer. The dash line represents the universal law of the wall for smooth surface with the dimensionless variables. The dimensionless variables are represented as followings.

$$u^+ = U/u^* \; and \; y^+ = u^* y/v$$

Where u^* is the friction velocity, U velocity tangential to the wall, and v is the kinematic viscosity. Generally, for viscous sub layer laminar law holds true ($u^+ = y^+$). Basically, laminar law is valid for almost all $y^+ \leq 5$ and the logarithmic law holds true for all y^+ above 30 and up to $y^+ = 500 - 1000$ [19].

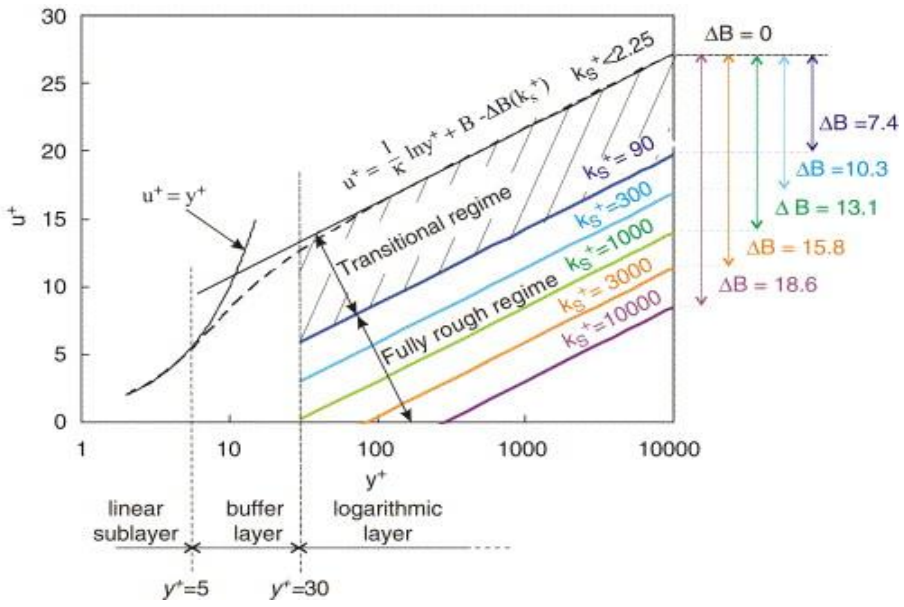

Figure 2-8. Wall Functions for Velocity (law of wall for rough surfaces) [19]

2.5.2 Other boundary conditions

A proper setting up of other boundary conditions for the entire domain becomes vital in order to visualize proper CFD simulations. Boundary conditions allow fluid to enter and leave the domain more pragmatic. Street canyons in the urban area generally have boundary condition set as pressure outlet. Usually, boundary condition at outlet represents outflow condition where backflow does not occur. The pressure outlet condition considers the static pressure of the fluid entering environment and the boundary face values of other variables as velocity is extrapolated from the interior of the domain solution. In case of the recirculation, pressure outlet boundary condition allows several methods such as extrapolated, boundary normal, components and angles to control the backflow directions.

Regarding side-walls and top, boundary condition for the domain can be symmetric if the geometry and the flow are symmetric. Symmetric plane boundary condition does not require one to specify any conditions and is valid for both compressible and incompressible flows. This boundary condition in STAR-CCM+, computes values at the boundary faces for velocity, static pressure, and the static temperature. The normal velocity and the gradient of all other variables

have zero values with zero fluxes across the symmetric plane in the symmetric boundary conditions.

For the ground surface, roughness effect is a critical issue which can lead to noticeable flow imperfections, and create disturbances in the velocity field and overall flow behavior. For a very fine mesh, roughness effect can be reduced by mesh itself. But for most cases, mesh cannot resolve it as roughness structure can be very small. Considering all these, roughness model at the ground surface can be a good option to eliminate flow imperfections due to small surface roughness by using appropriate roughness model. Table 1 illustrates the recommended boundary conditions for a standard k-ω model

Table 1. Recommended boundary condition for normal cases

Turbulence model	Standard k-ω model
Inlet	$u = \frac{u_*}{k} \ln(\frac{y_0+y}{y_0})$, $k = \frac{u_*^2}{\sqrt{c_\mu}}$, $\in = \frac{u_*^3}{k(y+y_0)}$, $u_* = \frac{ku_h}{\ln(\frac{h+y_o}{y_o})}$, k = 0.4, C_μ=0.253
Outlet	Pressure outlet with gauge pressure zero, same specific dissipation rate and turbulent kinetic energy as inlet
Ground	Roughness model using standard log law wall function, $r = \frac{Ey_o}{C_\mu}$, E = 9
Top	Symmetric boundary condition, free slip, and flux normal to the boundary is zero.
Sides	Symmetric boundary condition, free slip, and flux normal to the boundary is zero.

2.5.3 Turbulence models

For the turbulent kinetic energy K, and specific dissipation rate ω, the K-omega model generally solves transport equations. This model for turbulent flow is comprehensively originated by the D.C. Wilcox. K-Omega model is said to be superior to K-Epsilon model based on the performance for the boundary layers under adverse pressure gradients and it can be applied throughout the boundary layer including viscous dominated region without any need for the modifications [20]. Computation of wall distance is not required to make in this model and the boundary layer computations are sensitive to the values of ω in the free stream.

In this turbulent model, two variants of the K-Omega are implemented in the STAR-CCM+ as standard K-Omega and SST K-Omega. The standard K-Omega equation governing the turbulent kinetic energy and specific dissipation rate are:

$$\frac{\partial(\rho k)}{\partial t} + \frac{\partial\left(\rho u_j k\right)}{\partial X_j} = \frac{\rho\tau_{ij}\partial U_i}{\partial X_j} - \beta^*\rho k\omega + \frac{\partial}{\partial X_j}\left[\left(\mu + \frac{\sigma^*\rho k}{\omega}\right)\left(\frac{\partial k}{\partial X_j}\right)\right] \quad (15)$$

$$\frac{\partial(\rho\omega)}{\partial t} + \frac{\partial\left(\rho U_j\omega\right)}{\partial X_j} = \frac{\alpha\omega\rho\tau_{ij}}{k}\frac{\partial u_i}{\partial X_j} - \beta\rho\omega^2 + \sigma_d\frac{\rho}{\omega}\frac{\partial k}{\partial x_j}\frac{\partial\omega}{\partial X_j} + \frac{\partial}{\partial X_j}\left[\left(\mu + \sigma\frac{\rho k}{\omega}\right)\frac{\partial\omega}{\partial X_j}\right] \quad (16)$$

Where,

β^*, σ^* are the closure coefficients in the turbulent kinetic energy equation.

$\alpha, \beta, \sigma, \sigma_d$ are the closure coefficients in the specific dissipation rate

The turbulent kinetic energy equation (15) has no compressibility term in the pressure work, diffusion, and dilatation in order to remove severe effects in the shock separated flow predictions.

Similarly, the general transport equations for the kinetic energy k, and the specific dissipation rate ω are:

$$\frac{\partial(\rho k)}{\partial t} + \nabla(\rho k\vec{v}) = \nabla[(\mu + \sigma_k\mu_t)\nabla k] + P_k - \rho\beta^* f_{\beta^*}(\omega k - \omega_0 k_0) + S_k \quad (17)$$

$$\frac{\partial(\rho\omega)}{\partial t} + \nabla(\rho\omega\vec{v}) = \nabla[((\mu + \sigma_\omega\mu_t)\nabla\omega] + P_\omega - \rho\beta f_\beta(\omega^2 - \omega_0^2) + S_\omega \quad (18)$$

Menter addressed the sensitivity problem in freestream and inlet condition by recognizing the possibility of transforming Ɛ transport equation from K-Epsilon model to ω transport equation by a variable substitution.

SST K-Omega has additional non conservative cross diffusion term containing the dot product of ∇ k. $\nabla\omega$ which facilitates one to achieve identical outcomes as that of K-Epsilon model. This inclusion allows the benefit of looking into the far field as that of K-Epsilon model and the near field with K-Omega. The shear stress transport (SST) makes the model directly usable through the inner viscous sub layer at low Reynold number without using any extra damping function.

2.6 Domain

In order to conduct a successful CFD simulation for cases like this, a suitable domain must be created. The domain can be explained as a box around the area of buildings. The domain represents the boundaries of what will be the volume that is later meshed and simulated. It is important to obtain a domain large enough to achieve proper fluid flow in consensus with practicality, however, an unnecessary large domain will increase the complexity of the mesh, making the simulations more time consuming. The problems that can occur are due to the boundary conditions not being able to fully represent the real situation. This can include that artificial accelerations appears, or that the flow is not able to re-develop behind the wake region [21].

A vertical extension of the domain is necessary to prevent the flow over buildings getting an artificial acceleration due to the boundary conditions not allowing fluid to leave the domain. There are several recommendations for single buildings, where many are not the same. According to Franke and Baklanov, the vertical extension for multiple building urban areas should be five times the height of the tallest building, from the top of this same building [21]. This means that the total height of the domain should be six times the height of the tallest building.

When deciding the sizes of the lateral extension of the computational domain, the recommendations are based on the blockage ratio, which is the area of the buildings in relation to the area of the domain as seen from the inlet. In CFD the recommended blockage is normally set as 3%, based on the results of Baetke et el. [17, 21]. Franke and Baklanov adds that for urban areas with multiple buildings the lateral boundaries can be placed closer than five times the height of the tallest building to a part of the area that surrounds the area of interest. Another recommendation that is given, which usually correlate with the maximum blockage ratio, is that the lateral boundaries should be placed with a distance minimum five times the height of the tallest building away from the buildings [17].

In the flow direction the distance between the inlet and buildings is recommended to be at least five times the height of the tallest building, according to Blocken [17]. He also states that the distance between the buildings and he outflow should be at least 15 times the height of the tallest building. The distance between the buildings and outflow is longer to allow for a full flow re-development behind the wake region. Franke and Baklanov states that this distance can

be somewhat reduced if the area of interest is surrounded by other buildings, however, this should be tested to make sure it does not cause any problems [21].

2.7 Mesh

Creating a good mesh is a time-consuming process, especially since the trial-and-error method must be used to find the correct settings for each mesh. The goal when meshing is to create a mesh which allows the simulation to be initialized and run to achieve results. If these criteria are not met, the mesh is considered invalid. It is also important to remember that the mesh is closely linked to the physics in the simulation, and that different physics can require different attributes from the mesh.

When performing simulations for wind conditions inside an area, a volume mesh must be used. A volume mesh is a representation of the interior volume of an object, and in this case, it is the volume surrounded by the domain and the buildings. The volume mesh is generated from a previously made surface mesh, hence, it is also important to create a good and clean surface.

2.7.1.1 Meshing in STAR-CCM+

The information regarding the meshing in STAR-CCM+ in the chapters below is gathered from the Simcenter STAR-CCM+ User Manual [18].

Surface mesh

There are three different main tools in STAR-CCM+ for surface meshing; Surface Wrapper, Surface Remesher and Automatic Surface Repair.

Surface Wrapper is a tool that can be used to provide a closed, manifold, non-intersecting surface when starting from poor CAD data. This data is often described with intersecting surfaces, holes, and gaps. It can often be effective to use for cases with complex geometry. The resulting surface from the surface wrapper is often not of a high quality, and it is therefore normal to use together with the surface remesher.

The Surface Remesher is used to retriangulate a surface in to improve the quality and obtain a high-quality surface mesh. The resulting mesh is then often used to create a volume mesh. The Surface Remesher is normally used when the existing surfaces needs to be improved, either surfaces from the Surface Wrapper or directly imported surfaces.

The Automatic Surface Repair is a tool which is used after the Surface Remesher has been made. This tool is used to automatically correct several geometric errors that can occur in the surface. In cases where a surface is both wrapped and remeshed, it can be beneficial to also use the Automatic Surface Repair.

Volume mesh

STAR-CMM+ offers five different types of meshing models which can be used to create a volume mesh. These models are Tetrahedral, Polyhedral, Trimmed, Thin Mesh, and Advancing Layer Mesh. The three first mentioned models are used to create a full core volume mesh and are the ones most commonly used.

The Tetrahedral mesh model uses cells shaped as tetrahedrons to create a core volume mesh. The tetrahedrons are created from the triangulated input surface. In comparison to the other available models, the Tetrahedral mesh is the fastest and it uses the least amount of memory. However, it requires about five to eight times the number of cells to achieve the same accuracy of result.

The Polyhedral mesh creates a core mesh using cells shaped as polyhedrons. This process automatically creates polyhedral cells from the triangulated surface, and then goes on to create the core polyhedral mesh. Compared to the Tetrahedral mesh, it can produce results that are more accurate. However, it should be considered that it is slower and require more memory than the Tetrahedral mesh.

The Trimmed mesher creates a core mesh by using mostly hexahedral shaped cells. Along the surface, these cells are trimmed to fit within the surfaces, which means that these cells will be other shapes. As for the Polyhedral mesher, the Trimmed mesher can produce a more accurate result than the Tetrahedral mesher, but it is more time-consuming considering the number of cells.

Cell sizes

Setting the cell sizes can be the most difficult part of creating a good mesh. You want many cells to be able to achieve an accurate result, while at the same time you want less cells to be able to run the simulations within reasonable time. Finding the correct balance between a fine mesh and smooth simulations is key. In a study from 2015, Blocken states that the grid should be fine enough to capture important physical phenomena like shear layers and vortical structures with a sufficient resolution [17]. There are some more specific guidelines for cell sizes off different parts of the model, these are mentioned below.

Buildings

The buildings are often the most complex part of the geometry and is likely to demand the smallest cell sizes. According to Franke et al. the resolution of the built area should be minimum 10 cells per cube root of the building volume [22]. They also state that the minimum number of cells in street canyons should be 10. In another study from 2015, Blocken recommends that for studies where pedestrian-level wind is a focus area, the 3^{rd} or 4^{th} cell above ground level should be at a height of $1.5 - 2m$ above the ground [17].

Ground

The cell sizes on the ground can vary severely. In street canyons the sizes must be relatively small to meet the recommendations for a minimum of ten cells between buildings. However, further away from the buildings it can be increased as these areas are not of the same interest regarding the results. Increasing the cell sizes in these areas is key to avoid having a mesh too large to simulate. However, it is still important to keep the near surface cell sizes relatively small as this is the area most relevant for the simulation.

3 Methodology

3.1 Creating 3D-model

To be able to perform a CFD simulation it is important to create a good 3D-model of the area that should be used. In this project, two different areas will be used, both with an area of approximately $2x2\ km$ within the city of Oslo. One area will contain the geometry of buildings around the city center of Oslo, and will include such as the City Hall, the opera and Bjørvika. This area mainly consists of a combination of high and medium-rise buildings. This area will be referred to as *Downtown* in this report. The other area is the area of Bygdøy, which is a residential area located on a peninsula in Oslo. This consists mainly of low-rise residential buildings. This area will be referred to as *Bygdøy*. These areas are similar in its location and orientation, but different in its urban geometry, which makes it good for comparisons.

Figure 3-1 shows the workflow of creating the model from the input data to the finished model ready to be used in the CFD-simulation. This process is further described in the paragraphs below.

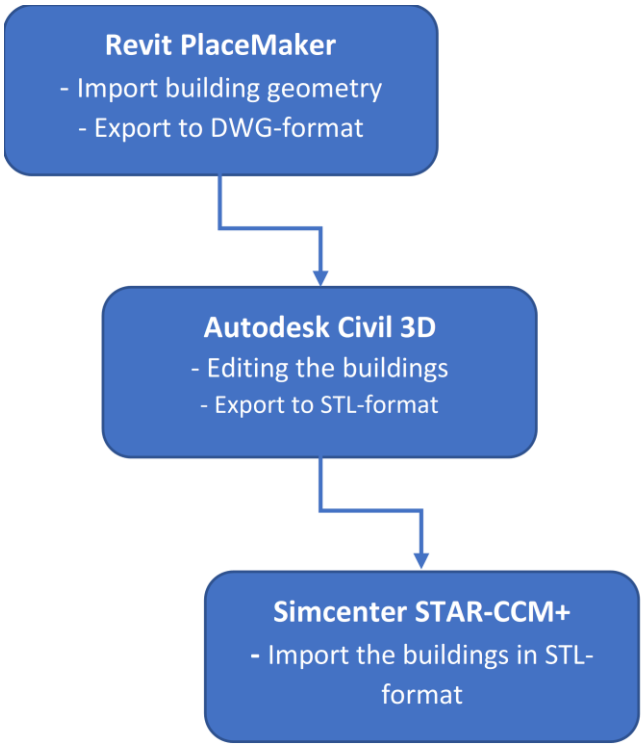

Figure 3-1. Workflow of the process of creating the 3D-models

The software Placemaker is used to create the models. Placemaker is a plugin compatible with Autodesk Revit and SketchUp, and in this project Autodesk Revit has been used. Placemaker

is a software which easily imports real data in the form of 3D or 2D-models, which can contain terrain, buildings, roads, etc. To create the models for this project, the buildings for the respective areas has been imported into Revit. This was done by first selecting the respective area, and then importing the buildings available in this area. The databased used for importing the buildings (OpenStreetMap) contains the outlines for all the buildings, as well as an assigned height for parts of the buildings. The buildings without a height tag are imported with a default height that can be selected by the user. For these buildings, the height is found later in the process by using Google Earth Pro.

It is important that the model is solid and watertight, if not it will cause problems in the CFD software. A watertight model means that the model is an entirely closed volume, that would hold water if it were filled. The buildings retrieved from Placemaker are not always watertight, especially for the buildings with more complex geometry. Therefore, some work with CAD tools is necessary, and in this case Autodesk Civil 3D is used. After exporting a .dwg-file from Revit and opening it in Civil 3D, the file is cleaned up so only the bottom surface of the buildings are remaining. This is done by exploding all buildings to the point where each wall, roof and floors acts as one surface, and then deleting everything above the bottom level. At this point all that is left is the bottom surfaces, but before starting the extrusion it is necessary to look at which surfaces will cause problems and fixing these.

Generally, buildings with overlapping geometries where surfaces are inside other surfaces will be problematic. This could still be possible if they are built correct and those extrusions later are unionized. What seems to cause the most problems are where two surfaces are seemingly connected, but when zooming in it is connected on one end, but not the other. The distance can be lower than a millimeter, so it is required to zoom significantly to see this. This type of error is illustrated in Figure 3-2. These small errors must be fixed in a CAD software (AutoCAD or Civil 3D). First, the surface is exploded, so that it is possible to edit the lines. Then, the line not connected must be moved to be in the exactly correct place, which must be done by use a snapping tool. After the lines are fixed, they should be converted into a surface by using the “Region”-command, and furthered extruded into a solid. If these errors are not fixed, they will cause a problem in STAR-CCM+, saying the model is *not closed and manifold* when doing the boolean subtract. To locate these errors, smaller parts of the geometry has been imported into

STAR-CCM+ to see which part has the errors. By doing this it will narrow down the searching area, and the error can be found using a CAD tool.

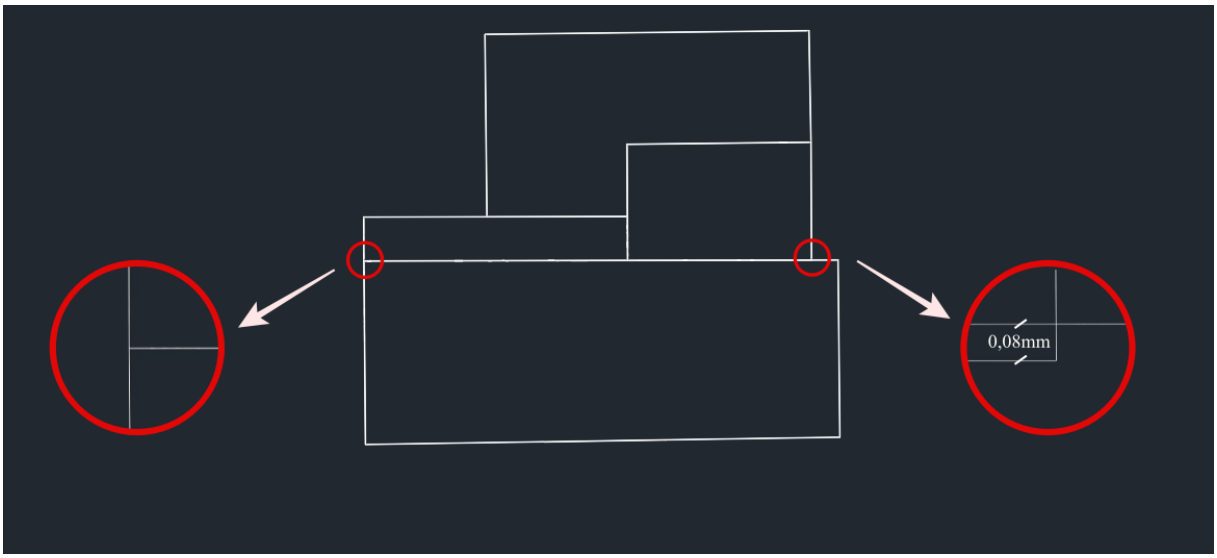

Figure 3-2. Illustration of the problems with the dwg-file imported from Revit Placemaker

When all the bottom surfaces are fixed, it is extruded in Civil 3D by using the extrusion tool. When using the extrusion tool, the result will be a 3D solid, which functions well in the CFD software. The buildings that came with an assigned height from PlaceMaker will be extruded to the same height. For the buildings without, the height is found by using Google Earth Pro. This will not give a perfectly accurate height; however, the degree of error will be insignificant for a simulation like this. After extruding all the surfaces, it remains with only 3D solids which can be exported and used in STAR-CCM+.

There are several file formats which can be both exported from Civil 3D and imported into STAR-CCM+. For this project it was found that stereolithography (STL) functioned better than the others. With other file types, the main problems were either that the file sizes ended up too large or that only parts of the area could be imported to the CFD software. By using STL none of these were problematic.

3.1.1 Downtown

The Downtown-model contains buildings of an area of a bit less then $2x2\ km$. It is chosen to be a bit smaller to make sure the file will not cause any unnecessary problems because of the file size. As mentioned, the model consists of a combination of high and medium-rise buildings. To get a clean and smooth model some of the small buildings and sheds have been removed.

This would not have played a major part in the simulations, and therefore it is seen beneficial to remove to lower the file sizes.

Figure 3-3. Placemaker model of the imported buildings from Downtown

A large part of the buildings in this area came with an assigned height from PlaceMaker. Most of the buildings without a height tag were centered in the same place and were of approximately the same height. The height given during the extrusion for these buildings were obtained by using Google Earth Pro.

3.1.2 Bygdøy

Most of the buildings in the Bygdøy-model are detached buildings of a relative low height compared to the Downtown-model. Some buildings are larger, these are mainly schools and museums. There are also a lot of small sheds which have been removed to make the processes smoother. Removing these will simplify the model and the mesh without significantly influencing the simulations. Also, some outlying buildings have been removed as they would not influence the wind conditions.

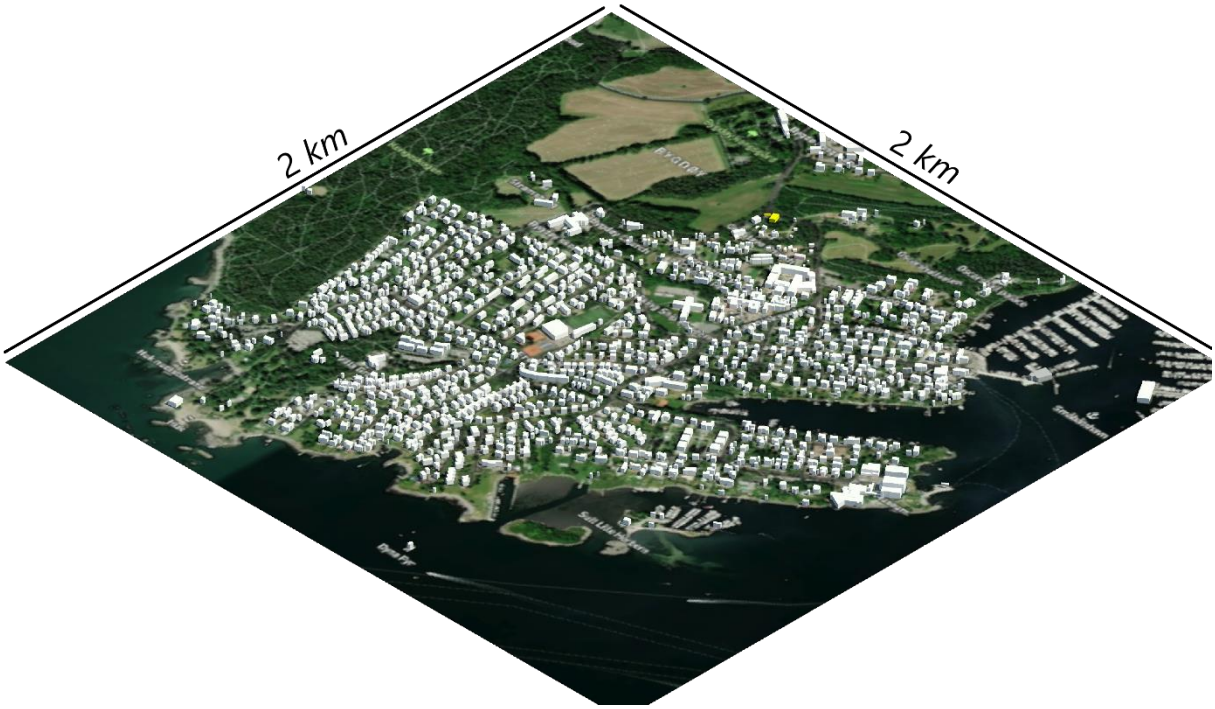

Figure 3-4. Placemaker model of the imported buildings from Downtown

For this area, most of the building came without an assigned height, and therefore when extruding the buildings, the heights had to be found from Google Earth Pro. When doing this it was found that most of the two-story buildings had a height of $8m$, and the one-story buildings had a height of $5m$. In order to create the model in a reasonable time, these heights were used for all one and two-story buildings. The rest of the buildings without an assigned height that were not one or two stories, the height was found from Google Earth Pro.

3.1.3 Other Methods

The process of creating the 3D-model was long, and several methods were considered and tested. The next section will briefly describe what has been considered, as well as the main problems with those methods.

3.1.3.1 Placemaker with terrain

An option that was considered was to include the terrain in the simulations. Placemaker has an import option which easily allows to import the terrain surface of an area, and then place the real buildings on top of this. This terrain surface could be made into a solid in Civil 3D by importing the surface and use the "Extract Solid from Surface"-tool. By working with the buildings in the same way as explained above, a model functioning in STAR-CCM+ should be possible to create.

The problem of doing this is that the terrain data obtained from Placemaker is not as accurate as desirable. The terrain data for Norway and Oslo is obtained from the *Copernicus Land Monitoring Service - EU-DEM database* and comes with a geographic accuracy of $25m$. This lack of accuracy will cause some problems as parts of buildings will be placed below the terrain surface because the terrain is inaccurate. This is not realistic and would not be functioning as wanted in the simulations. As of this reason it was chosen to do the simulations without the terrain.

3.1.3.2 SOSI data

The Norwegian Mapping Authority possesses accurate geodata of the whole of Oslo. This includes buildings (FKB-Bygning) and terrain (FKB-Høydekurve). By using these data, a more accurate model could be made than the PlaceMaker model. However, using these data demands some work. After downloading the files for the given area in SOSI format, the buildings and terrain must be handled separately.

The building data contains the outer lines of the buildings. By using the software Trimble Novapoint, the buildings can be created as surfaces, and then exported into other formats. To be able to use the model in STAR-CCM+, these surfaces must be created into solids. As the buildings are complex with overlapping surfaces and difficult roof geometries, this could be a time-consuming process. Therefore, it was not further evaluated in this project. However, if this could be done in an efficient way, it would be a good option to Placemaker, much because it will include the roof geometries.

The terrain data consists of contour lines. To make this a solid, the software Autodesk Civil 3D can be used, along with the plugin Naviate for Civil 3D which allows the import of SOSI files. The contour lines will be imported as a surface, which then can be created into a solid. This can be done by using the “Extract Solids from Surface”-tool. This operation will leave a solid surface, which can be used in STAR-CCM+.

If the buildings and the surface could both be created as solids, they can be merged to create a realistic 3D-model containing terrain and buildings. It could also be an option to use the terrain from SOSI-files along with the buildings from Placemaker, if using the buildings from the SOSI-files is not possible. Anyway, it should be noted that adding terrain to a CFD simulation will increase the complexity of the mesh, which makes it require better hardware and more time.

3.2 Creating CFD model

When the 3D-model is created with adequate quality, the CFD models can be created. In this project the models are created by the following steps:

- Import geometry
- Model domain
- Subtract buildings from domain to create the simulation volume
- Set up the mesh
- Set up the physics
- Run simulation

3.2.1 Domain

The first step of creating the CFD model is to import the geometry into STAR-CCM+. The 3D-models consists of only the buildings with no ground surface; therefore, a block was created to represent the ground. The top of this block was placed on the same level as the bottom of the buildings and was then merged with the buildings by using the function *Boolean Unite*. The united part that is created is representing the buildings and the terrain. From this point the outer domain can be created.

The outer domain is made by creating a new block. This block is placed with the bottom on the ground, and the other sides relating to how large the domain should be. After the domain is created in the correct size, the function *Boolean Subtract* is used to subtract the buildings and ground from the domain. This leaves the volume that will be used in the simulation. When this is successfully done, the geometry is ready to be meshed.

Domain sizes

In the vertical direction, i.e. the height, the recommendation given by Franke and Baklanov of a distance of five times the height of the tallest building from the domain to the top of the tallest building is followed [21]. This means that the height of the domain should be a minimum of $702m$ and $174m$ for the Downtown and Bygdøy model respectively. The domain height used in the models are $850m$ and $700m$ respectively.

In the lateral direction the recommendation of a distance of five times the height of the tallest building from the built area to the boundaries is used [17]. This gives a distance of $585m$ and $145m$ for the Downtown and Bygdøy model respectively. The distances used in this project is

$800m$ and $500m$. Using these distances, the recommendation of a maximum blockage ratio of 3% based on the results of Baetke is also followed [17, 21].

In the flow direction, based on the study of Blocken, it is recommended to use a distance of minimum five times the height of the tallest building from the inlet to the buildings, and 15 times the height from the outlet to the buildings [17]. This means that for the Downtown model the distance should be minimum $585m$ and $1755m$ for the inlet and outlet respectively. For the Bygdøy model these numbers $145m$ and $435m$. The distances that are used in the project is $800m$ and $2400m$ for Downtown, and $700m$ and $1200m$ for Bygdøy.

The domain sizes in all directions have been increased further beyond the recommendations. This is done to make sure there will be no errors due to an insufficiently small domain. Especially for the Bygdøy model, the sizes have been increased as the tallest building is relatively low compared to the large area. It has been taken into consideration that an increased domain will increase the mesh and computational time, however, it has been seen that it is within a reasonable limit.

Table 2. Domain sizes and recommendations

Domain	Downtown		Bygdøy	
	Size [m]	Recommendation [m]	Size [m]	Recommendation [m]
Lateral	800	585	500	145
Inlet	800	585	700	145
Outlet	2400	1755	1200	435
Vertical	850	702	700	174
Tallest building	117		29	

3.2.2 Mesh

When the simulation volume has been successfully created the meshing can start. Creating an adequate mesh is a time-consuming process, and many tests have been made to find the optimal mesh for this project. The biggest challenge is to find a balance between a high-quality mesh, and a mesh which runs within a reasonable time.

This chapter will describe the creation of the surface mesh and the volume mesh. For both models, the same meshing tools have been used, with the differences being mostly the sizes.

3.2.2.1 Surface Mesh

To create the surface mesh, the models Surface Wrapper and Surface Remesher have been used. The Surface Wrapper is used to create a closed, manifold, and non-intersecting surface. Since the model is quite large and complex, and perhaps contains some errors, the Surface Wrapper was seen as necessary. The use of the Surface Wrapper was significant in this project. When it was not used, the resulting surface mesh ended up with edges that were rounded in comparison to the original geometry. When the Surface Wrapper was added, this problem was non-occurring, and the surface mesh had the correct sharp edges. It was also seen that the Wrapper Scale Factor had a big influence on a problem where nearby geometries melted together. As the Wrapper Scale Factor decreased, the number of these errors decreased. It is still important to notice that a low Wrapper Scale Factor contributes to a longer CPU time.

The Surface Remesher was chosen to use together with the Surface Wrapper. The Surface Remesher improves the quality of the surface mesh by retriangulating it, and it is used to prepare the surface for the volume mesh. The cell sizes of the retriangulated surface are closely linked to the cell sizes of the volume mesh, therefore it is important to get the correct cell sizes also in the surface mesh. Also, when extracting results from the surfaces it is the surface mesh cells that are used.

Different cell sizes have been used for different parts of the model. This is done by using custom minimum and target sizes for the respective boundary under the *Regions* tab. On the buildings, the recommendation given by Blocken that the 3_{rd} or 4_{th} cell above the ground level should be $1.5 - 2m$ above the ground is followed as closely as possible [17]. However, for some cases the recommendation has not been possible to fulfil, especially in the Bygdøy model. In this model the number of buildings is higher, and the size of the buildings are smaller. The number of cells required to fulfil this recommendation would be too high, making the computing time

unreasonably long. In these cases, the cell sizes have been made as small as possible to close in on the recommendation. For the Downtown model, the minimum and target cell sizes for the buildings is set to $0.5m$ and $1.5m$ respectively. For the Bygdøy model these numbers are $0.5m$ and $0.75m$.

To get a high-quality result in the street canyons it is important that there are enough cells on the ground in these areas. The recommendation given by Franke et.al. that the minimum number of cell sizes in the street canyons is ten is followed as closely as possible [22]. There still might be cases where it is not fulfilled in order to keep the mesh within a reasonable size. In the outlying areas and areas not of interest, the cell sizes for the ground are increased. It is still kept relatively low in order to get a higher density volume mesh near the surface. To obtain these features, the minimum and target sizes have been set to $0.5m$ and $5m$ for the Downtown model, and $1m$ and $5m$ for the Bygdøy model.

All the parameters specified in the surface mesh is shown in the table below. For parameters that are not shown in the table, the standard value of the software has been used.

Table 3. Surface mesh parameters

Surface Mesh		Downtown		Bygdøy	
Base Size		$5m$		$5m$	
		Minimum	Target	Minimum	Target
Relative Sizes	General	10 %	1400 %	10 %	1200 %
	Buildings	10 %	30 %	10 %	15 %
	Ground	10 %	100 %	20 %	100 %
	Inlet	25 %	1200 %	10 %	1000 %
	Boundaries	50 %	1400 %	100 %	1200 %
Surface Growth Rate		1.1		1.1	
Wrapper Scale Factor		30 %		25 %	

3.2.2.2 Volume Mesh

The volume meshes has been created based on the existing surface meshes. To create the core volume mesh, the polyhedral mesher has been used. This was chosen as it is known to produce an accurate result. It is slower and requires more memory than the tetrahedral mesher, and for such large models it requires powerful hardware. Since such hardware was available to use in the project, the polyhedral model was considered the preferable method.

To capture good results in the area around the buildings, two volumetric controls have been placed in each model. These are used to create a denser mesh in the chosen areas, which are

around the buildings. For the Downtown model, the innermost volumetric control has cell sizes of $5m$, while the outermost has cell sizes of $10m$. For the Bygdøy model, these numbers are $5m$ and $7.5m$.

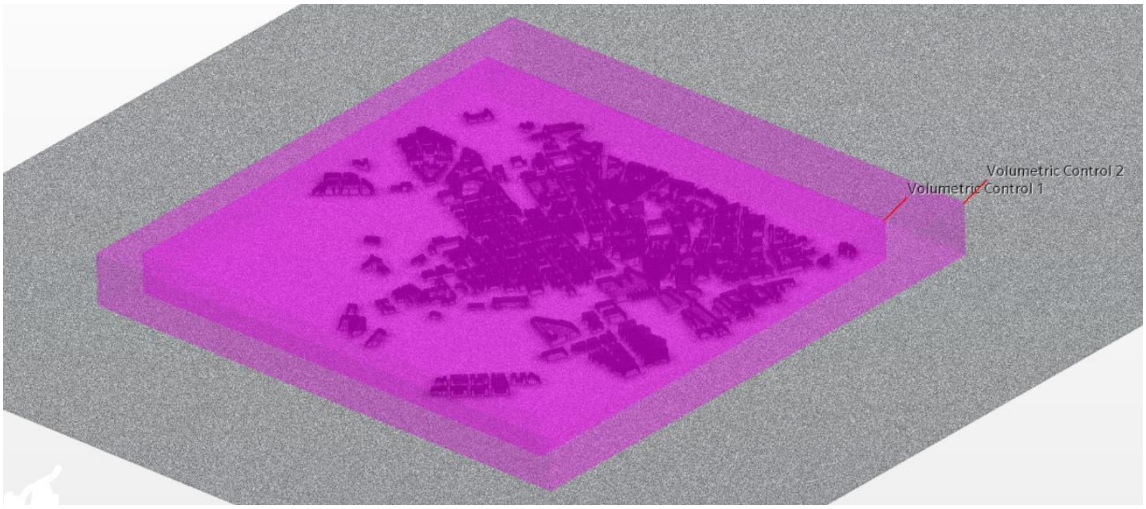

Figure 3-5. Representation of the two volumetric controls for the Downtown-model

The attributes and sizes of the volume mesh is mostly determined by the existing surface mesh. In this case, the parameter that was specified for the volume mesh was the polyhedral density and growth factor. For both models the density is set to 0.7 and the growth factor to 1.3.

Another detail that is added to the mesh is prism layers, which are prismatic cells near surfaces and boundaries. These are added to increase the number of cells near the ground, to make sure the near ground behavior is adequately captured. For both models 1 prism layer is added with a thickness of $1m$.

All the parameters specified in the volume mesh is shown in the table below. For parameters that are not shown in the table, the standard value of the software has been used.

Table 4. Volume mesh parameters

Volume Mesh	Downtown		Bygdøy	
Polyhedral Density	0.7		0.7	
Polyhedral Growth Rate	1.3		1.3	
Number of Prism Layers	1		1	
Prism Layer Stretching	1.5		1.5	
Prism Layer Thickness	$1m$		$1m$	
Volumetric Control 1	Cell Sizes	$5m$	Cell Sizes	$5m$
Volumetric Control 2		$10m$		$7.5m$

3.2.3 Physics

Primary variable of the simulation and the mathematical formulation that is used to generate the solution is defined under physics model. STAR-CCM+ is a multi-physics platform that allows user to model the fluid flow based on the scope of the study.

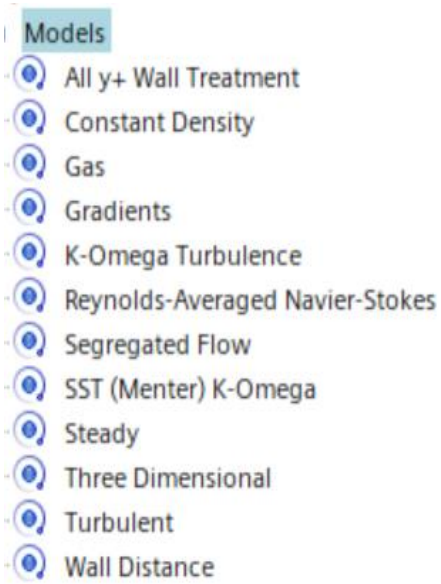

Figure 3-6. Physics used in the model

The physics model for this study involves the use of K-Omega model with constant density and segregated flow. SST (Menter) K-Omega inclusion in the study makes the model to have the advantage of both K-Omega and K-Epsilon model. Study involves the use of all y^+ wall treatment. The figure above shows the models which has been used in this project.

3.2.4 Extracting results

When the simulation is completed using the abovementioned parameters, the final results can be extracted from STAR-CCM+. As this project focuses on pressure coefficient and wind velocity, these are the results that will be gathered.

In both the Downtown- and Bygdøy-model six different areas will be created when extracting the results. This is done to also be able to investigate how the wind conditions varies within each model, not only between each model. The areas are selected with the goal to represent as different features as possible. The division of the areas can be seen in Figure 4-8 and Figure 4-43.

3.2.4.1 Pressure coefficients

To export the pressure coefficient values from STAR-CCM+, a *XYZ Internal Table* is created, adding the pressure coefficient for the relevant boundaries. This is done both by adding all the building boundaries, and by adding the building boundaries for each area. These tables are exported to csv-files and opened in Excel where the data is processed and created into histograms and other diagrams. It should be noted that the exported files could contain more data than can be exported directly to Excel, therefore it should be opened in Notepad and from there copied in smaller parts into Excel.

In addition to the histograms, the pressure coefficient will also be extracted as figures showing the variation of the values over the buildings. This is done by creating a scalar scene, adding the building boundaries as parts, and adding the pressure coefficient function. This gives a visual representation of the pressure coefficient values on the building facades.

3.2.4.2 *Wind velocity*

When it comes to the wind velocity, the magnitude of the velocity in the street canyons it what will be focused on. These results will be captured by creating *resampled volumes* in the respective areas. These resampled volumes are then added to scalar scenes, and are given the correct scalar field, and will then show as a representation of the wind velocity in the street canyons of the chosen area.

For both models seven different resampled volumes will be created. One for each of the six areas, and one which includes all the buildings and street canyons. To be able to connect the results to the pedestrian wind comfort, the volumes will have a height of $2.5m$. This means that the wind velocity from the ground and up to $2.5m$ will be captured. In addition to this, results

from the height of $17m$ will also be captured for the Downtown-model. This is done to see the differences from the street level to the higher parts of the building. This was chosen not to do for the Bygdøy-model, as the relatively small size of the buildings would cause the difference to be small.

4 Results

This chapter will show the obtained results from the simulations. First, the results from the Downtown-model will be given, then the results from the Bygdøy-model.

4.1 Downtown

4.1.1 Simulation

4.1.1.1 Domain

The figure below shows the computational domain which was used in the simulation. The dimensions of the domain are according to what was described in 0 and 3.2.1. As mentioned, the distances have been somewhat increased over the recommendations to make sure it would not cause any problems.

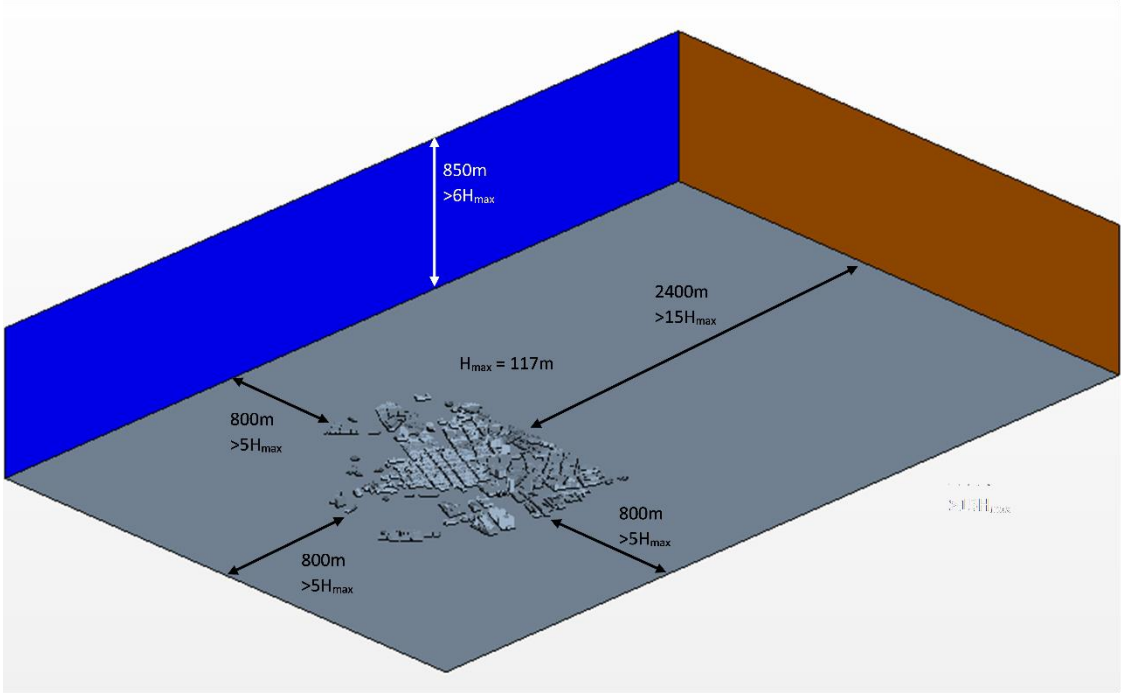

Figure 4-1. Domain with dimensions and recommendations

4.1.1.2 Mesh

The resulting mesh that was further used to do the simulations is shown in the figures below. The remeshed surface ended up with a total of 4 417 456 faces. From this, the volume mesh was created, which in total contains 11 558 746 cells.

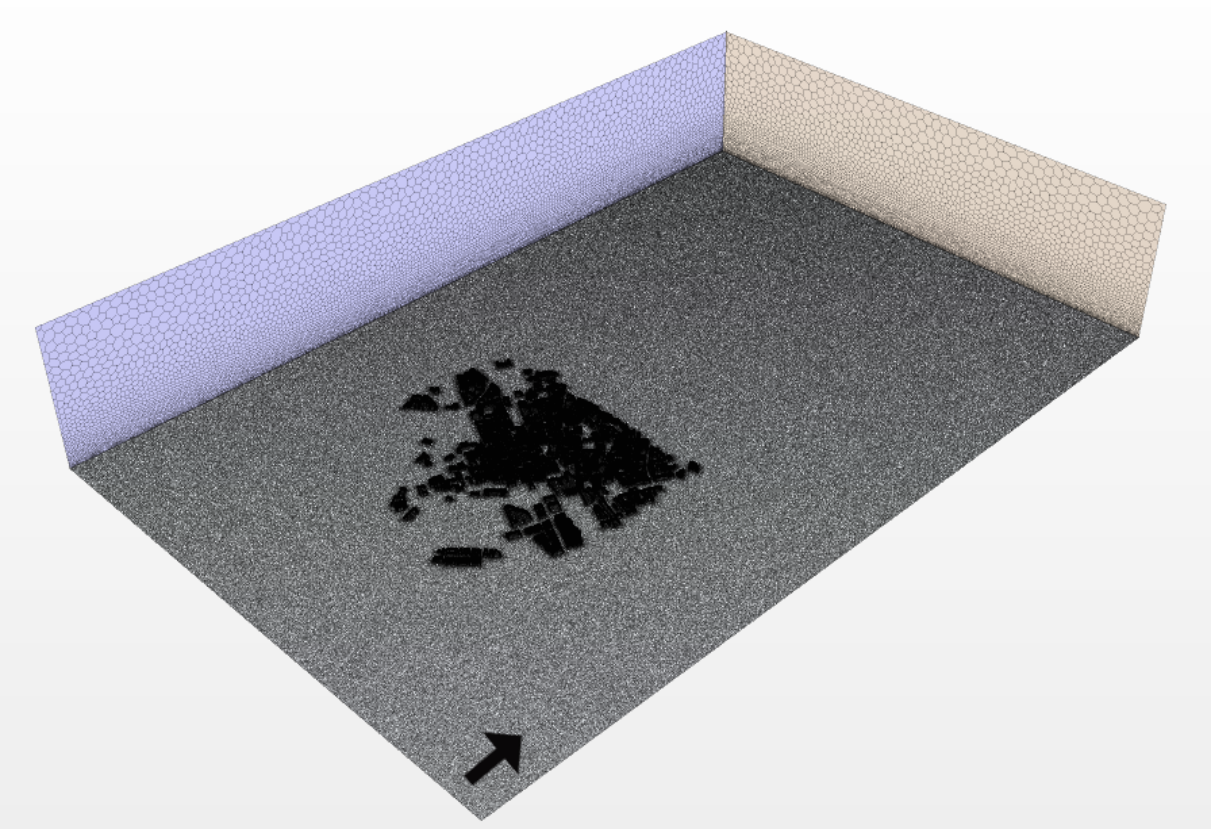

Figure 4-2. Overview of the surfaces in the volume mesh for the whole computational domain. Arrow shows wind direction from south to north

The figure below shows a cross-section of the volume mesh. It can be seen that the mesh gradually increases from the bottom to the top. This was the aim, as the areas of interests are located near the ground surface. What can also be seen in the figure is the two volumetric controls around the buildings.

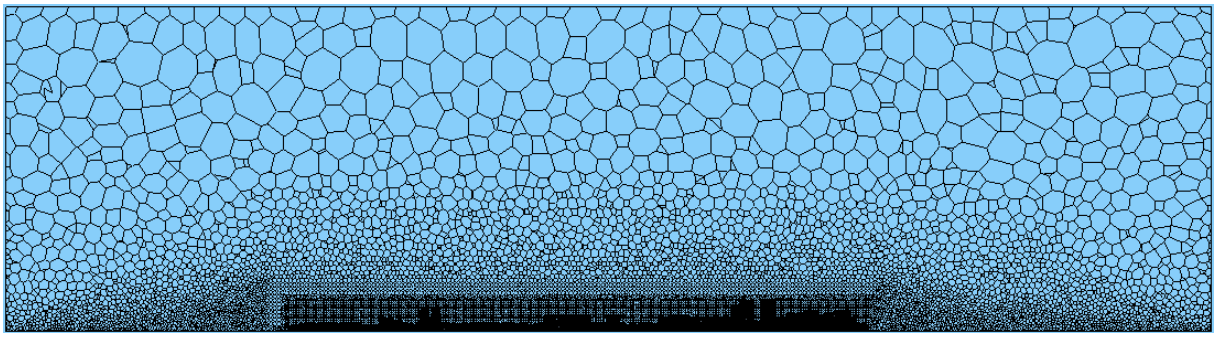

Figure 4-3. Cross-section of the volume mesh

The figure below shows a close-in on buildings and street canyons, and the number of cells on the surfaces cann be seen. The polyhedrons in the surfaces of the volume mesh (right) is created from the remeshed surface (left). The average height of the buildings in the figure is $23m$.

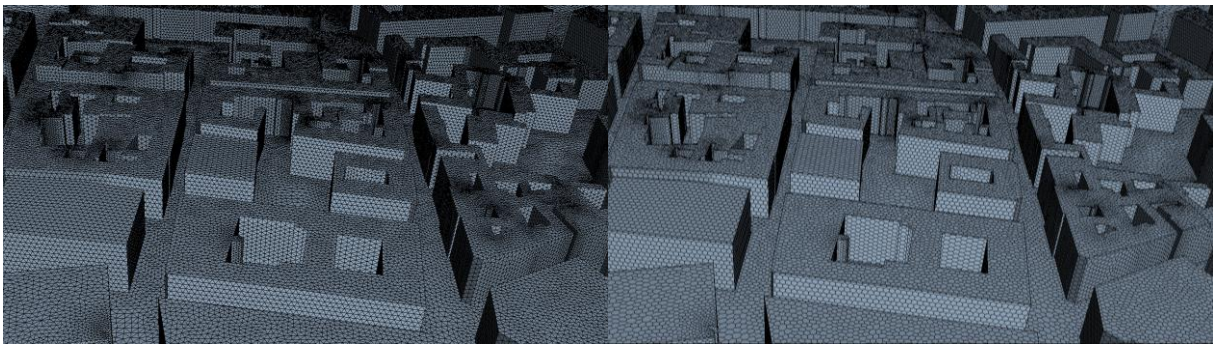

Figure 4-4. Close-in on buildings and street canyons. Left shows the remeshed surface, right shows the surfaces of the volume mesh

4.1.1.3 Residuals

The residual monitor plot shown in the figure below shows that the solution has successfully converged. In total, the simulation was run for 1030 iterations.

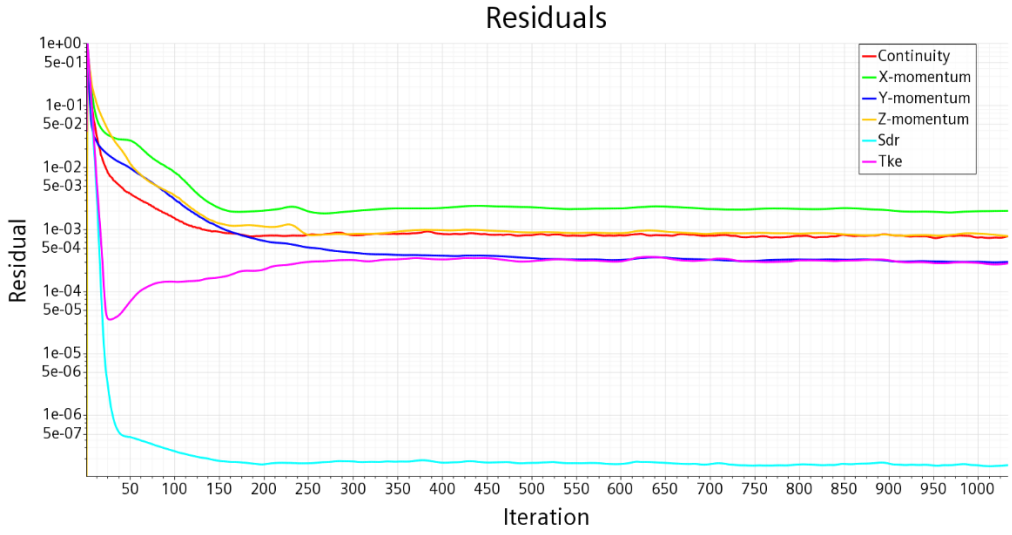

Figure 4-5. The residuals shown over the number of iterations

4.1.2 Pressure coefficient

The figure below shows the pressure coefficient on the building facades for all buildings in the model. The highest occurring pressure coefficient value in the area is 0.80, while the lowest is -2.21. From the figure it can be seen that the positive values mainly occur on the facades facing the inlet, while the negative values mainly occur on all other facades, both facades facing the outlet, the sides, and the roofs.

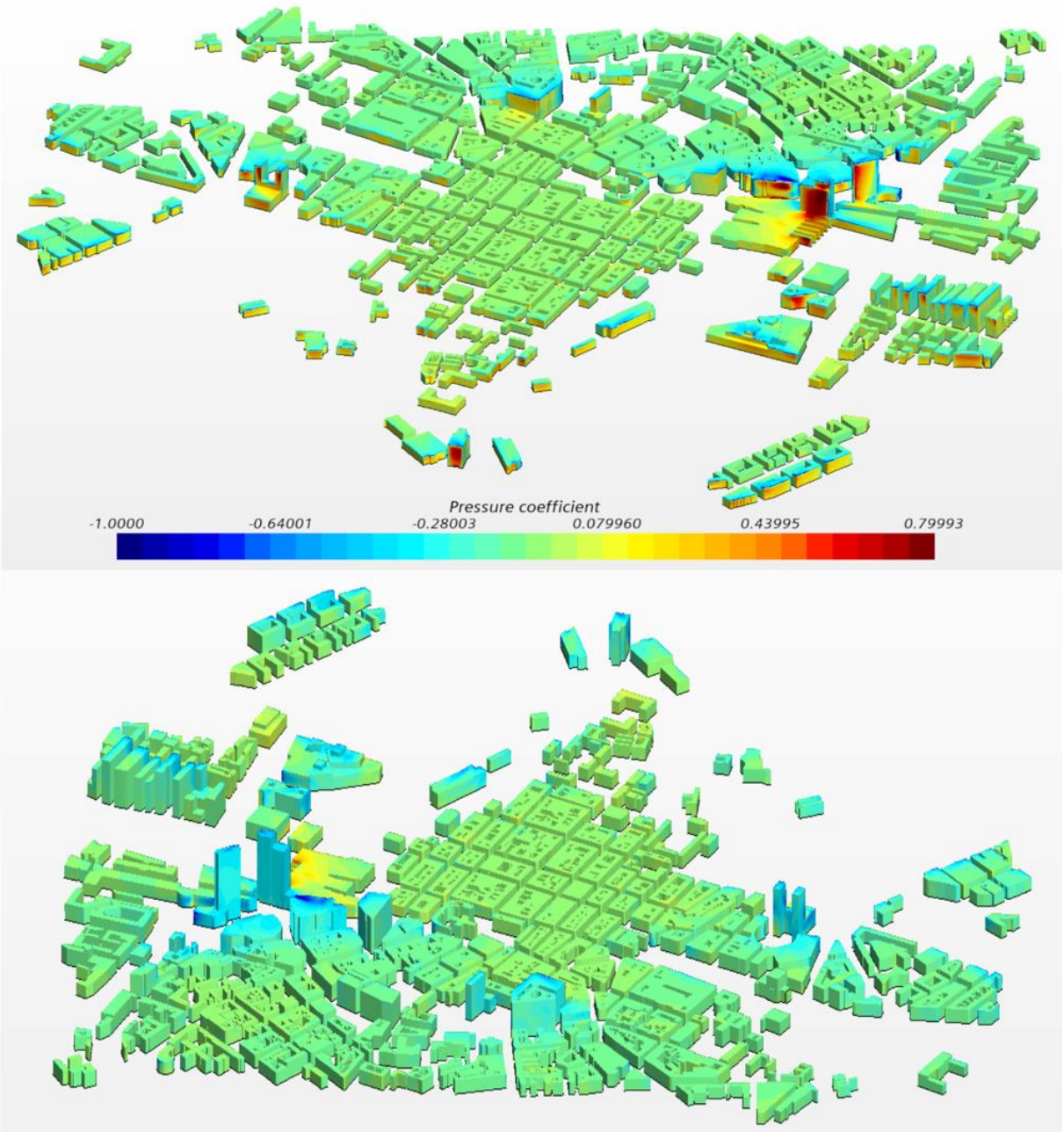

Figure 4-6. Pressure coefficient on building facades shown from inlet (top) and outlet (bottom)

What can also be seen from Figure 4-6 is that the highest values occur on and around the highest buildings, and buildings most exposed to direct wind.

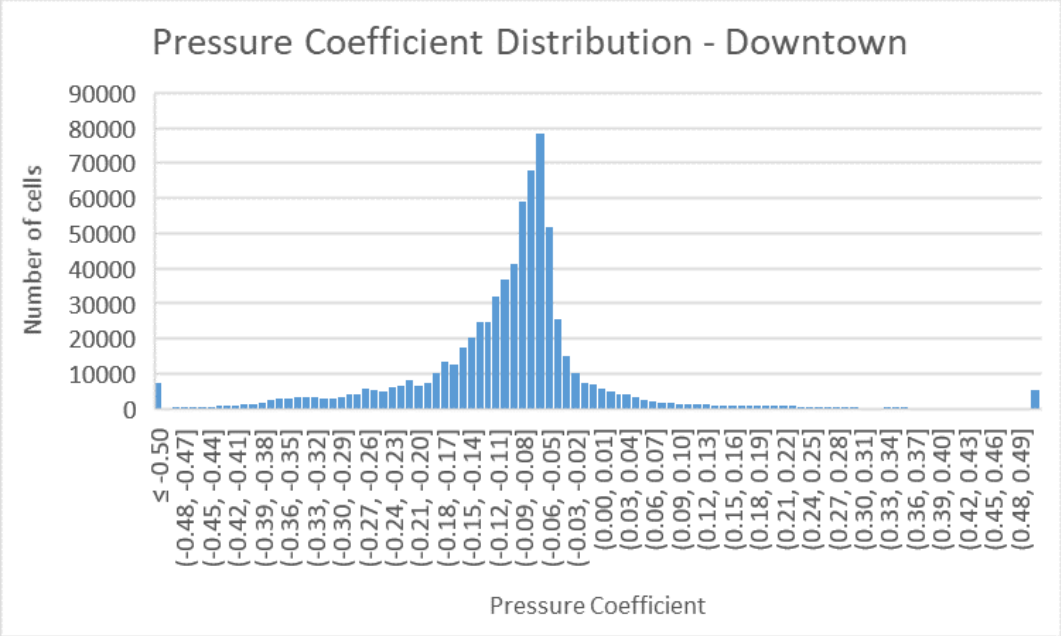

Figure 4-7. Pressure coefficient distribution of all buildings in the Downtown-model

Figure 4-7 shows the distribution of C_p values within the whole model. It shows that the main part of the values range between -0.30 and 0.03. This also indicates that the main part of the values is negative, which is seen from the distribution. The average of all the values is -0.11.

4.1.2.1 Pressure coefficient by area

To capture results and differences within the Downtown-model, the areas have been chosen as shown in the figure below. The areas are spread as much as possible, and contains different sized buildings, in order to see many different situations.

Figure 4-8. The six areas of the Downtown-model. Wind direction is from the bottom to the top

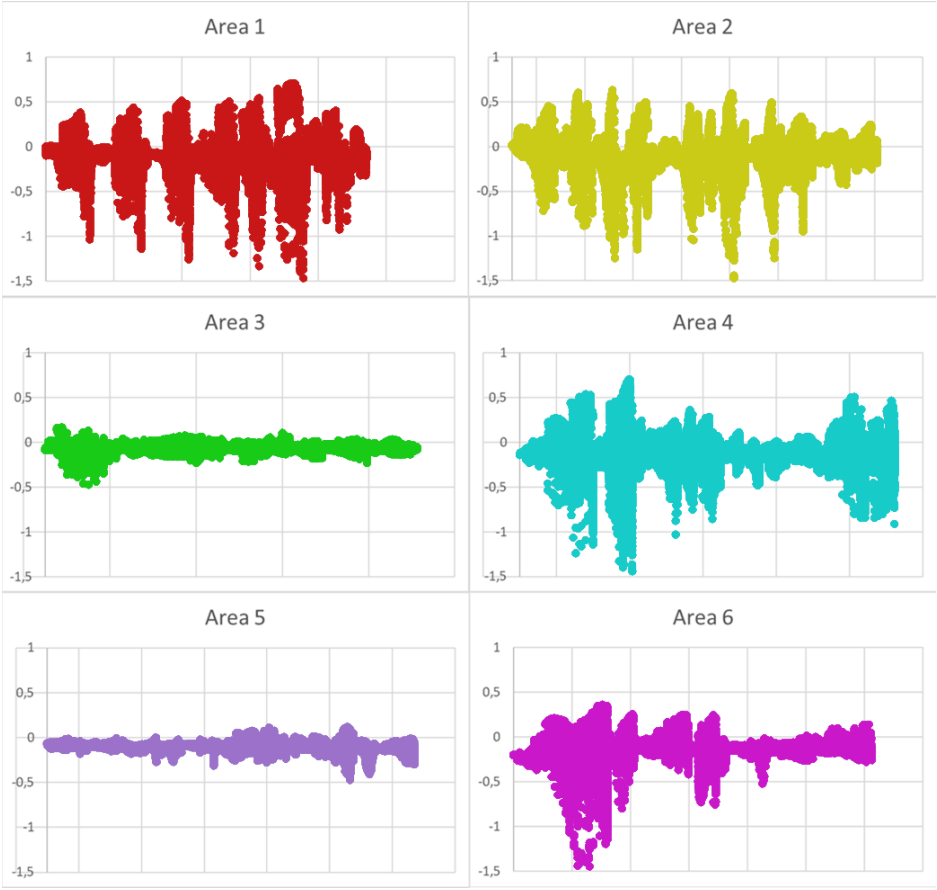

Figure 4-9. Comparison of the pressure coefficient for each area. The Y-axis shows the C_p values, and it shows an overview of the values for all cells (X-axis)

Figure 4-9 shows a comparison of the C_p values for all the areas. It can be seen that Area 1 and 2 contains consistently high values. Area 4 and 6 has parts with high values and parts with low values. In Area 3 and 5 all values are relatively small. Further description of the different areas is done below.

Area 1

This area is located closest to the inlet. It consists of mostly average height buildings, with a few buildings that are taller. The area is really exposed to the wind as it has no buildings in front to protect it.

Figure 4-10 shows the distribution of pressure coefficients within the area. Compared to the other areas, the distribution is more spread out, meaning that higher values occur more often in this area than others. The amount of positive value C_p compared to negative value C_p is also higher than in the other areas. This is due to the fact that most facades facing the inlet is directly exposed, and it is these facades that obtain positive C_p.

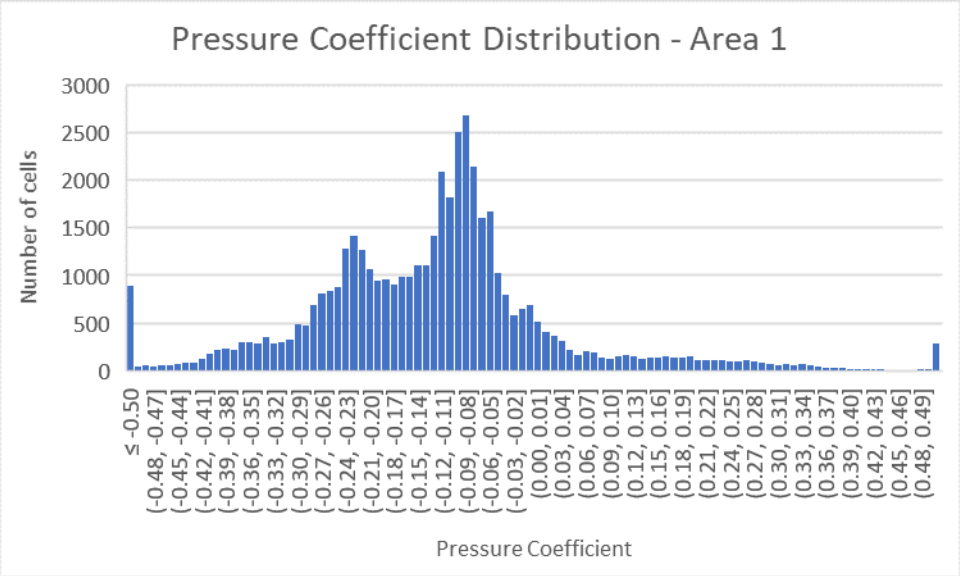

Figure 4-10. Pressure coefficient distribution of Area 1 in Downtown

Area 2

This area is also relatively exposed to the inlet, however, with a bit more shielding than area 1. Area 2 consists of more high-rise buildings, which mainly are buildings from the "Barcode Project". Between these high-rise buildings and the inlet is a bunch of more average sized buildings, which does a bit of shielding. Area 2 has quite similar results to area 1 with a relatively spread-out distribution, however, there are some small differences. It can be seen that the amount of positive C_p values is higher than for Area 1, even though Area 2 is more protected for the wind. The reason for this could be the taller buildings in Area 2 which gives a larger surface area towards the inlet.

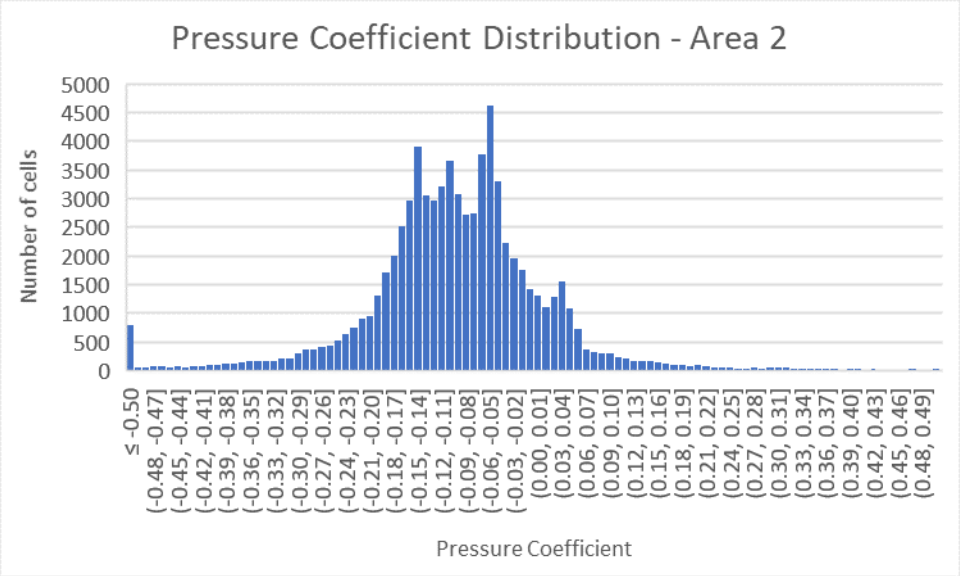

Figure 4-11. Pressure coefficient distribution of Area 2 in Downtown

Area 3

Area 3 is located in the middle of the model and consists only of average height buildings. It is surrounded on all sides by buildings with the same heights, and the buildings mass is dense. As seen from Figure 4-9 and Figure 4-12 the pressure coefficients in this area are consistently low. It is also seen that there are almost no positive C_p values in this area. This is due to the area being surrounded by other buildings of the same height, which makes close to no wind hitting the facades directly.

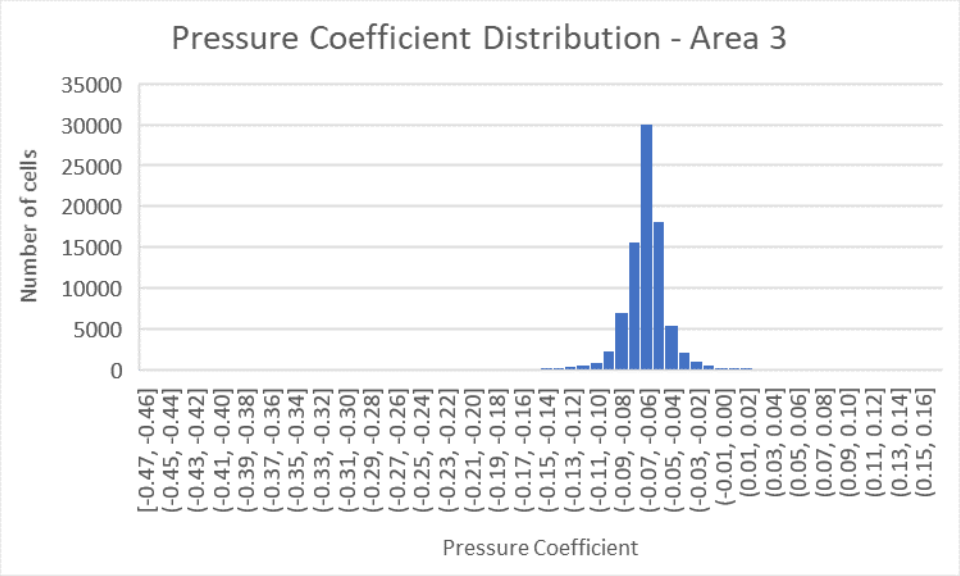

Figure 4-12. Pressure coefficient distribution of Area 3 in Downtown

Area 4

Area 4 is one of the most exposed areas, however, it is a bit more shielded than Area 2. This area consists of average sized buildings and one taller building, the Oslo City Hall. From Figure 4-9 it is seen that the area contains some higher C_p values, but it does not tell the frequency of these values. The pressure coefficient distribution in Figure 4-13 shows that these values occur rarely. This tells us that it is only the tall buildings and the close by facades that receives higher C_p values, while the other buildings have relatively low values.

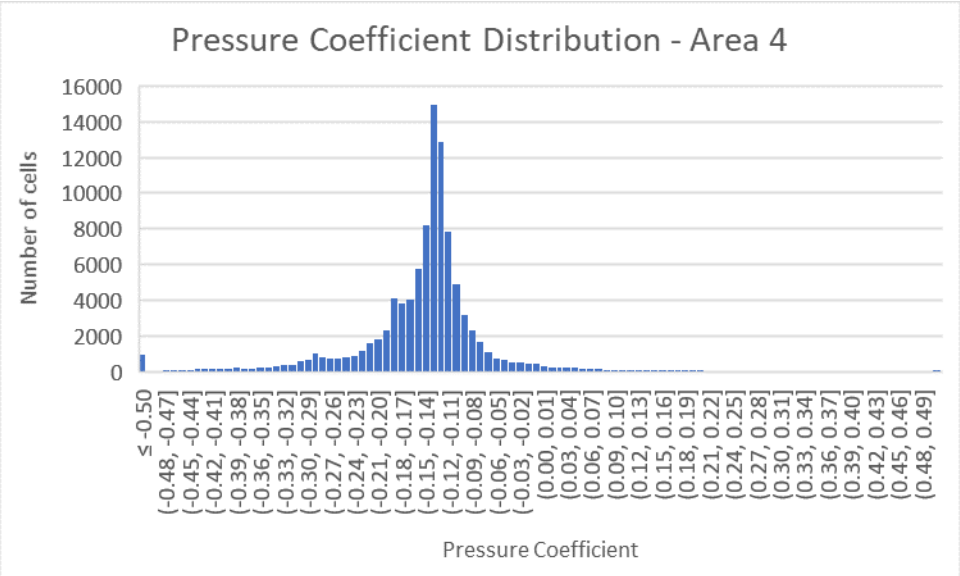

Figure 4-13. Pressure coefficient distribution of Area 4 in Downtown

Area 5

This area is located in the back of the domain and is well shielded by surrounding buildings of the same heights. The buildings in this area are all average sized. The results of this area can be compared to Area 3, which is to be expected. However, it can be noticed that the C_p values are a bit higher for this area. In Area 3 the buildings are placed and shaped as rectangles, whereas for Area 5 the buildings have more complex shapes and placement, this could be a factor of the slightly increased C_p values.

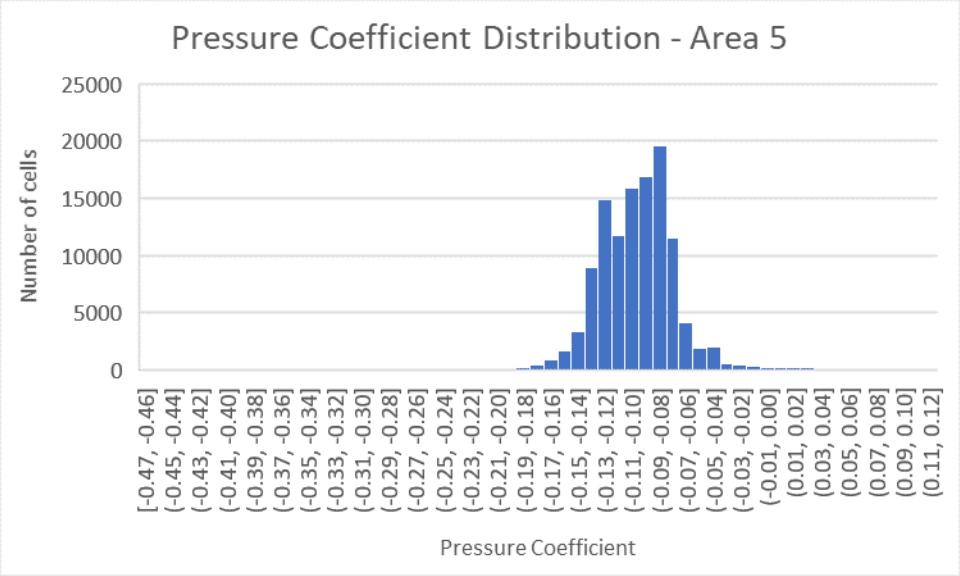

Figure 4-14. Pressure coefficient distribution of Area 5 in Downtown

Area 6

Area 6 is placed in the back of the domain and has a similar geometry to Area 5. However, it contains one building which is significantly larger than the others in the area. It is seen from Figure 4-9 and Figure 4-15 that it influences the pressure coefficients. In Area 6 the values are higher than in Area 5, and the distribution of values is more spread out.

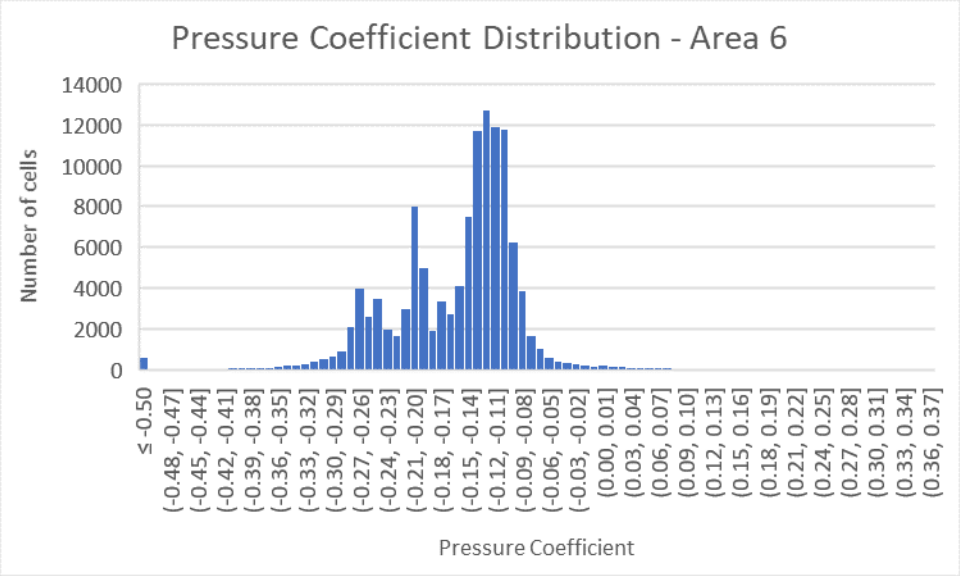

Figure 4-15. Pressure coefficient distribution of Area 6 in Downtown

4.1.3 Wind velocity

When analyzing the results for the wind velocity in the street canyons in the Downtown-model, two different heights are used. These heights are from the ground up to $2.5m$ and $17m$.

Figure 4-16 shows an overview of the wind velocity in the whole domain at the height of $2.5m$. Generally, the wind velocity is decreasing as it moves through the domain as the buildings are shielding. However, it is also seen that the wind velocity is significantly increasing in some areas, which can be seen by the green and red colors. The tendency is that in more open areas, even though they are placed further in the back of the domain, the wind velocity is increasing. It is also seen that around the taller buildings the highest values occur. The highest occurring wind velocity at this height is $15.0m/s$ and is located next to the two tallest buildings in the model.

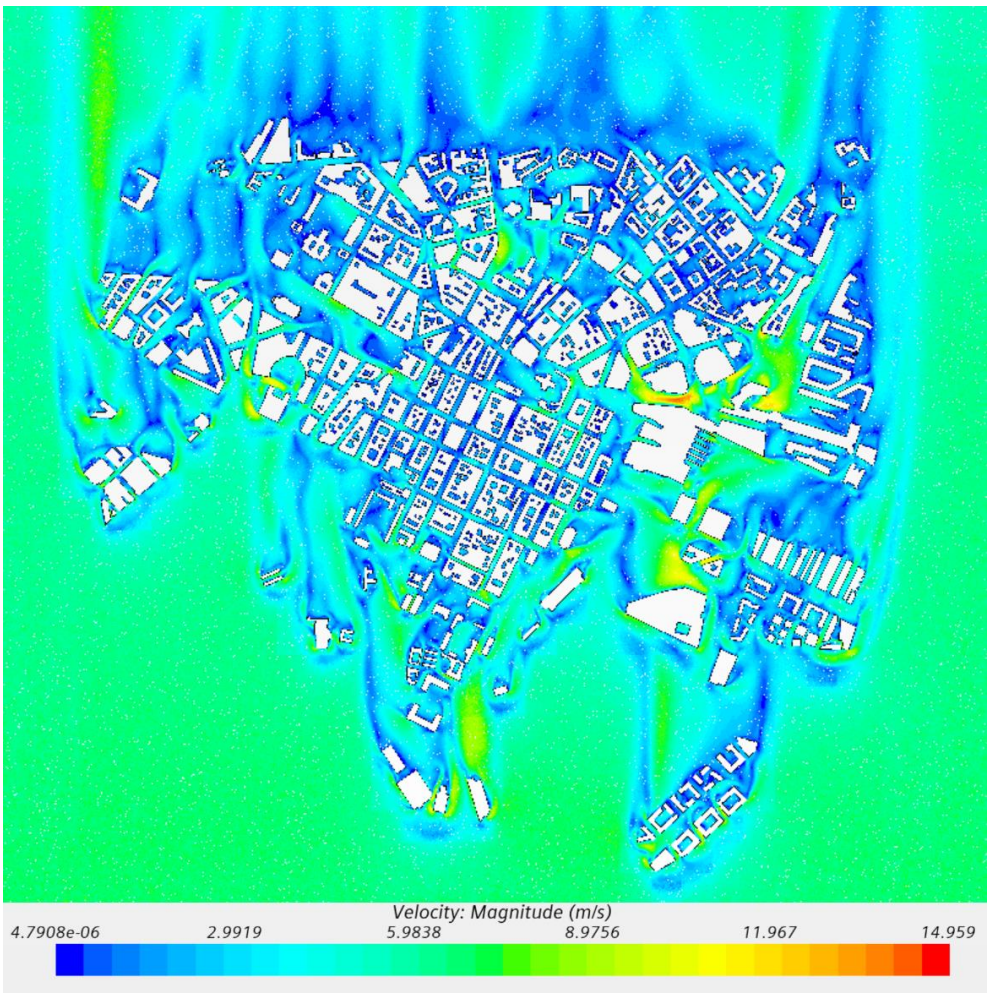

Figure 4-16. Wind velocity for the whole Downtown-model, up to a height of 2.5m

Figure 4-17 shows the wind velocity for the whole area up to $17m$. It can be seen that the incoming wind velocity at this height is higher than at the pedestrian level, without it increasing as much in the street canyons. The increase is still happening in the same areas, but not to the same degree. At this height, the maximum wind velocity is measured to $16.4m/s$.

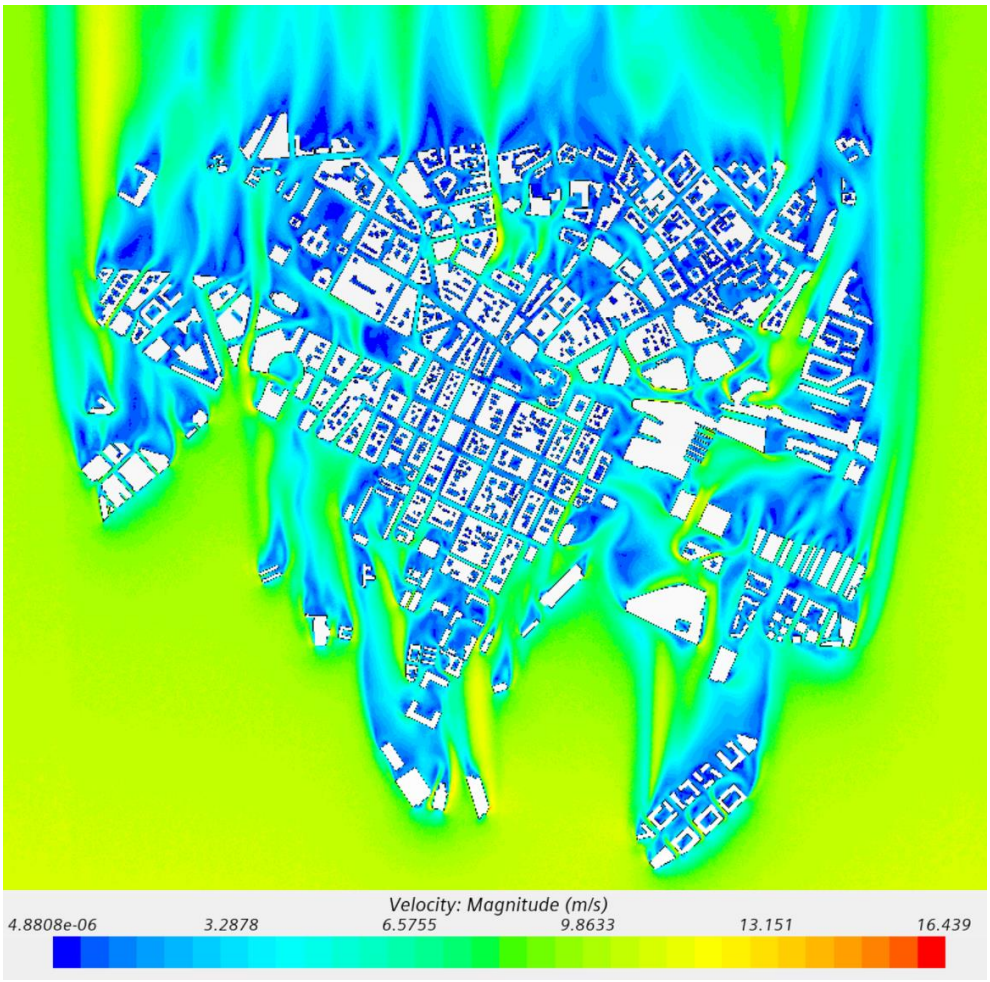

Figure 4-17. Wind velocity for the whole Downtown-model, up to a height of 17m

4.1.3.1 Wind velocity by area

Area 1

Figure 4-18 shows the wind velocity up to $2.5m$ for Area 1. It shows that the wind velocity increases in some street canyons. The highest values occur on the corners going around the buildings, and on the side of the buildings, seen from the inlet. The areas straight behind the buildings has a significantly decreased wind velocity. The maximum wind velocity is $14.0m/s$ and it occurs on the front corner of the building on the left side, where the red color slightly can be seen.

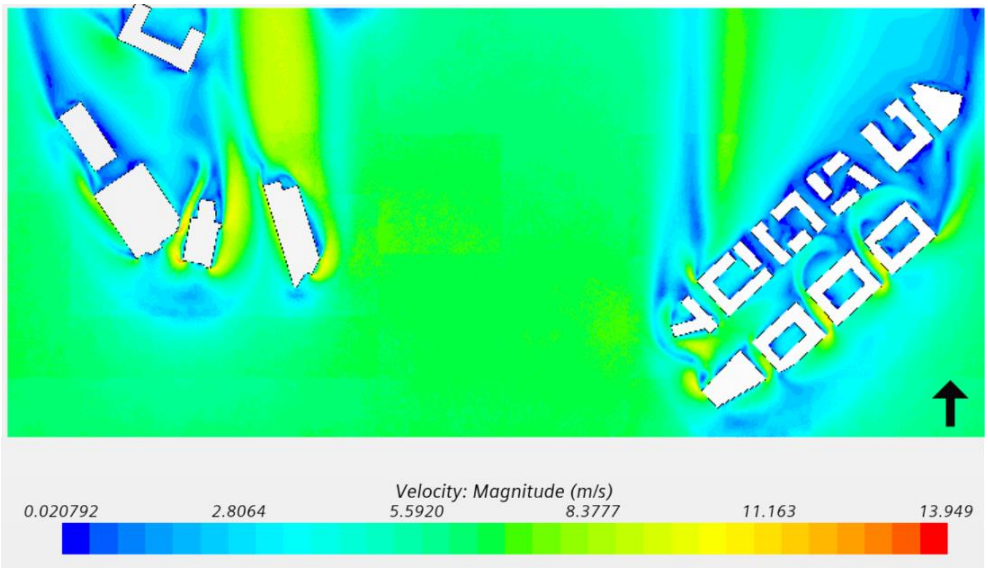

Figure 4-18. Wind velocity for Area 1, up to 2.5m

Figure 4-19 shows the wind velocity for the same area, and a height up to $17m$. In general, the increase of wind velocity in street canyons and around buildings has almost disappeared. However, there are some very small areas on the corner of buildings with a high wind velocity. The maximum wind velocity in this area is $16.2m/s$.

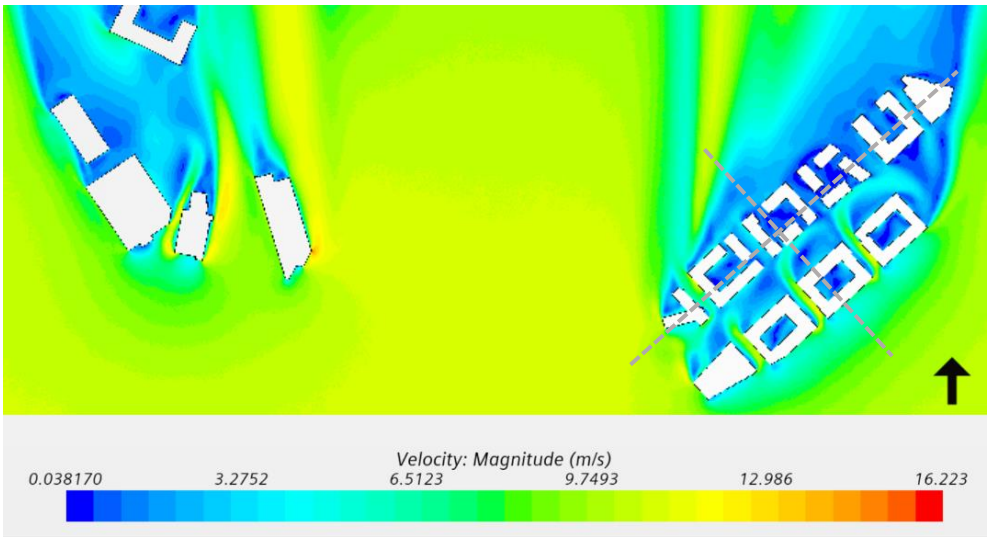

Figure 4-19. Wind velocity for Area 1, up to 17m. The dotted lines show the placement of planes for the vorticity result

Figure 4-20 depicts velocity field revealing wind vortices in a plane section passing through buildings in the wind direction and normal to the wind direction. In both direction, wind vortices seem to be more prominent and matured for better aspect ratio. Buildings normal to the wind direction seems to be of same height with varying width between them so, vortices seem to be in developing stage and less prominent.

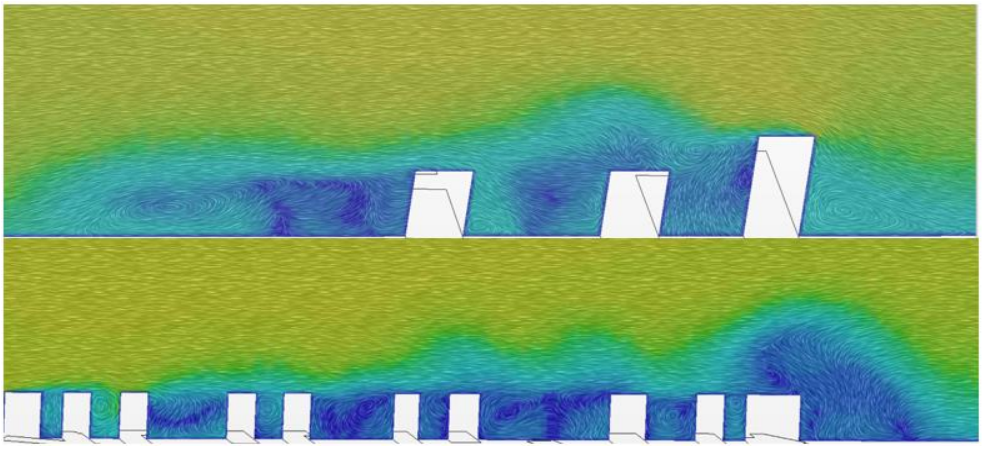

Figure 4-20. Velocity field revealing vorticity structures, wind direction (top) and normal to wind direction (bottom), Area 1

Area 2

Figure 4-21 shows the wind velocity in area up to the height of $2.5m$. In this area, significant increases in the wind velocity can be seen. These increases are also over larger areas when comparing to Area 1. These areas are mainly occurring around the largest building. It can also be seen that around the tallest buildings, which is located in the top-right part of the figure, there are no significant increase in wind velocity. This could be to the buildings lying in front, even though they are lower. Lastly, it is seen that in the bottom-right there is an increase in wind velocity in front of the building. The maximum wind velocity in this area is $12.7m/s$.

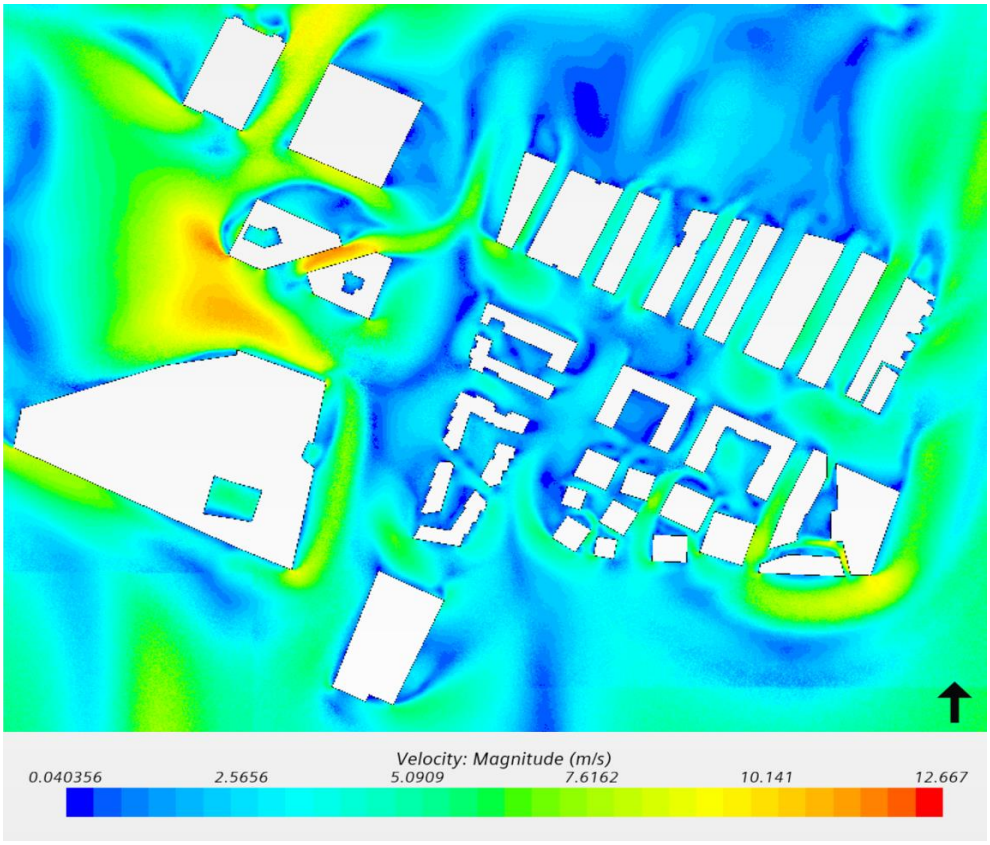

Figure 4-21. Wind velocity for Area 2, up to 2.5m

Figure 4-22 shows that Area 2 has quite similar attributes for wind velocity both at $2.5m$ and $17m$ height. The main difference is that the areas with increased wind velocity are smaller at $17m$. The maximum wind velocity has increased to $13.6m/s$, which is a small increase compared to the other Area 1.

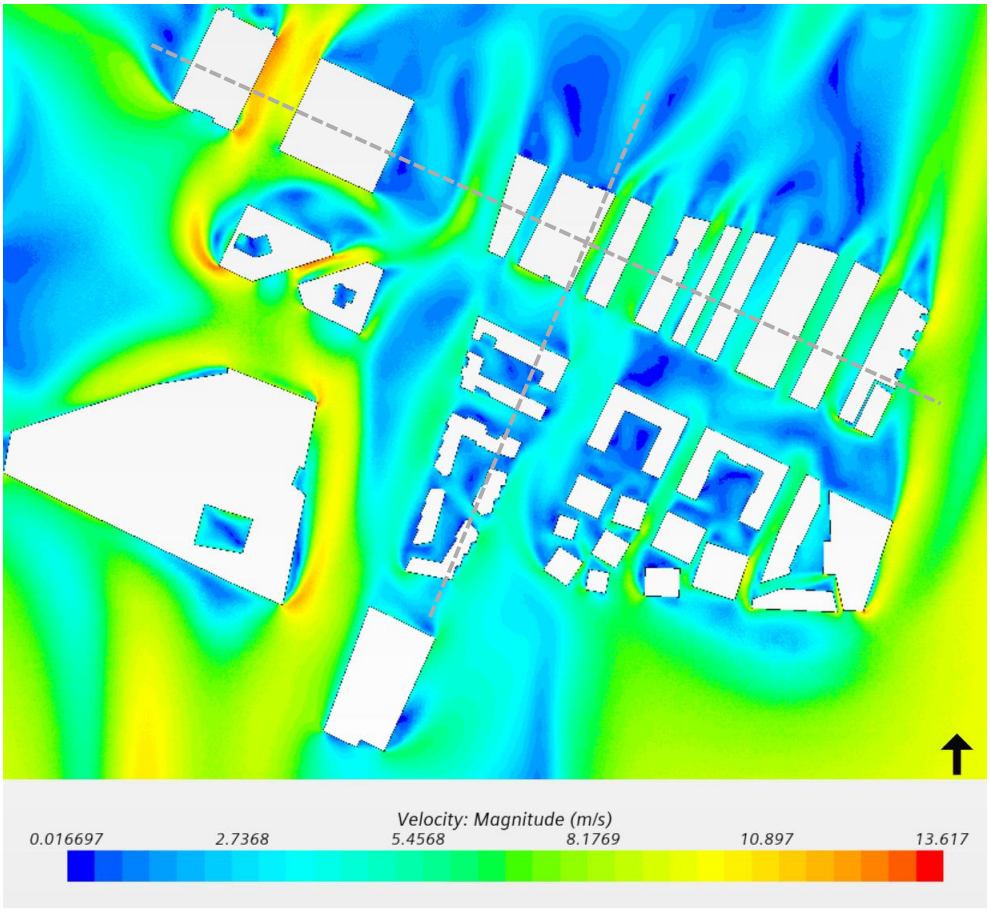

Figure 4-22. Wind velocity for Area 2, up to 17m. The dotted lines show the placement of planes for the vorticity results

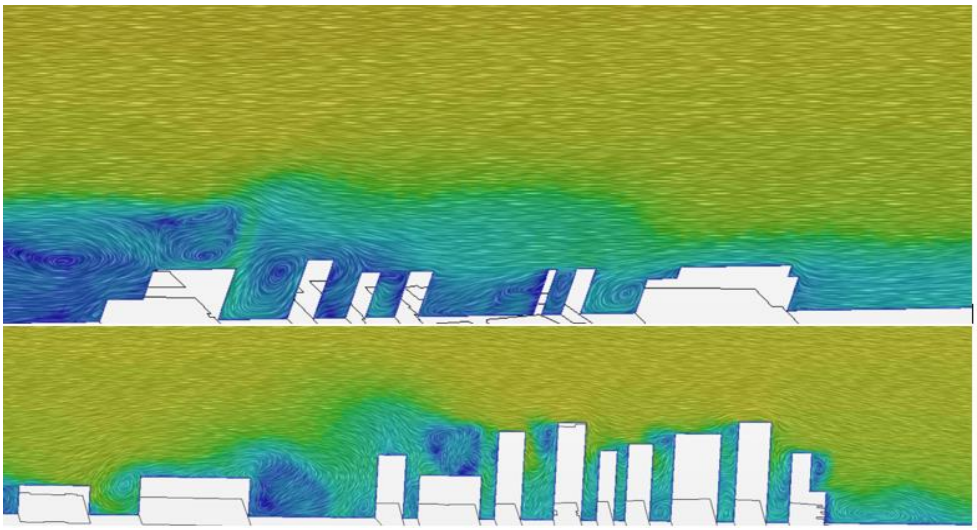

Figure 4-23. Velocity field revealing vorticity structures, wind direction (top) and normal to wind direction (bottom), Area 2

Velocity field illustrating vortices structures in a plane section passing through buildings is presented in the Figure 4-23. Buildings in both wind and its normal direction are of different heights mostly. As a result of this, developed vortices are observed with increased height-width ratio (aspect ratio). But, for higher width between the buildings, vortices are less developed.

Area 3

The wind velocity for Area 3 up to $2.5m$ is shown in Figure 4-24. This figure also includes the buildings and street canyons surrounding the area. It can be seen that the wind velocity values inside the actual area is really low, as it is well shielded by other buildings. On the outside of the area where the geometry is more open it can be seen that the wind velocity increases.

Figure 4-24. Wind velocity for Area 3, up to 2.5m

The figure below shows the situation up to $17m$ for the same areas. It is seen that inside Area 3 the wind velocities are still low and increases a bit outside the area. This shows that a compact building mass with same heights and geometry will contribute towards low wind velocities in the street canyons.

Figure 4-25. Wind velocity for Area 3, up to 17m. The dotted lines show the placement of planes for the vorticity results

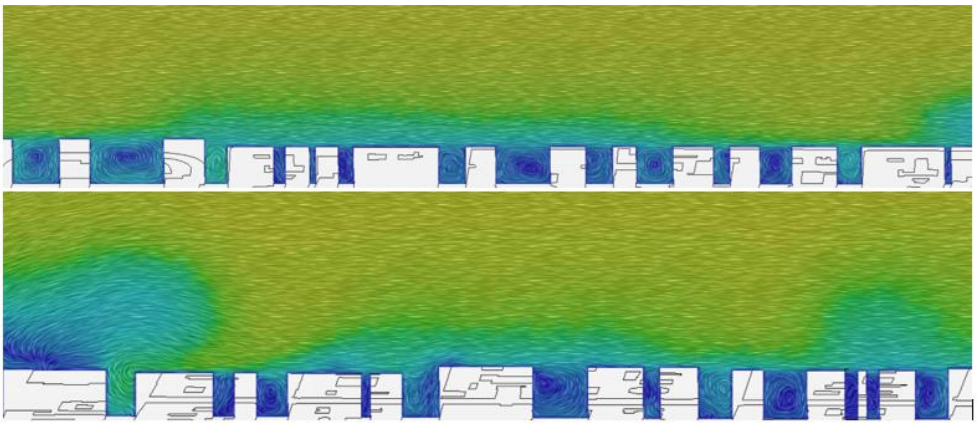

Figure 4-26. Velocity field revealing vorticity structures, wind direction (top) and normal to wind direction (bottom), Area 3

Figure 4-26 shows velocity field illustrating vorticity structures in a plane section passing through buildings in wind direction (top) and its normal (bottom). Buildings have almost same height in this area with varying width between them in both wind and its normal direction. Vortices in the wind direction are less prominent whereas, in the normal direction, interaction between winds in canyons, shows higher vortices.

Area 4

At pedestrian level in Area 4 there can be seen several places with increased wind velocity. The main increases can be seen around the tallest building, Oslo City Hall, on the right side of the figure. The main increases can be seen both on the corners and around this building, as well as on the corners of the building behind. The maximum wind velocity in this area is $12.3 m/s$.

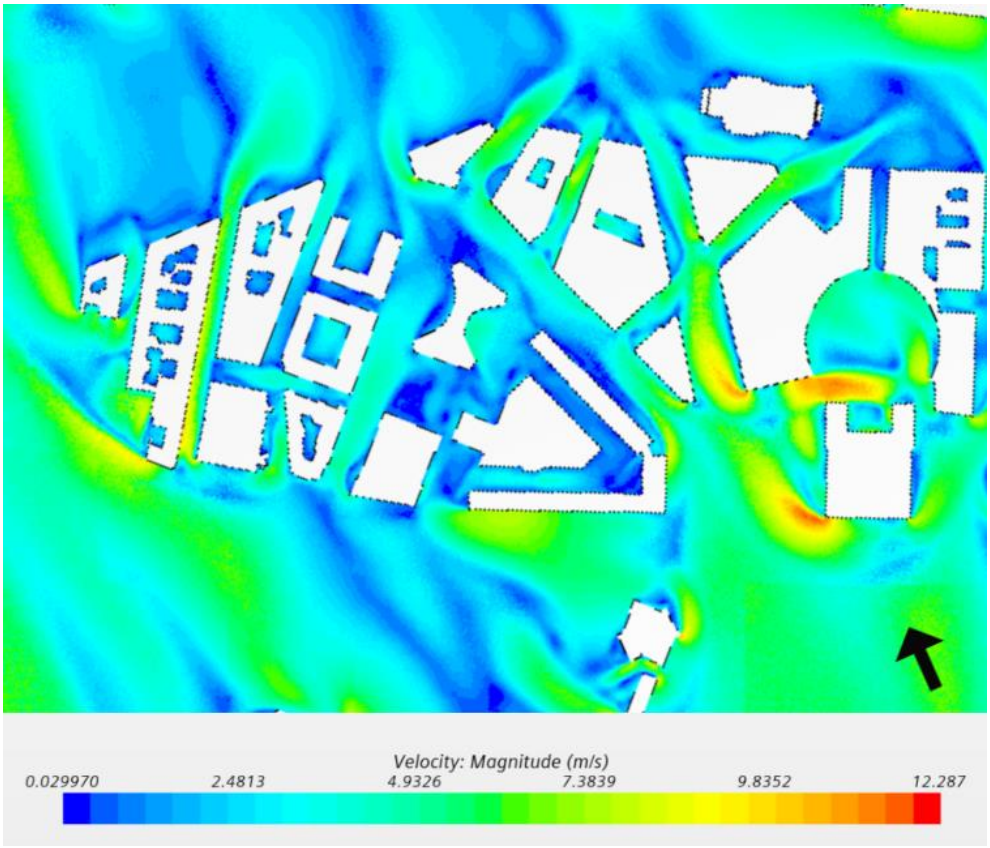

Figure 4-27. Wind velocity for Area 4, up to 2.5m

At the height up to $17m$, which is shown in Figure 4-28, there are less increases in wind velocity. The places with increases can be seen on the same spots as the case above. The maximum wind velocity in this case is $13.4m/s$.

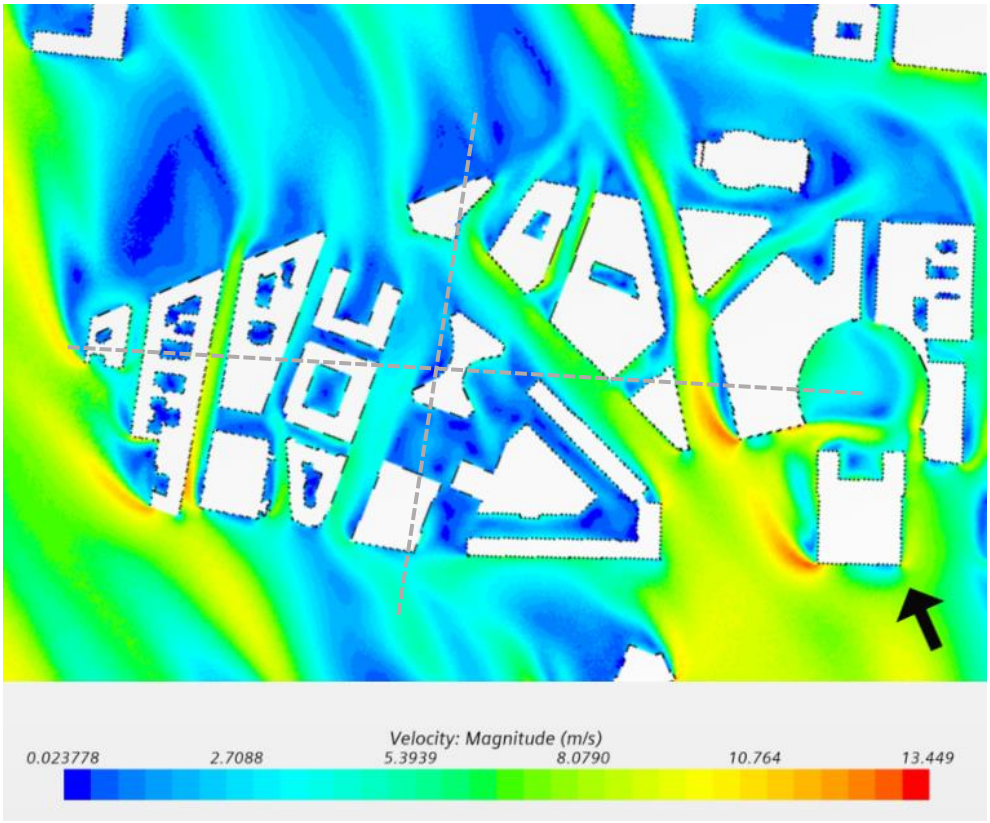

Figure 4-28. Wind velocity for Area 4, up to 17m. The dotted lines show the placement of planes for the vorticity results

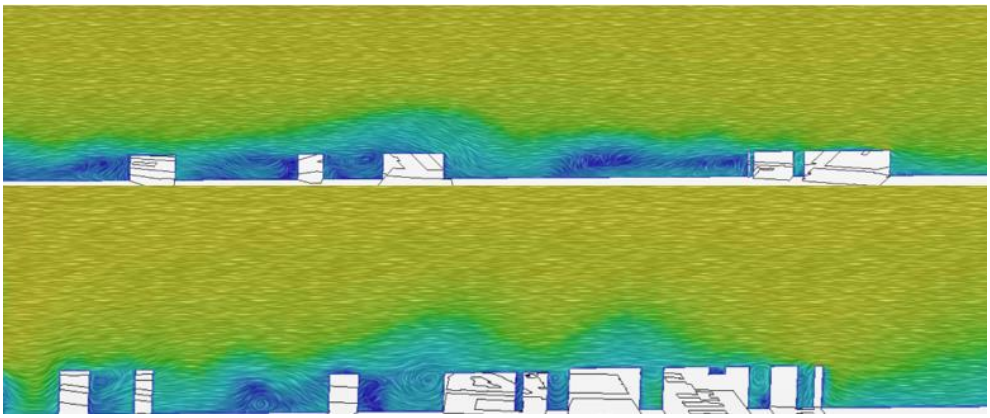

Figure 4-29. Velocity field revealing vorticity structures, wind direction (top) and normal to wind direction (bottom), Area 4

Velocity field showing wind vortices in a plane passing through the buildings is presented in the Figure 4-29, in the wind and its normal direction. Similar to the Area 3, buildings are of almost same height with developed but small vortices at the downfall of wind.

Area 5

Area 5 is well shielded and has no buildings significantly taller than others. In this whole area, the wind velocity has been decreased by the building morphology. The maximum wind velocity in this area at pedestrian level is $6.1 m/s$, and as can be seen from the figure, this is actually occurring outside the buildings in the area.

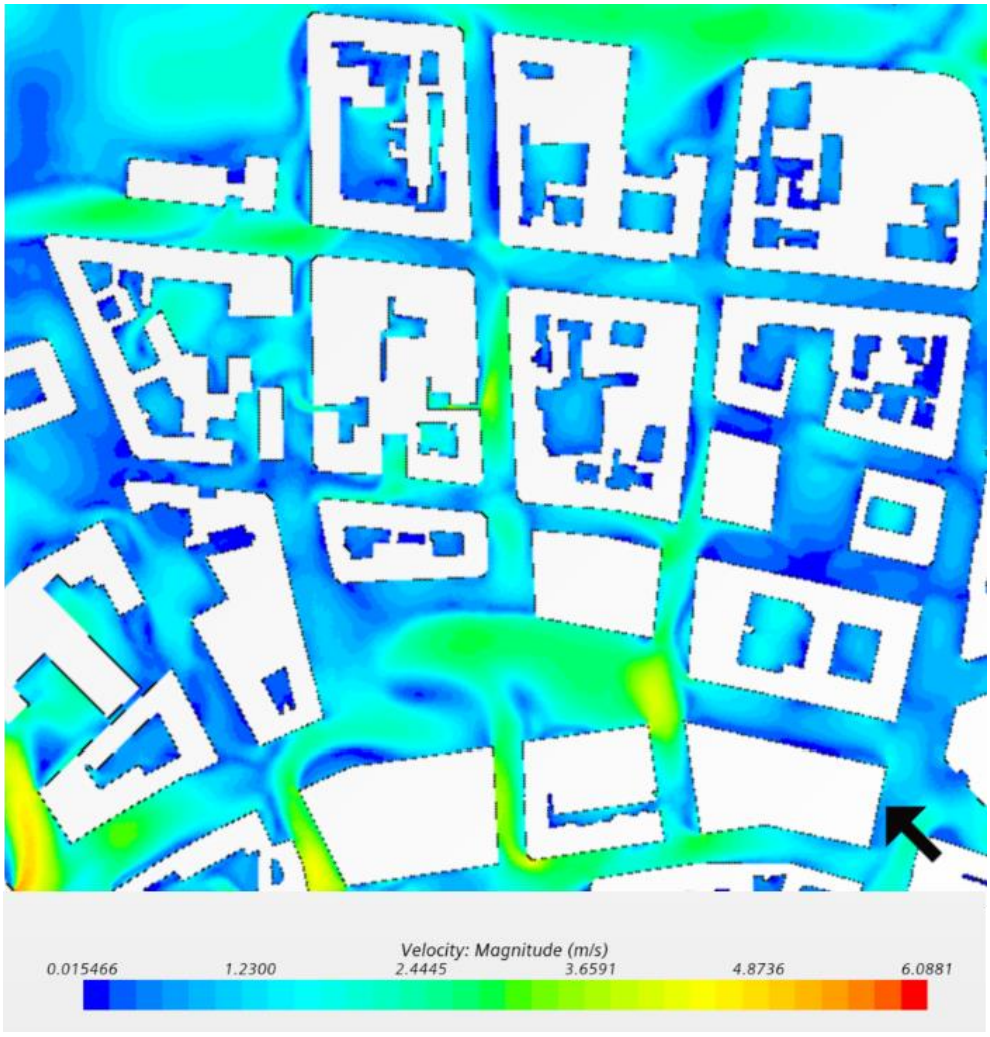

Figure 4-30. Wind velocity for Area 5, up to 2.5m

Up to a height of $17m$, there are small differences in Area 5. The maximum wind velocity at this height is $8.1m/s$, still located right outside the area.

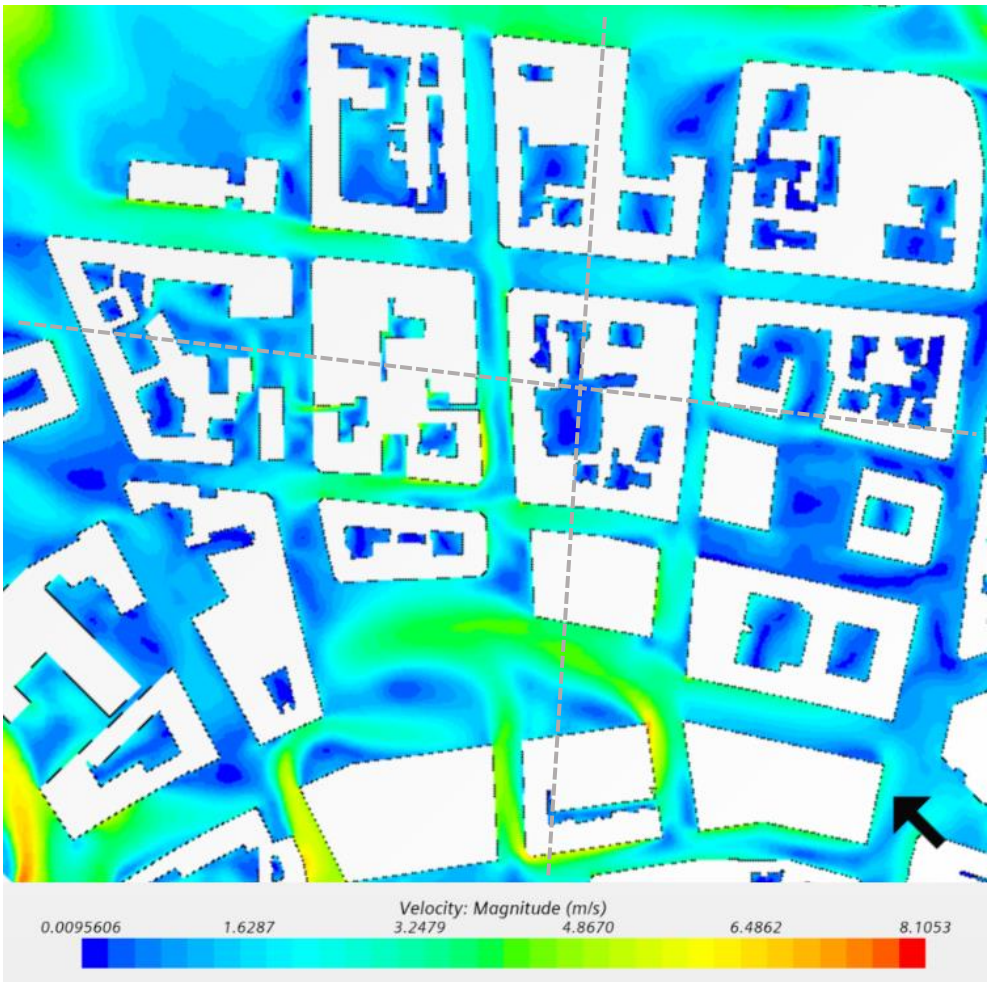

Figure 4-31. Wind velocity for Area 5, up to 17m. The dotted lines show the placement of planes for the vorticity results

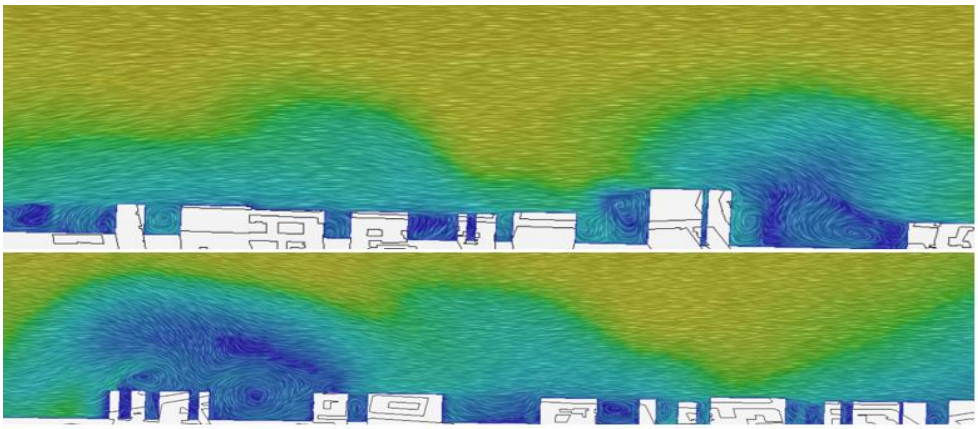

Figure 4-32. Velocity field revealing vorticity structures, wind direction (top) and normal to wind direction (bottom), Area 5

Area 5 has varying aspect ratio, therefore wind vortices depicted in the Figure 4-33 are more complex and developed. In the plane passing through the building in the wind direction, vortices in upwind is developed and vortices at the down-wind are less developed. Wind vortices in the normal direction plane seems to be more complex at the back.

Area 6

At pedestrian level in Area 6, the wind velocity has been decreased for the main parts of the area. However, around the one tall building in the area, the wind velocity has increased. The maximum wind velocity around this building is $12.8 m/s$, however, this is very local. It still tells that even though an area is well shielded, one tall building that stands out from the rest will cause changes to the wind conditions.

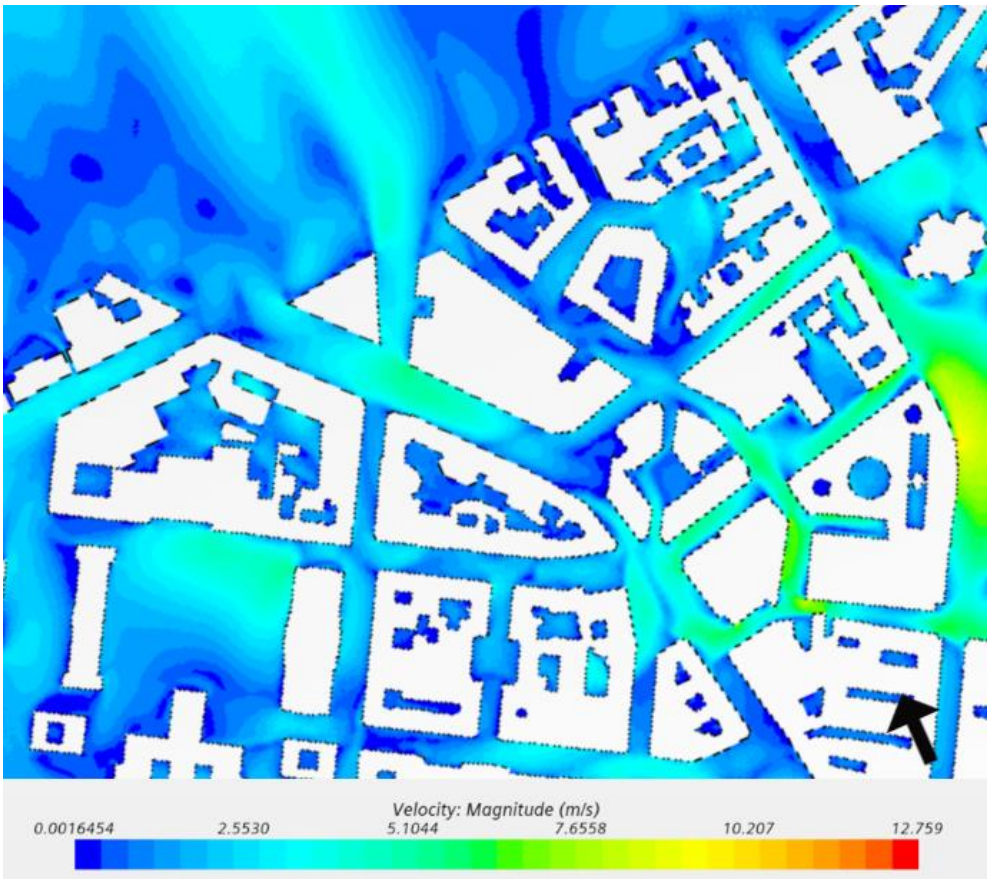

Figure 4-33. Wind velocity for Area 6, up to 2.5m

At the height of $17m$, the wind is moving almost identical as at pedestrian level. The difference is in the magnitude of the values, as it is slightly increased at $17m$ height. Here, the maximum wind velocity is $14.4 m/s$.

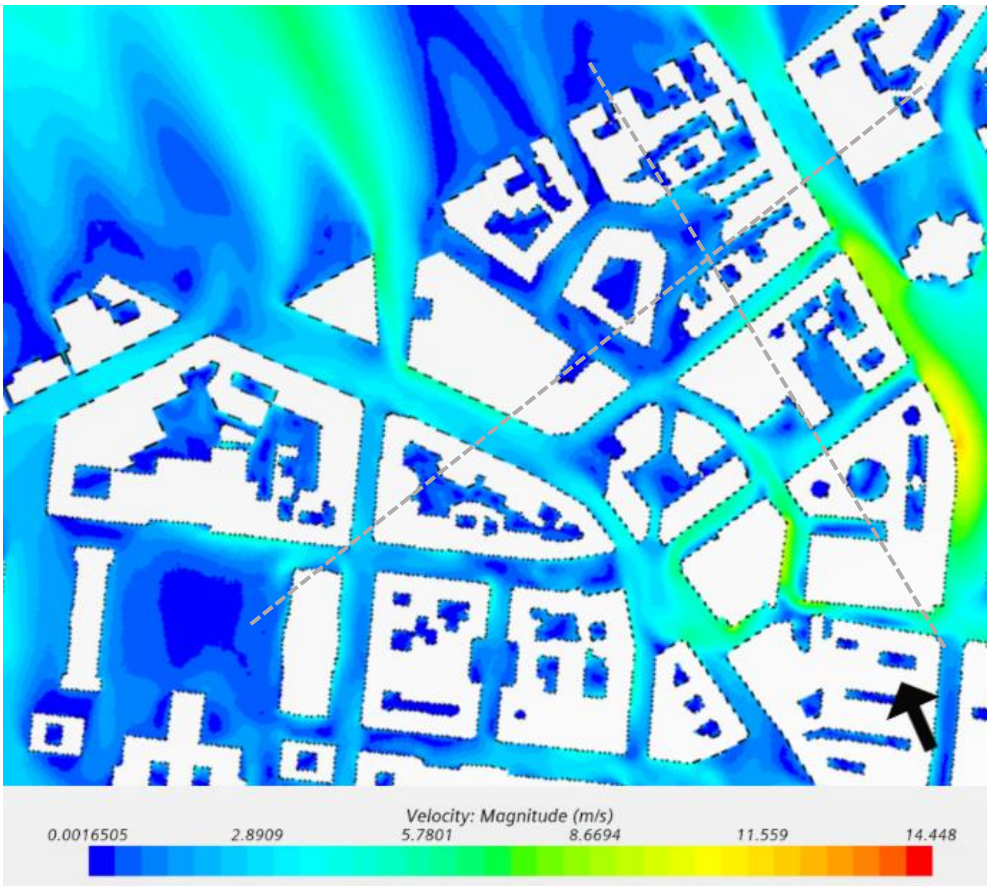

Figure 4-34. Wind velocity for Area 6, up to 17m. The dotted lines show the placement of planes for the vorticity results

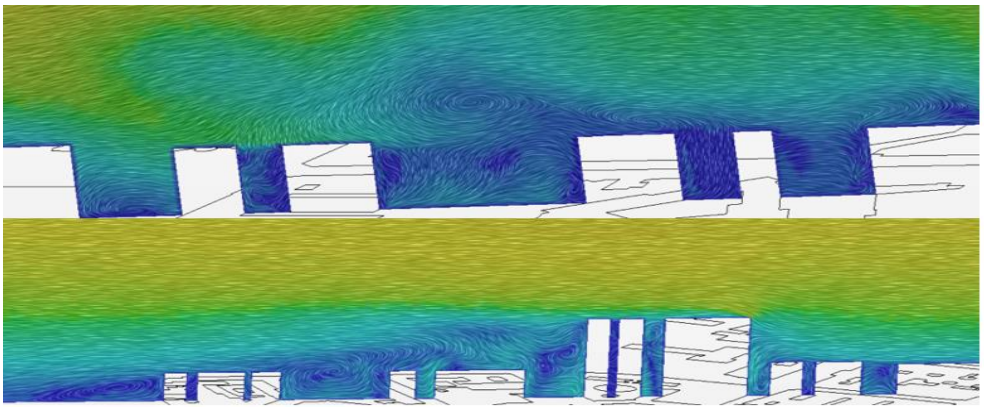

Figure 4-35 . Velocity field revealing vorticity structures, wind direction (top) and normal to wind direction (bottom), Area 5

Wind vortices in the velocity field for planes passing through the buildings in wind and its normal direction is illustrated in the Figure 4-35. Wind vortices at the down-wind condition seems to be fully developed at the middle of the plane in the wind direction.

4.2 Bygdøy

4.2.1 Simulation

4.2.1.1 Domain

Figure 4-36 shows the computational domain used for the Bygdøy-model, including the dimensions and recommendations. Also, for this model, the distances have been increased to make sure it would not cause any problems in the simulation.

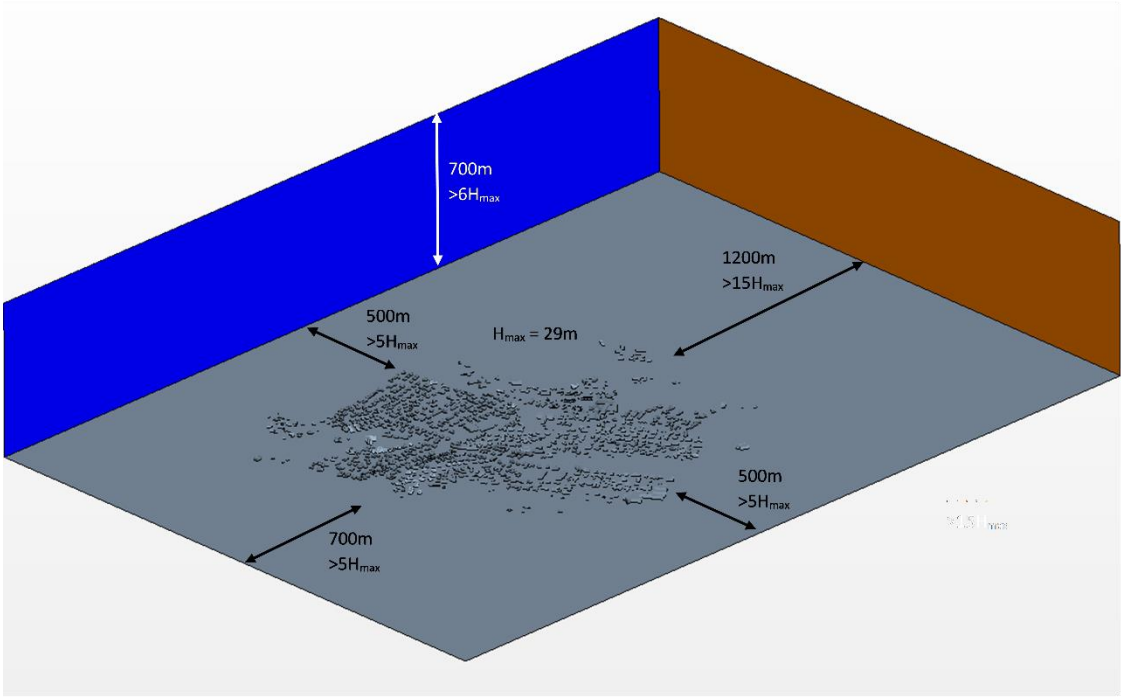

Figure 4-36. Domain with dimensions and recommendations

4.2.1.2 Mesh

Figure 4-37 shows an overview of the surfaces in the volume mesh for the whole domain. The remeshed surface had a total of 6 530 078 faces. From this, the volume mesh was created, which in total contains 13 891 296 cells. Figure 4-38 shows a cross-section view of the volume mesh. In this figure the two volumetric controls near the surface can be seen, as well as the gradually increasing cell sizes from the bottom to the top.

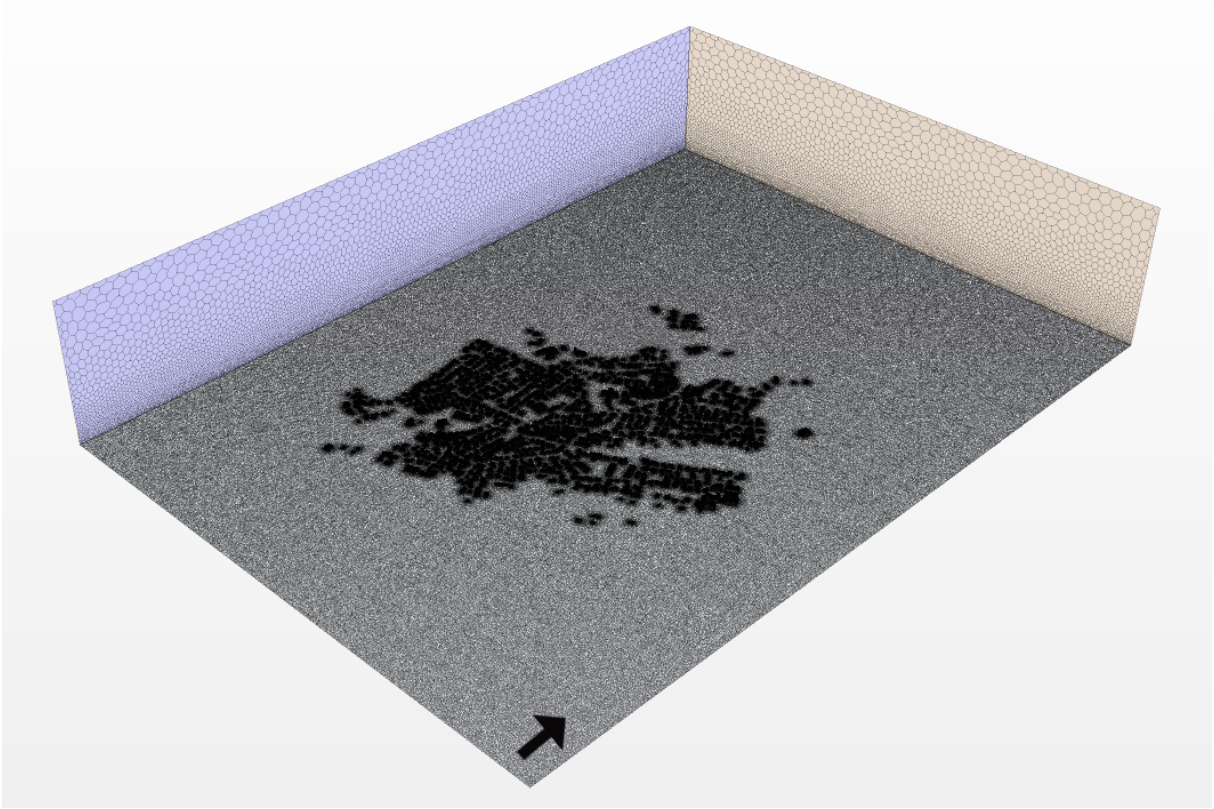

Figure 4-37. Overview of the surfaces in the volume mesh for the whole computational domain. Arrow shows wind direction from south to north

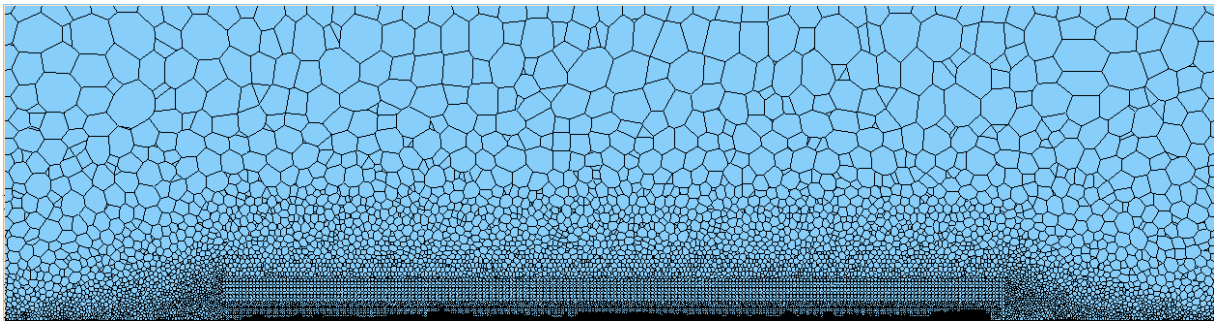

Figure 4-38. Cross-section of the volume mesh

A close-in on buildings and street canyons can be seen in Figure 4-39. Due to more spread-out buildings in this model, there are no obvious street canyons as there are in the Downtown-model. The figure shows the number of cells on the different surfaces. The average height of the buildings in the figure is $8m$.

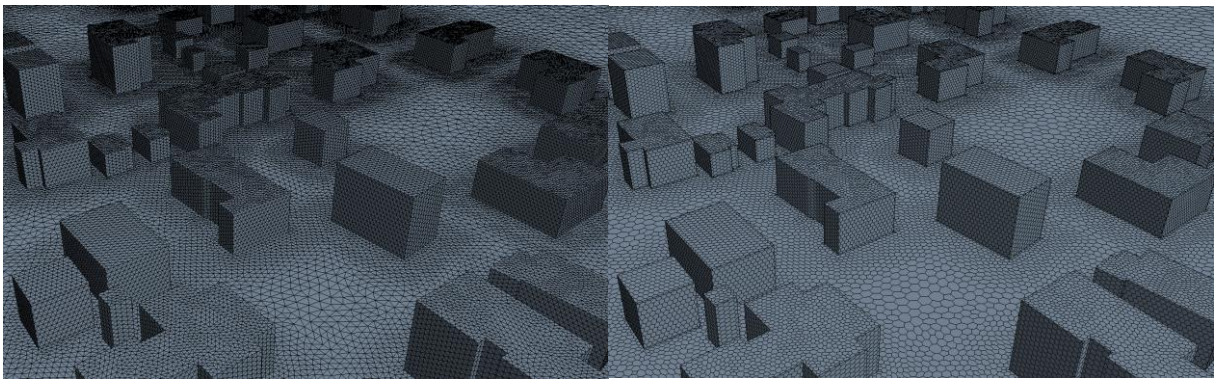

Figure 4-39. Close-in on buildings and street canyons. Left shows remeshed surface, right shows the surfaces of the volume mesh

4.2.1.3 Residuals

Figure 4-40 shows the residual monitor plot for the simulation. The simulation was run for 801 iterations, and as can be seen in the figure, the solution has successfully converged.

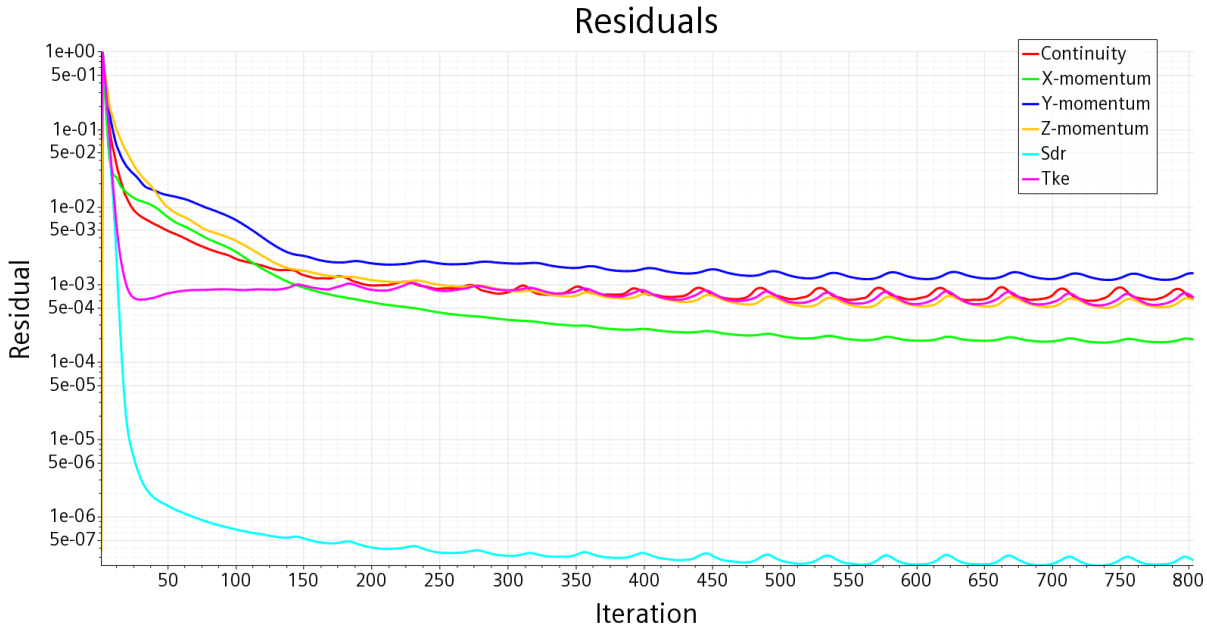

Figure 4-40. The residuals shown over the number of iterations

4.2.2 Pressure coefficient

Figure 4-41 shows the pressure coefficients on the building facades in the Bygdøy-model, from both inlet and outlet. The C_p values varies from a minimum of -1.68 to a maximum of 0.65. The figure shows that the positive values mainly occurs on the facades facing the inlet, while the negative values occur on the other facades. It can also be seen that the taller and larger buildings has the highest C_p values.

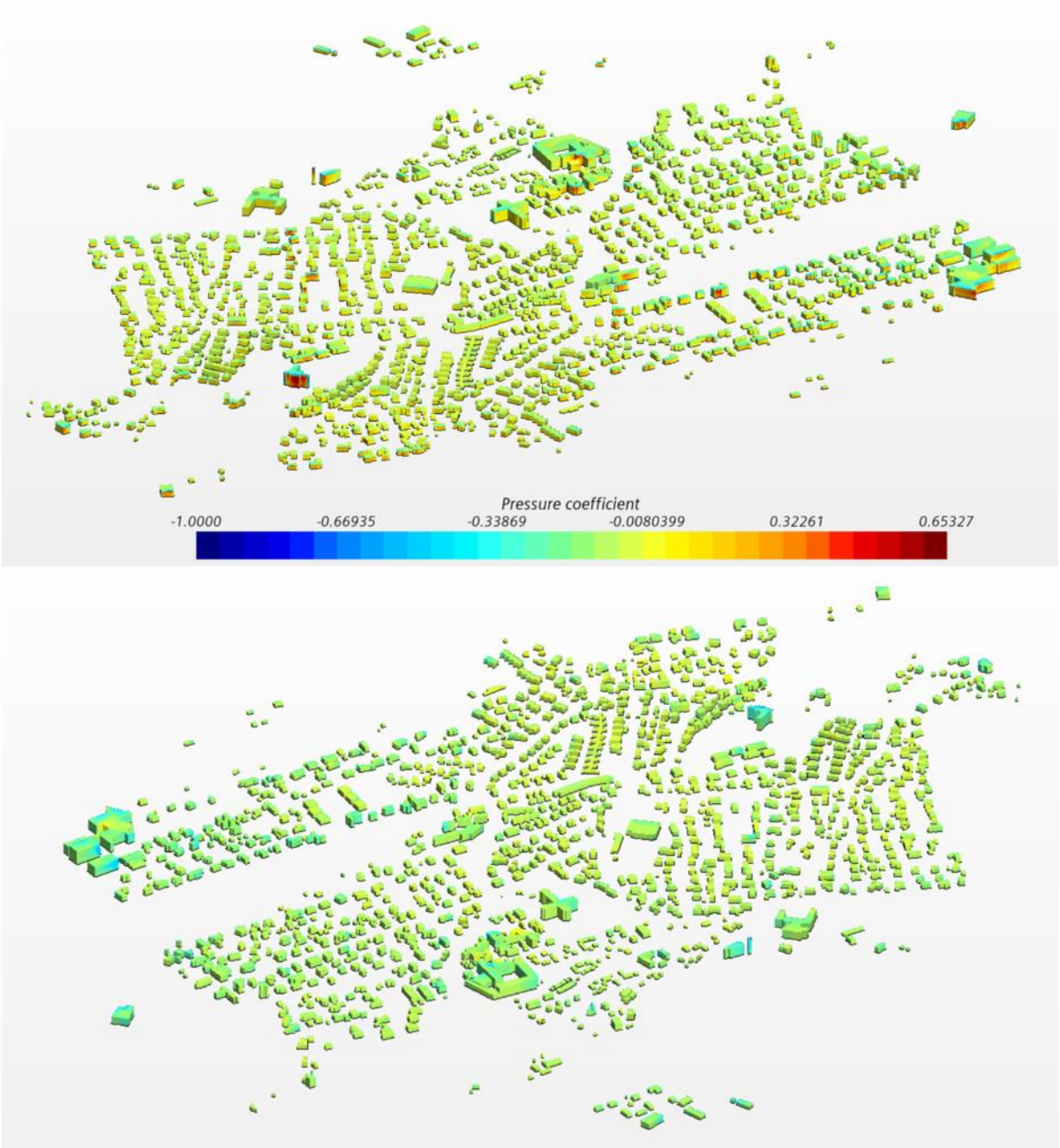

Figure 4-41. Pressure coefficient on building facades shown from inlet (top) to outlet (bottom)

Figure 4-42 shows the distribution of C_p values of all buildings in the model. The main part of the values is within the range of -0.25 to 0.06. The number of values with a higher magnitude than these are really limited. The average C_p value is -0.08.

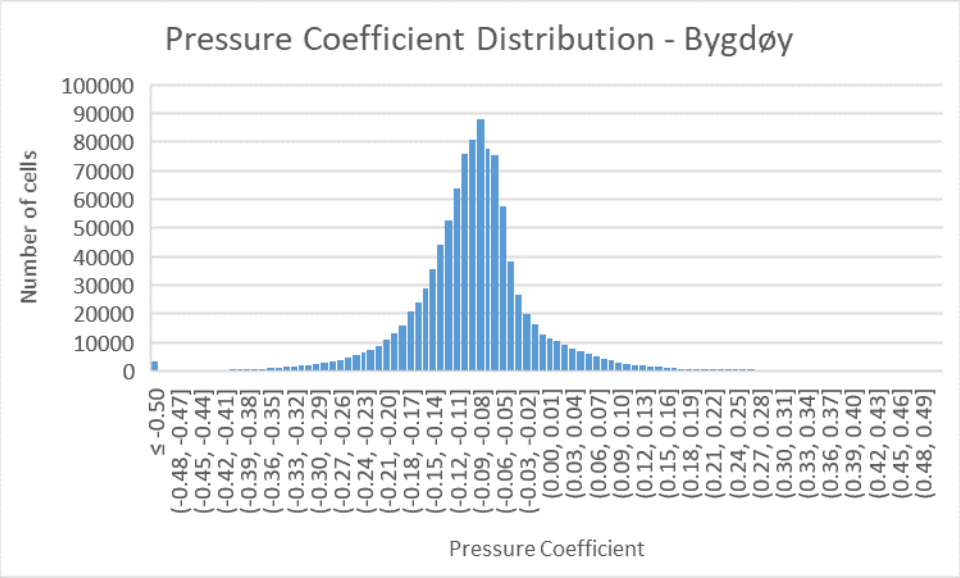

Figure 4-42. Pressure coefficient distribution of all buildings in the Bygdøy-model

4.2.2.1 Pressure coefficient by area

The areas of the Bygdøy-model have been divided as shown in Figure 4-43. The aim with the division was to create as many different areas as possible, both regarding location and morphology.

Figure 4-43. The six areas of the Bygdøy-model. Wind direction is from the bottom to the top

From the chart below some differences can be seen. Area 3, 4 and 6 contains mostly low C_p values, which is to be expected as they consist of only small residential buildings, and they are well shielded. Area 6 still has some increased values. This is due to the open area in front where the wind velocity increases after having been increased by the buildings in Area 2. Area 1 and 5 both have some increased values and look quite similar from the chart. However, the reason for this is totally different between the two. Area 1 has higher C_p values due to the area being directly exposed to the inlet. Area 5 is shielded in the back of the domain, but due to some large and tall buildings the C_p values increases. Area 3 and 4 are both well shielded and contains small buildings, which makes the C_p values low.

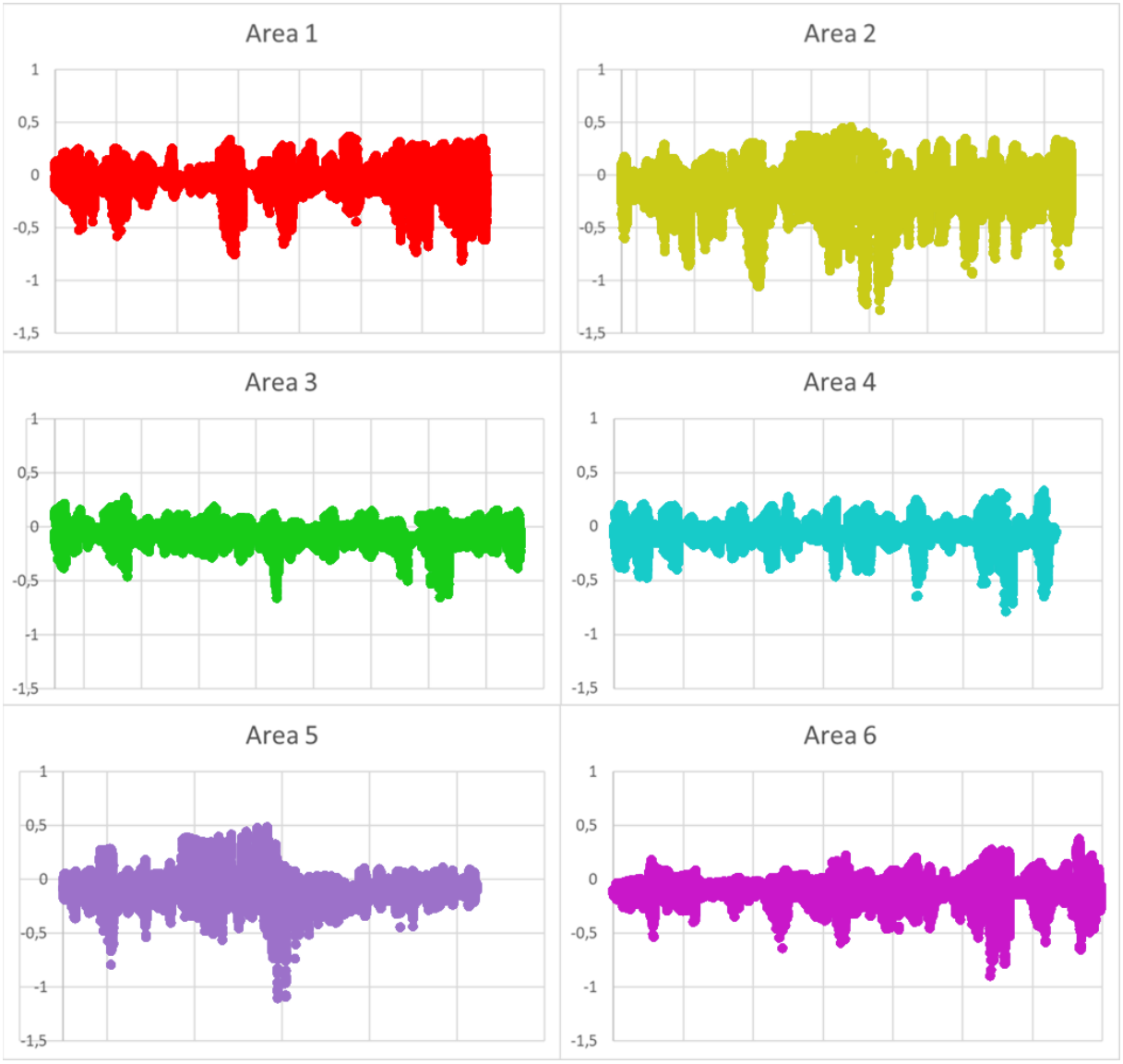

Figure 4-44. Comparison of the pressure coefficients for each area. The Y-axis shows the C_p values, and it shows an overview if the values for all cells (X-axis)

Area 1

Area 1 is located closest to the inlet and consist of small residential buildings. It is not protected by any buildings in the wind direction and is quite exposed. Figure 4-45 shows that the pressure coefficient distribution is relatively spread out, and that the number of positive values is higher than in most of the other areas. This is due to a larger area of facades being exposed directly to the wind.

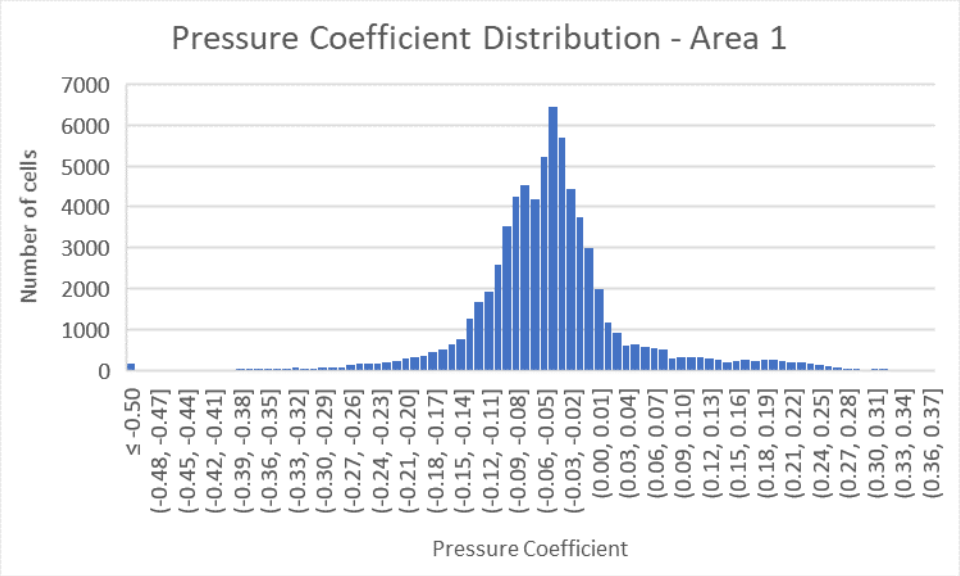

Figure 4-45. Pressure coefficient distribution of Area 1 in Bygdøy

Area 2

Figure 4-44 showed that Area 2 contained consistently higher C_p values than the other areas, and this is also reflected in the pressure coefficient distribution in Figure 4-46. This distribution is the most spread out with the highest values. The reason for Area 2 having this result is that it is directly exposed to the wind, and it contains some buildings that are significantly taller than the average building height.

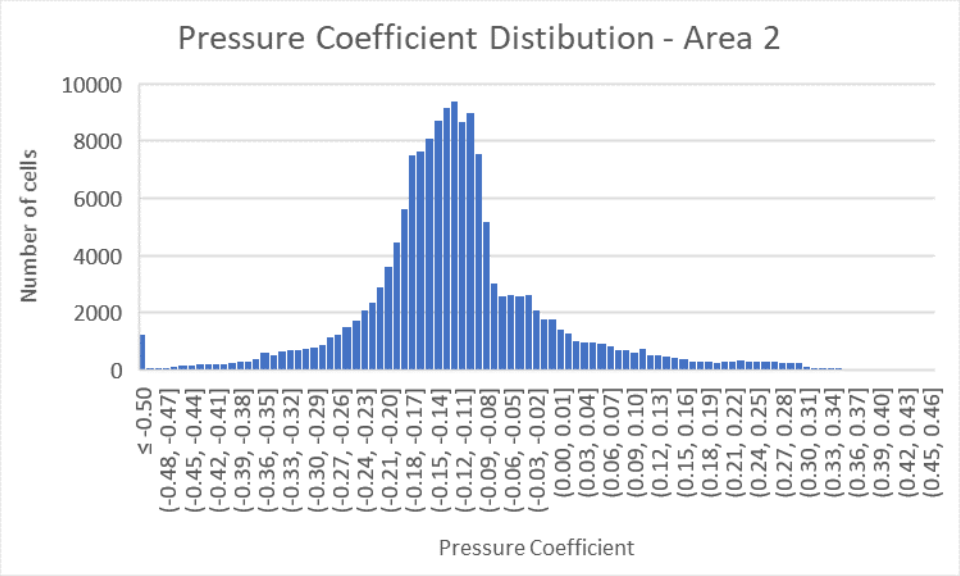

Figure 4-46. Pressure coefficient distribution of Area 2 in Bygdøy

Area 3

Area 3 is well shielded and contains small buildings, which means it should not contain large C_p values. This can be seen in Figure 4-47.

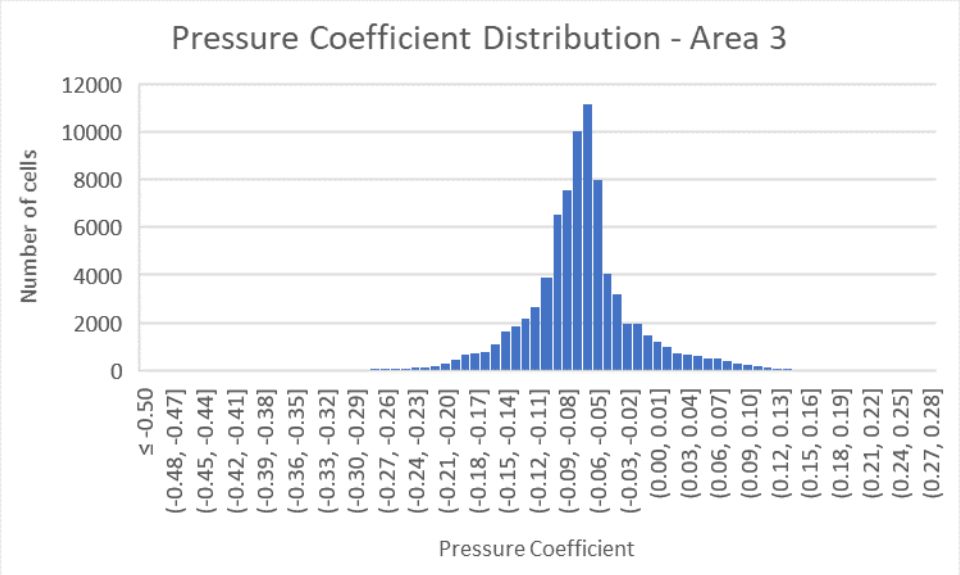

Figure 4-47. Pressure coefficient distribution of Area 3 in Bygdøy

Area 4

The attributes of Area 4 in terms of location and morphology are almost the same as Area 4. The pressure coefficient distribution also shows that by being really similar.

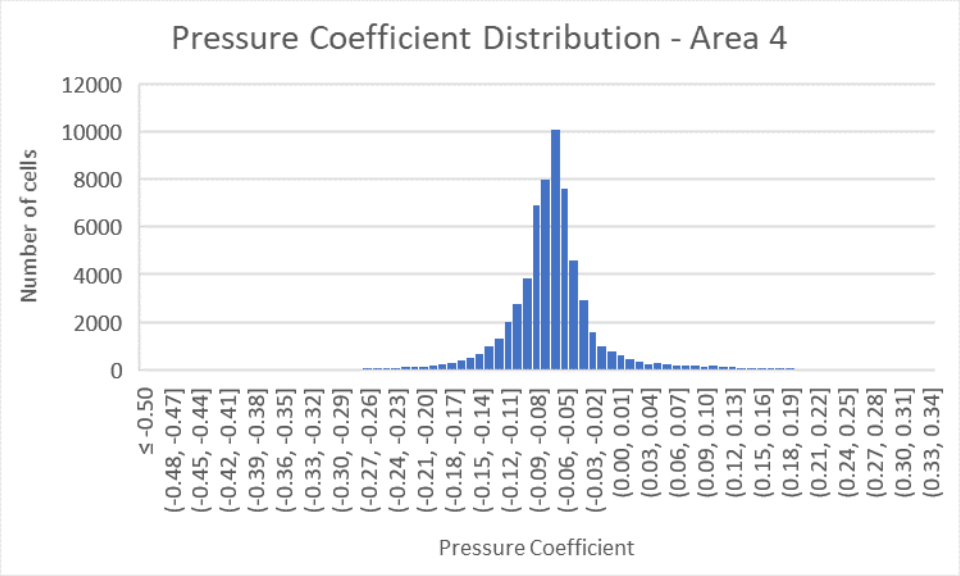

Figure 4-48. Pressure coefficient distribution of Area 4 in Bygdøy

Area 5

Area 5 is well shielded with its location in the back of the domain. There is one building that is significantly larger and taller than other buildings nearby. This has an influence on the pressure coefficients in the area. As seen in Figure 4-49, there are some C_p values that are relatively high, and the highest value of all the areas is found here. However, there are not many high values compared to Area 1 and 2. This is due to only one of the buildings sticking out and obtaining a high C_p value.

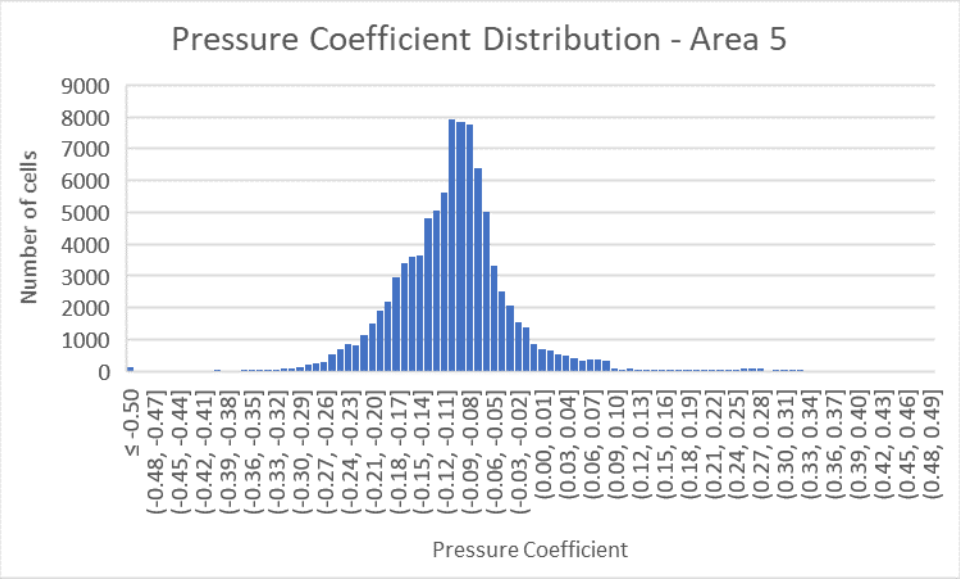

Figure 4-49. Pressure coefficient distribution of Area 5 in Bygdøy

Area 6

Area 6 consists of only small buildings, and it is located in the back of the domain. However, there is some open space in front of it towards the inlet where the wind velocity has space to increase. This has an influence on the pressure coefficients in the area, and it is quite similar to what is seen in Area 1.

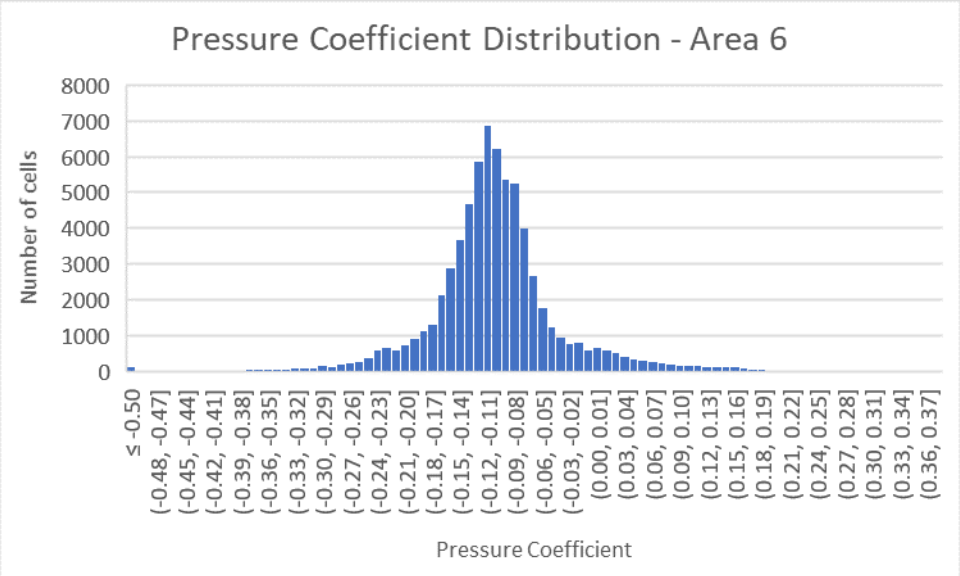

Figure 4-50. Pressure coefficient distribution of Area 6 in Bygdøy

4.2.3 Wind velocity

Unlike for the Downtown-model, only the pedestrian level height will be concerned when analyzing the results for wind velocity in street canyons for the Bygdøy-model. A higher level has been chosen to not be analyzed as the low buildings would require a height so low that the differences would not be significant. The height of the analysis for the pedestrian level for this model is also $2.5m$.

Figure 4-51 shows the wind velocity at pedestrian level over the whole domain. It shows that the wind velocity is decreasing almost within the whole building mass. The areas where it is increasing around buildings are limited, however, there are still some, and this is where the highest values occur. It can also be seen that in the wake regions of the domain, the wind velocity in some places increases. This can also be seen in the gap in the building mass on the right side of the model. After buildings have shielded the wind, it has time to re-establish and also slightly increase before hitting the next row of buildings. The maximum wind velocity occurring in this model is $8.49m/s$.

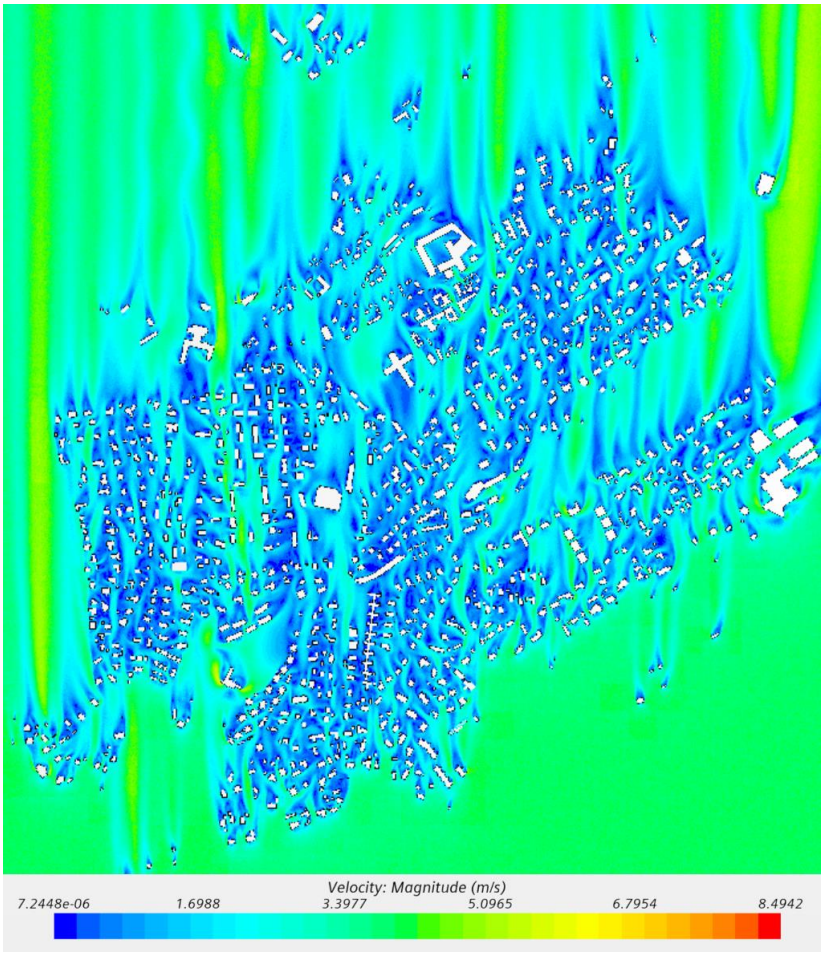

Figure 4-51. Wind velocity for the whole Bygdøy-model, up to a height of 2.5m.

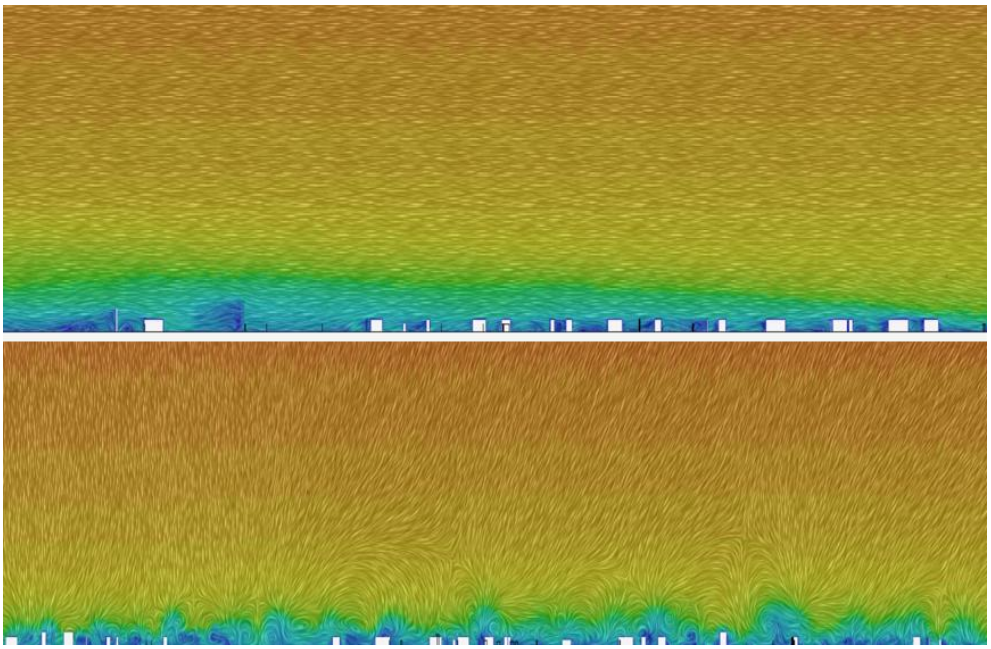

Figure 4-52. Velocity field revealing vorticity structures, wind direction (top) and normal to wind direction (bottom), Bygdøy

Vorticity structure revealed in the velocity field above shows no major vortices for Bygdøy, in both directions. The aspect ratio seems to be more or less similar in Bygdøy.

4.2.3.1 Wind velocity by area

Area 1

Area 1 consists of only small houses and is directly exposed to the inlet. Figure 4-53 shows the wind velocity within the area. The maximum wind velocity in this area is $5.52 m/s$. It is seen that the incoming wind velocity is being significantly decreased as it passes through the buildings. Some street canyons do however get a flow with higher velocities.

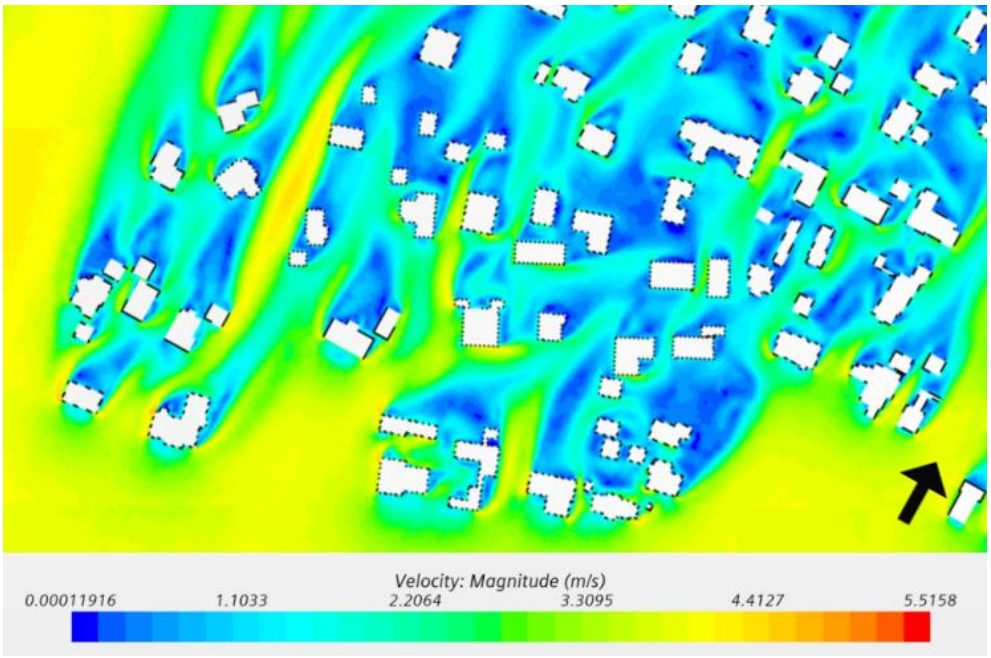

Figure 4-53. Wind velocity for Area 1, up to 2.5m

Area 2

Area 2 is also exposed directly to the inlet, and in addition, it contains some taller and larger buildings. Figure 4-54 shows that around these buildings the wind velocity is slightly increasing. As for the other areas, the wind velocity is generally decreasing when passing through the building mass. The maximum wind velocity in this area is $5.86 m/s$.

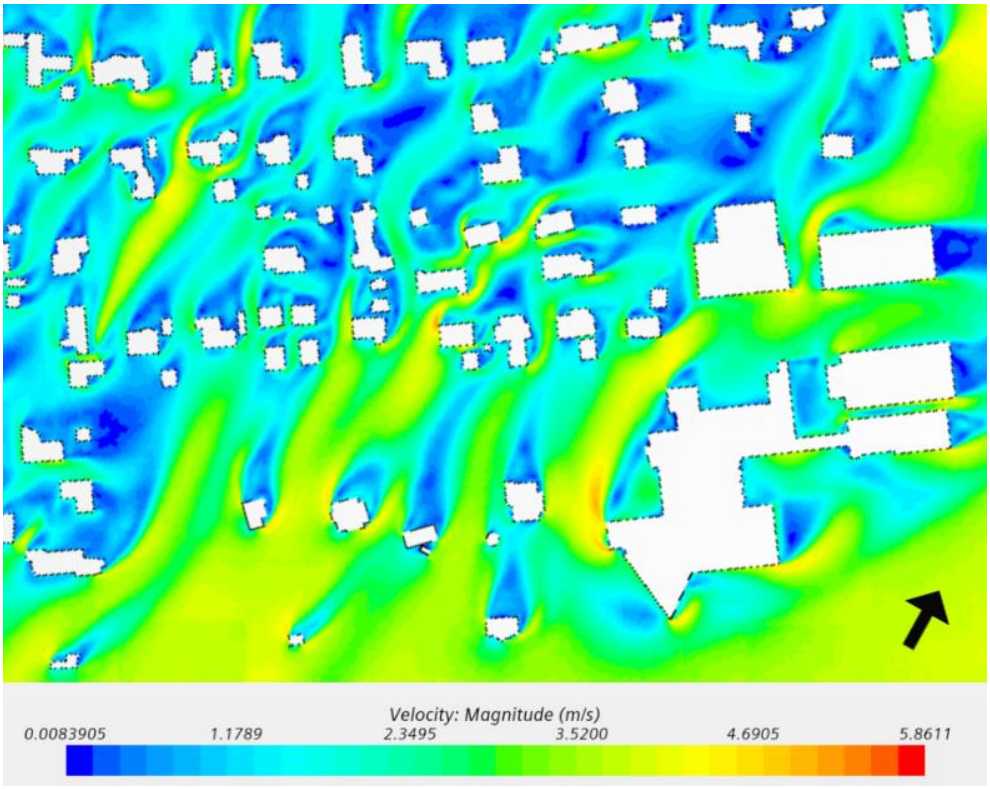

Figure 4-54. Wind velocity for Area 2, up to 2.5m

Area 3

Area 3 is located in the middle of the domain and contains mostly small buildings. From Figure 4-55 it can be seen that the incoming wind velocity is not as high as in Area 1 and 2, due to this area being more shielded. Even though the wind velocity is relatively low throughout the whole area, the maximum wind velocity is $5.70 m/s$, which is around the same as for Area 1 and 2.

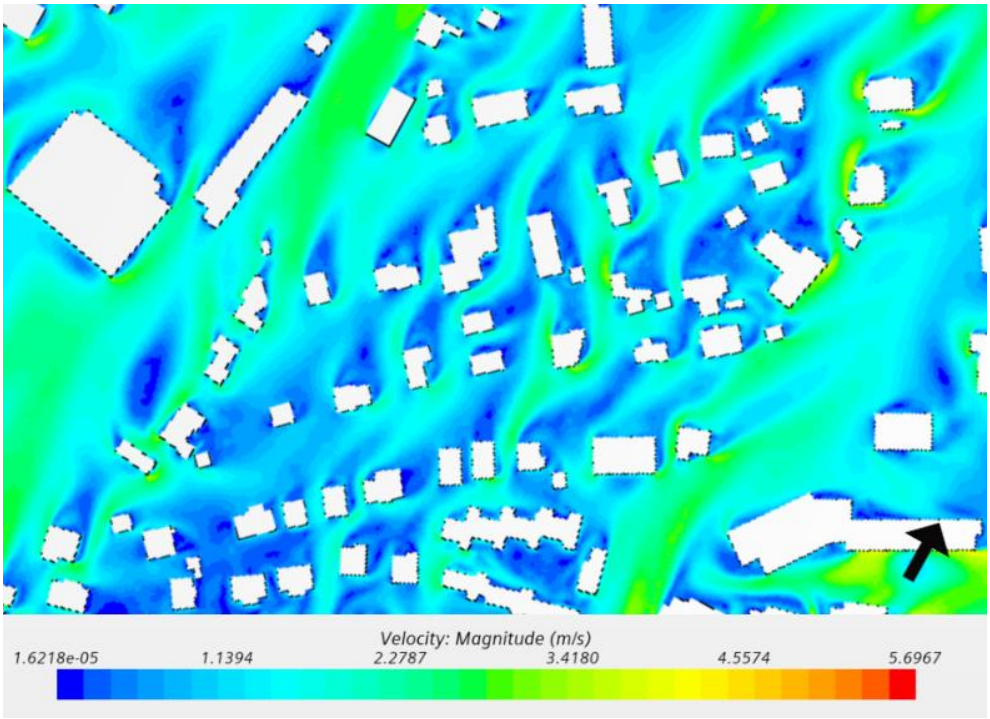

Figure 4-55. Wind velocity for Area 3, up to 2.5m

Area 4

Area 4 is well shielded from the inlet and contains mostly small buildings. Figure 4-56 shows the wind velocities within the area, which is quite similar to Area 3. However, on the right side of the area, the wind velocity is increasing within a street canyon. This also gives an increased maximum wind velocity of $6.44 m/s$.

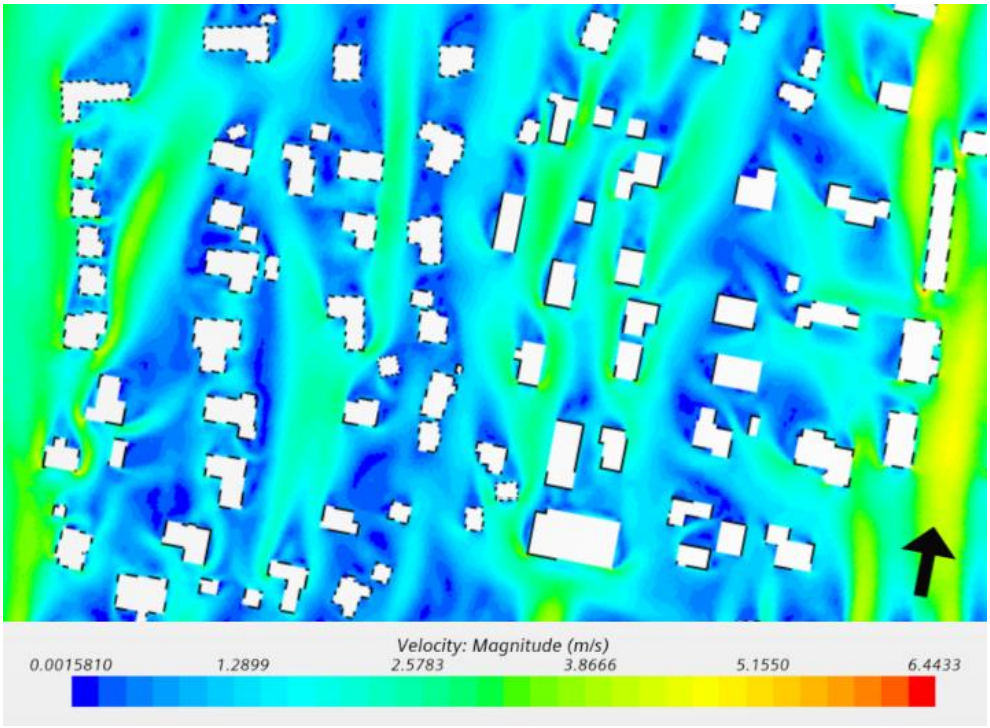

Figure 4-56. Wind velocity for Area 4, up to 2.5m

Area 5

Area 5 is located in the back of the domain. The building mass is less dense than other areas, and it contains on building larger and taller than the rest. This building is well shielded by a group of buildings with high density. This could be a factor of the relative low maximum wind speed in the area. This still occurs around the tall buildings, but with a magnitude of $5.40 m/s$, it is lower than in all of the other areas.

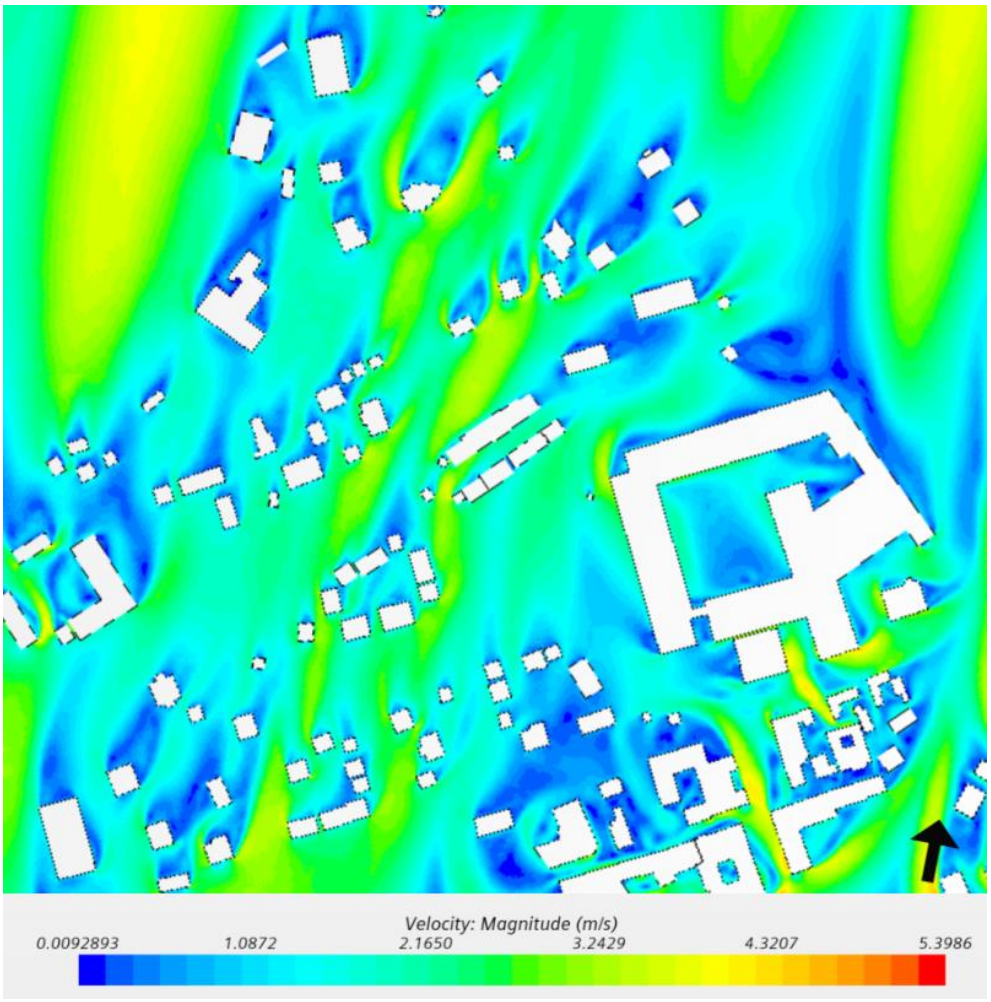

Figure 4-57. Wind velocity for Area 5, up to 2.5m

Area 6

This area is located in the back-right of the domain. The building mass is dense and consists of only small buildings. It is shielded by many buildings from the inlet, however, there is a gap in front of the area which allows for the wind velocity to re-establish. As can be seen in Figure 4-58, the wind velocity enters quite high, and does not increase significantly within the area, apart from a couple small spots around some buildings. The maximum wind velocity in the area is $6.05 m/s$.

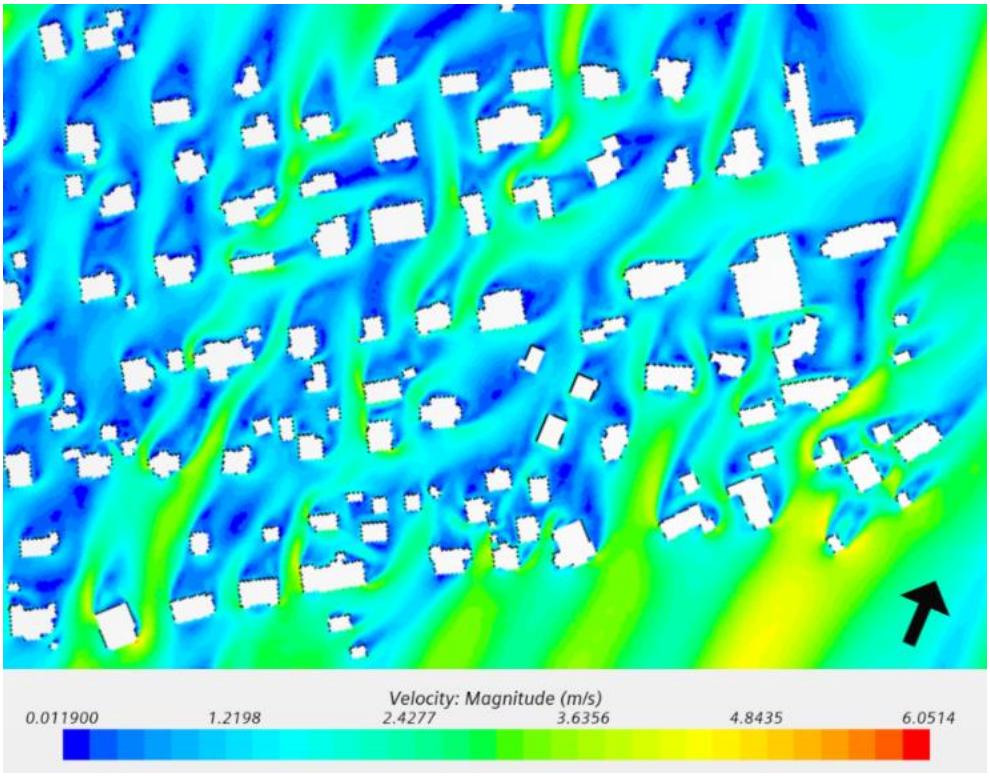

Figure 4-58. Wind velocity for Area 6, up to 2.5m

5 Discussion

To analyze the impact of urban morphology on wind conditions, two different areas within the city of Oslo has been studied. These areas represent very different buildings, where one contains mostly high and medium-rise buildings, and the other contains mostly low-rise buildings. Six smaller areas have been chosen within both main areas to be further analyzed. All of these as different as possible regarding morphology and exposure to the wind inlet. By running simulations in the CFD-software STAR-CCM+ results have been found, which are further discussed in the chapters below.

5.1 Pressure coefficients

When considering the pressure coefficients in the Downtown-model, it is clear to see that the facades facing the inlet obtain positive C_p values, while the other facades obtain negative C_p values. This also reflects in the pressure coefficient distribution, where it can be seen that the majority of values are negative.

By comparing the different areas, it is seen that the areas in the back of the domain, which are more shielded, generally obtains lower C_p values than the exposed areas in the front. This deviates if the area in the back has buildings that rises high above the surrounding buildings, making the surface area that is not shielded higher. The differences between the shielded and exposed areas in a city center like this is large, which can be seen from Figure 4-9.

In the Bygdøy area the buildings are smaller, and the building mass is less dense. Also, in this case it is seen that the positive values appear on the facades facing the inlet, while the negative values appear on the other facades. This is also reflected in the pressure coefficient distribution where the majority of values are negative.

There are some differences on the areas in the back of the domain, as it obtains lower C_p values than in the front. More determining is the size and height of the buildings, and a large effect can be seen on these variations. This is due the area not being as dense, which will let some wind through the domain, and the buildings being smaller, so it will not catch as high C_p values.

There are severe differences between the two areas. The Downtown-model has higher and more variated C_p values than the Bygdøy-model. This is due to the larger size of the buildings and the higher number of high-rise buildings. It is still seen that in Downtown there are some areas with really low C_p values, as Area 3 and 5. Due to the dense building mass this area is well

shielded, which leads to low C_p values. In Bygdøy, no areas are shielded as well as this and obtains as low values, which is due to the building mass being less dense.

5.2 Wind velocity

In the Downtown model the wind velocity has been assessed both at heights up to $2{,}5m$ and $17m$. The former is to assess the wind condition at pedestrian level, while the latter is to see the wind conditions on the upper parts of the buildings. For both cases, it is seen that the wind velocity generally decreases through the domain as it is passing the building mass, as the buildings are shielding the wind. However, there are areas where the wind velocity significantly increases. These areas are mostly in open areas and around large buildings. At pedestrian level, the increases in wind velocity are more significant than at $17m$ height. The sizes of areas with increased wind velocity are also larger. At $17m$, there are smaller spots that has a high increase. However, these spots are located in the same place at both heights.

There are large differences between the areas in the Downtown-model. The areas which are shielded and contains only average sized buildings has significantly lower wind velocity than the other, which can be seen for Area 3 and 5. This is due to the dense building mass which shields the areas, as well as no tall buildings getting exposure, and no large open areas which allows the wind velocity to increase.

For the Bygdøy-model, only the wind velocity at pedestrian level ($2.5m$) was considered. In this model, less increases in wind velocity occurs, and the one that occurs are mainly small spots on the corners of the taller buildings. There are no larger areas with increased wind velocity, which is due to a combination of the small buildings and larger distances between the buildings. This also makes the whole domain quite uniform, and the differences from area to area is small.

The differences between the two models are big when it comes to the wind velocity. As expected, the higher velocities occur in the Downtown-model, as it contains taller buildings and the distances between the buildings is not too large. Within the Downtown-model the situation is varying, where some areas have small velocities, and some areas has significantly increased velocities. This is not the case for the Bygdøy-model, where the whole model is more uniform with lower velocities.

Wind vortices structure revealed in the velocity field shows major and developed vortices both at the down-wind and up-wind condition for the downtown model. This is primarily due to

varying aspect ratio. Buildings are tall and the width between them is not constant in Downtown, and which leads to greater aspect ratio. Greater aspect ratio shows major and developed vertices in the velocity field plane. The reason behind small and developing vertices in the wind direction in Area 3 and Area 4 could be due to similar aspect ratio but, vortices in the normal plane are complex in this area due to intermixing of wind flowing in the street canyons. Bygdøy on the flipside, has dispersed and low-rise buildings with almost similar heights. Aspect ratio does not vary much thus, wind vortices in the Bygdøy is not more prominent and developed as that of downtown.

5.3 Model and simulation

Model

The creation of the 3D-models has been a large part of this project, as it turned out to be more difficult and time-consuming than planned. Problems were occurring both in the process of converting the input data into a format compatible with STAR-CCM+, and in STAR-CCM+ with buildings not being closed and manifold. To find a solution to these problems took a lot of time which ideally should have been used on other parts of the project, however, getting workable models is necessary to move on with the simulations.

The two models that was being used in the end has some simplifications as mentioned in chapter 1.3, regarding the geometry of the buildings, especially the roofs which are all considered flat, and the height of some buildings. However, these simplifications are believed to not play a big influence in the results of the simulation. What could have had a larger impact is if the terrain were included, however, this was not possible to do within the time-scope of this project.

CFD-simulation

Reliability and the accuracy of every CFD studies solely depends on how good the model is and how well the driving parameters such as mesh, boundary conditions, domain, physics, flow types with respective turbulence model and so on are addressed. For appropriate mesh refinement, use of polyhedral mesh model with proper control on mesh condition and mesh value allowed this study to have greater control.

The use of logarithmic low for velocity profile at inlet, roughness model for the bottom wall treatment, K-Omega turbulence model, RANS equations, field function for turbulent kinetic energy, specific dissipation rate, bottom wall roughness, pressure coefficient, friction velocity and inlet velocity and SST-Menter model have been a solid foundation for this study. The sub-layers which are more sensitive in these studies are better addressed with the use of SST-Menter, field function for the bottom wall roughness and K-Omega model. SST-Menter allows the advantage of both K-Omega and K-Epsilon model.

6 Conclusion

In this project two models containing buildings of urban areas within the city of Oslo has been created by using Revit Placemaker and Autodesk Civil 3D. These have been imported into STAR-CMM+ where meshes has been created and relevant physics has been applied. CFD-simulations have then been run and results for the pressure coefficients on building facades and wind velocity in street canyons has been extracted.

The results have shown that the urban morphology does severely affect the wind conditions. Regarding the pressure coefficient on building facades, it is seen that facades which are facing the inlet wind receives a positive pressure coefficient, while other facades mainly receive negative pressure coefficients. Buildings which are exposed in the front of the domain receives higher magnitude pressure coefficients than buildings in the back which are more shielded. The same applies for taller buildings, and buildings that rises above nearby buildings, making parts of the façade exposed to the inlet wind. In the Downtown model, it is seen that areas with a dense building mass and same heights building will receive real low pressure coefficient values compared to the rest of the area. These differences are not so significant in the Bygdøy model with smaller buildings and a less dense building area.

As for the wind velocity, it is seen that it generally decreases throughout the domain as it passes buildings. However, there are areas where the wind velocity is increasing significantly. These areas tend to be around taller buildings and in open areas, and especially a combination of the two. These increased velocities occur more often and over larger areas at pedestrian level than higher in the street canyons ($17m$). The Downtown model has high differences between open areas around tall buildings, where the wind velocity is higher, and areas with dense building mass and same height building, where the wind velocity is low. These differences are much less significant in the Bygdøy model, due to a much less dense building mass, and lower buildings.

Recommendations for future work

This report has analyzed two relatively large areas within the city of Oslo regarding the impact of urban morphology on wind conditions. The process has been challenging and time consuming, and not all aspects that could be interesting to include in such an analysis has been possible to do. Therefore, some recommendations on further work which has not been done in this project is given below.

- Include the realistic terrain in the analysis. This will require some extra work in the process of creating the model, which is briefly explained in chapter 3.1.3. It must be noted that an advanced terrain surface will make the meshing more complicated.
- Include the realistic roofs in the analysis. As this project has considered all roofs as flat, it could be interesting to see what differences would occur if the roofs had their real geometry. These geometries are available in the files given by The Norwegian Mapping Authority as explained in chapter 3.1.3.2.
- Improve the mesh. When working with CFD, it is difficult and very time consuming to create a perfect mesh. If more time could be put into creating the mesh, it would be interesting to see if that would affect the results in some way.
- Do analysis for thermal comfort. Thermal comfort is an important part of the overall pedestrian comfort. Doing simulations that includes the thermal comfort is possible to do within STAR-CCM+.

References

[1] United Nations, Department of Economic and Social Affairs, Population Division, "World Urbanization Prospects: The 2018 Revision," New York, 2019.

[2] Y. Liu, Y. Xu, F. Zhang, and W. Shu, "A preliminary study on the influence of Beijing urban spatial morphology on near-surface wind speed," *Urban Climate*, vol. 34, p. 100703, 2020/12/01/ 2020, doi: https://doi.org/10.1016/j.uclim.2020.100703.

[3] J. Srebric, M. Heidarinejad, and J. Liu, "Building neighborhood emerging properties and their impacts on multi-scale modeling of building energy and airflows," *Building and Environment*, vol. 91, pp. 246-262, 2015/09/01/ 2015, doi: https://doi.org/10.1016/j.buildenv.2015.02.031.

[4] A. Jurelionis and D. G. Bouris, "Impact of Urban Morphology on Infiltration-Induced Building Energy Consumption," *Energies*, vol. 9, no. 3, 2016, doi: 10.3390/en9030177.

[5] UN Environment and International Energy Agency, "Towars a zero-emission, efficient, and resilient buildings and construction sector. Global Status Report 2017," 2017.

[6] D. Cóstola, B. Blocken, M. Ohba, and J. L. M. Hensen, "Uncertainty in airflow rate calculations due to the use of surface-averaged pressure coefficients," *Energy and Buildings*, vol. 42, no. 6, pp. 881-888, 2010/06/01/ 2010, doi: https://doi.org/10.1016/j.enbuild.2009.12.010.

[7] B. Blocken, W. D. Janssen, and T. van Hooff, "CFD simulation for pedestrian wind comfort and wind safety in urban areas: General decision framework and case study for the Eindhoven University campus," *Environmental Modelling & Software*, vol. 30, pp. 15-34, 2012/04/01/ 2012, doi: https://doi.org/10.1016/j.envsoft.2011.11.009.

[8] H. Kataoka, Y. Ono, and K. Enoki, "Applications and prospects of CFD for wind engineering fields," *Journal of Wind Engineering and Industrial Aerodynamics*, vol. 205, p. 104310, 2020/10/01/ 2020, doi: https://doi.org/10.1016/j.jweia.2020.104310.

[9] R. Yoshie *et al.*, "Cooperative project for CFD prediction of pedestrian wind environment in the Architectural Institute of Japan," *Journal of Wind Engineering and Industrial Aerodynamics*, vol. 95, no. 9, pp. 1551-1578, 2007/10/01/ 2007, doi: https://doi.org/10.1016/j.jweia.2007.02.023.

[10] J. Holmes and S. Bekele, *Wind Loading of Structures*. 2020.

[11] M. Fadl and J. Karadelis, "CFD Simulation for Wind Comfort and Safety in Urban Area: A Case Study of Coventry University Central Campus," *International Journal of Architecture, Engineering and Construction*, vol. 2, pp. 131-143, 06/01 2013, doi: 10.7492/IJAEC.2013.013.

[12] M. Bottema, "A method for optimisation of wind discomfort criteria," *Building and Environment*, vol. 35, no. 1, pp. 1-18, 2000/01/01/ 2000, doi: https://doi.org/10.1016/S0360-1323(98)00065-1.

[13] B. Blocken, T. Stathopoulos, and J. P. A. J. van Beeck, "Pedestrian-level wind conditions around buildings: Review of wind-tunnel and CFD techniques and their accuracy for wind comfort assessment," *Building and Environment*, vol. 100, pp. 50-81, 2016/05/01/ 2016, doi: https://doi.org/10.1016/j.buildenv.2016.02.004.

[14] W. D. Janssen, B. Blocken, and T. van Hooff, "Pedestrian wind comfort around buildings: Comparison of wind comfort criteria based on whole-flow field data for a complex case study," *Building and Environment*, vol. 59, pp. 547-562, 2013/01/01/ 2013, doi: https://doi.org/10.1016/j.buildenv.2012.10.012.

[15] B. Blocken, T. Stathopoulos, J. Carmeliet, and J. Hensen, "Application of computational fluid dynamics in building performance simulation for the outdoor environment: An overview," *Journal of Building Performance Simulation*, vol. 4, pp. 157-184, 06/01 2011, doi: 10.1080/19401493.2010.513740.

[16] P. Richards and S. Norris, "Appropriate boundary conditions for computational wind engineering models revisited," *Journal of Wind Engineering and Industrial Aerodynamics - J WIND ENG IND AERODYN*, vol. 99, pp. 257-266, 04/01 2011, doi: 10.1016/j.jweia.2010.12.008.

[17] B. Blocken, "Computational Fluid Dynamics for urban physics: Importance, scales, possibilities, limitations and ten tips and tricks towards accurate and reliable simulations," *Building and Environment*, vol. 91, pp. 219-245, 2015/09/01/ 2015, doi: https://doi.org/10.1016/j.buildenv.2015.02.015.

[18] Siemens. "Simcenter STAR-CCM+ User Manual." https://docs.sw.siemens.com/documentation/external/PL20200617112215329/en-US/userManual/userGuide/html/index.html (accessed 03.03, 2021).

[19] B. Blocken, T. Stathopoulos, and J. Carmeliet, "CFD simulation of the atmospheric boundary layer: wall function problems," *Atmospheric Environment*, vol. 41, no. 2, pp. 238-252, 2007/01/01/ 2007, doi: https://doi.org/10.1016/j.atmosenv.2006.08.019.

[20] "Turbulence Models," in *Computational Fluid Dynamics for Engineers: From Panel to Navier-Stokes Methods with Computer Programs*, T. Cebeci, J. P. Shao, F. Kafyeke, and E. Laurendeau Eds. Berlin, Heidelberg: Springer Berlin Heidelberg, 2005, pp. 81-94.

[21] J. Franke and A. Baklanov, *Best Practice Guideline for the CFD Simulation of Flows in the Urban Environment: COST Action 732 Quality Assurance and Improvement of Microscale Meteorological Models*. 2007.

[22] J. Franke *et al.*, "Recommendations on the use of CFD in wind engineering," *Proceedings of the International Conference on Urban Wind Engineering and Building Aerodynamics*, 01/01 2004.

Appendix

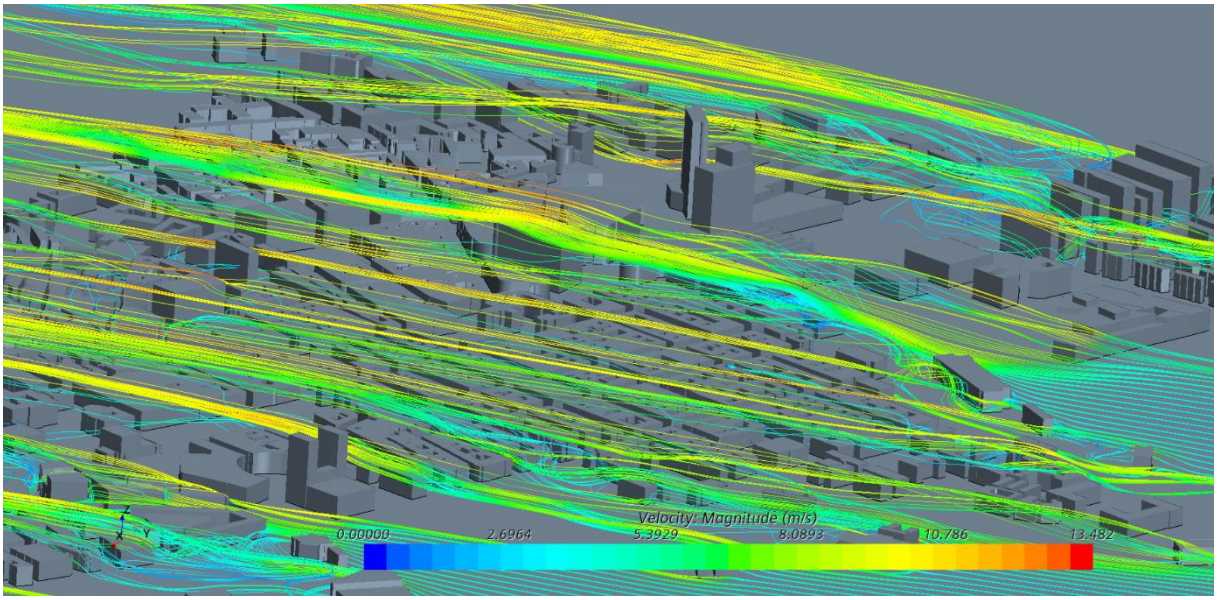

Figure A-1. Free stream flow in Downtown

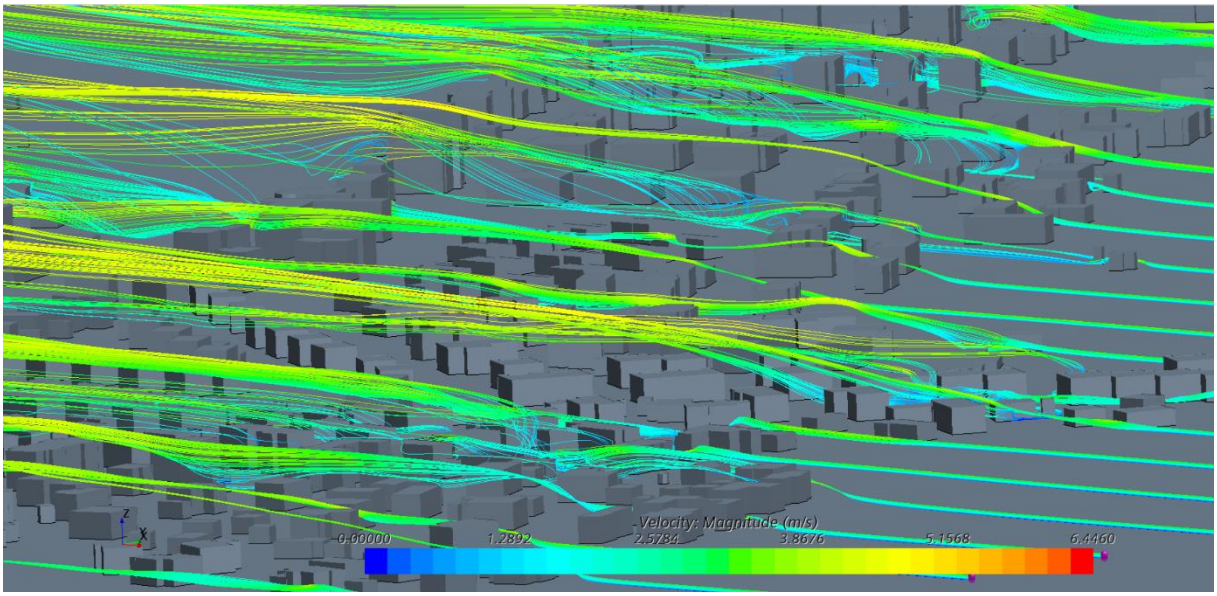

Figure A-2. Free stream flow in Bygdøy

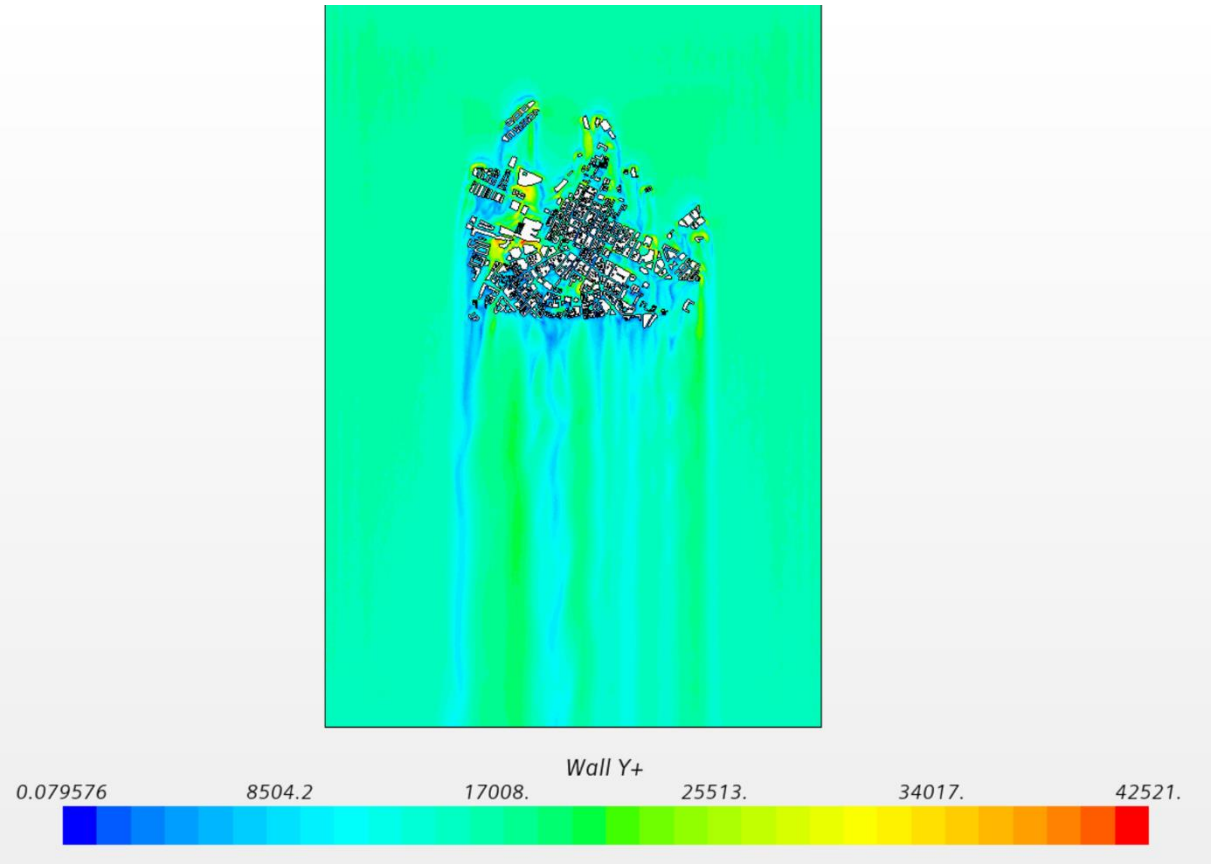

Figure A-3. y+ wall value from inlet to outlet for Downtown

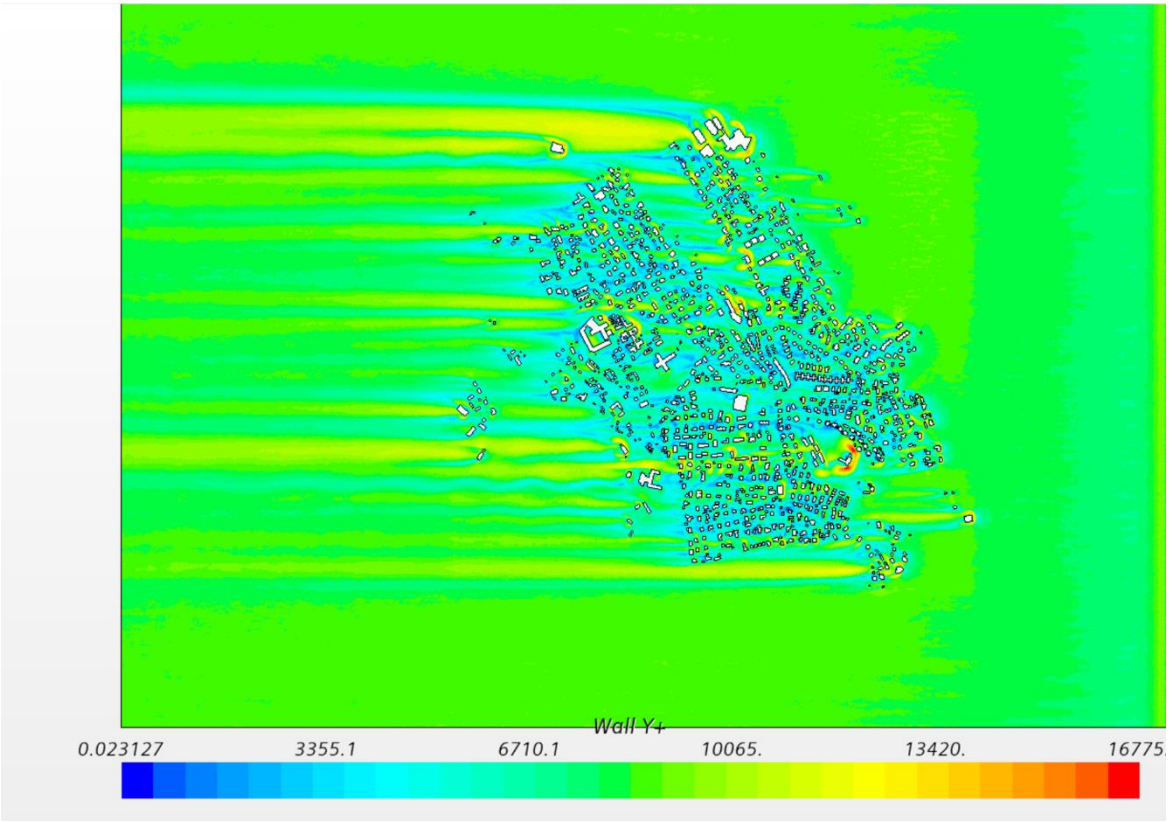

Figure A-4. y+ wall value from inlet to outlet Bygdøy